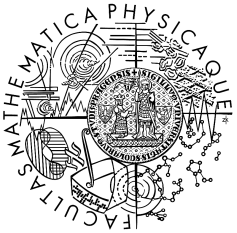

MATEMATICKO-FYZIKÁLNÍ
FAKULTA
Univerzita Karlova

RIGORÓZNÍ PRÁCE

Vojtěch Bednář

Počítačové modelování vývoje tkání

Katedra aplikované matematiky

Vedoucí rigorózní práce: Doc. RNDr. Zdeněk Hedrlín, CSc.

Studijní program: Informatika

Studijní obor: 4I4 – Diskrétní modely a algoritmy

Praha 2017

Prohlašuji, že jsem tuto rigorózní práci vypracoval samostatně a výhradně s použitím citovaných pramenů, literatury a dalších odborných zdrojů.

Beru na vědomí, že se na moji práci vztahují práva a povinnosti vyplývající zezákona č. 121/2000 Sb., autorského zákona v platném znění, zejména skutečnost, že Univerzita Karlova v Praze má právo na uzavření licenční smlouvy o užití této práce jako školního díla podle § 60 odst. 1 autorského zákona.

V …..... dne ..... podpis

Acknowledgement

I would like to thank to my advisor Doc. Hedrlín for his advices, ideas, kind supportiveness, patience and for providing creative environment in his seminars, which were source of inspiration for me. I am grateful to Tomáš Bílý, Martin Bálek, Michal Karásek, and Jiří Šejnoha. I would like to thank for the financial support provided by Europian Commission under the project 'ContraCancrum: Clinically Oriented Translational Cancer Multi-level Modelling' (FP7-ICT-2007-2-223979).

Název práce: Počítačové modelování vývoje tkání

Autor: Vojtěch Bednář

Katedra: Katedra aplikované matematiky

Vedoucí: Doc. RNDr. Zdeněk Hedrlín, CSc.

Abstrakt: Tato práce popisuje hybridní na individuální buňce založený přístup k modelování soustav biologických buněk. V první části je zaveden reakčně-difúzní model prostředí, vaxové ekvilibrium a model buňky postavený na zygotickém grafu a kumulačních stavech. Dále jsou představeny simulace modelující tři biologicky motivované situace: Vznik dutiny, růst nádoru a buněčnou migraci v chronickém zánětu. První model ukazuje scénář formování duté struktury založený na směrovém dělení a buněčné migraci. Druhý model se zabývá růstem potomstva mírně poškozené buňky. Výsledný nádor vykazuje tři stádia maligní transformace. Dále je pozorován jak vznik agresivního nádoru bez detekovatelného prekurzoru na jedné straně tak postupná transformace benigního útvaru na maligní na druhé, každý jako důsledek jiné parametrizace modelové situace. Poslední model se zabývá analýzou role membránové enzymatické aktivity na migrujících buňkách imunitního systému v chronickém zánětu. V tomto modelu je pozorováno, že absence této aktivity je zodpovědná za chování odpovídající chronickému zánětu, namísto fyziologicky relevantní imunitní odpovědi.

Klíčová slova: hybridní model, agentně založené modelování, digitální biologická buňka, zygotický graf

Title: Computer Modeling of Tissue Development

Author: Vojtěch Bednář

Department: Department of Applied Mathematics

Supervisor: Doc. RNDr. Zdeněk Hedrlín, CSc.

Abstract: This thesis describes hybrid individual cell-based approach to modeling of systems of biological cells. In the first part reaction-diffusion model of environment is introduced together with vax equilibrium and model of cell based on zygotic graph and cumulative states. Further, simulations modeling three biologically motivated situations are introduced: Lumen formation, tumour growth, and cellular migration in chronic inflammation. The first model shows a scenario of hollow structure formation based on directional division and cellular migration. The second model is concerned with the growth of a progeny of a slightly damaged cell. The resulting tumour exhibits three stages of malign transformation. Further, emergence of an aggressive tumour without detectable precursor is observed on one hand and a continual transformation of a benign neoplasm into a malign one is seen on the other hand. Each of these cases is a consequence of different parametrization of the model situation. The last model analyses the role of membrane enzymatic activity in migrating cells of the immune system in chronic inflammation. In this model it is observed that absence of this activity is responsible for occurrence of behavior corresponding to chronic inflammation instead of physiologically relevant immune response.

Keywords: hybrid model, agent-based modeling, digital biological cell, zygotic graph

Contents

Introduction

Computer modeling of biological phenomena has gained widespread attention, establishing itself as an acknowledged companion of experimental as well as theoretical research efforts of biology. In-silico simulations are powerful in generating hypotheses that go beyond the extent of conceptual models widely used to formulate biological understanding. In this thesis we provide a variant of hybrid cell-based modeling approach to simulation of behavior and development of systems of cells, together with particular biologically motivated models. Our model shares common basic properties with agent-based systems. It further involves reaction-diffusion environmental modeling based on discretization of continuous equations. Chemical substances and receptor-ligand interactions are essential for the system. Neither decision rules nor states of the agent cells are encodings of direct phenomenological observations, as it is usual in agent-based methodology. Instead, we accommodate simplistic yet flexible and versatile model originally inspired by a very basic function of neuron. Neural cell has a body, dendrites, and axon. By means of membrane-bound receptors the neuron collects chemical signals on its dendrites. If the signal collected is strong enough, the neuron fires, which causes secretion of neurotransmitters at the end of the axon. These neurotransmitters can bind to receptors of other neurons and the process may repeat. While the places of receiving the signal and sending the signal are spatially separated in a neuron, in our agent cell the receiving locus is the whole cell surface and the sending locus is the whole membrane as well. We have multiple kinds of ligands and multiple kinds of receptors. The cell has states that are in one-to-one correspondence with receptor kinds, generally with chemical substances. The cell decides which signal is seen most by the receptors and this signal determines cell state. The state then drives “firing“, which basically means secreting ligands, adding receptors on the membrane, and other actions like migration and apoptosis. As we see, the agents are using kind of rather low level rules. If willing to tell the agents to act according to some “if - then“ high level rules, one has to implement these in the low-level “language“. However, doing this is our goal rather implicitly than explicitly. One of the strengths of agent-based modeling is emergence [5]. When providing the rules and simulating interactions of multitude of agents, unexpected behaviors often occur, hardly guessable based on the sole knowledge of the axioms without executing the simulation. The type of emergent results depends on the kind of the primary encoded rules. If one encodes phenomenological rules, only the part of reality captured by the rules of this kind will produce emergent results. If one focuses on the use of rules embodied in transparent or transparently graspable properties like chemically-based receptor-ligand interactions or ligand secretion, it is expected that the results will have that degree of closeness to reality that the transparent assumptions had. This needn't mean that the results have to be biologically correct. But they are generally

traceable to the transparent axioms, simplifying the process of either result justification or error detection.

Our model is based on Digital Biological Cell approach [1]. In a grid based environment there are discrete cells generally occupying multiple sites, together with reaction-diffusion system of chemical substances. Many of the reaction-diffusion interactions are encapsulated in building blocks we call vaxes and vax equilibrium. Generic mechanism for expressing most rules for the cells is called zygotic graph. As we have stated beforehand, the cells may secrete ligands, add membrane receptors, move, and undergo apoptosis. Cell divisions can be driven by the zygotic graph rather indirectly, they have their own controlling mechanism. Scheme for simulating advection in bounded surroundings of a moving cell is incorporated in the model. It can be optionally used if constant flow velocities for the neighborhood are externally provided.

In the first part of the thesis, model of these above outlined properties is defined, conceptually building on [115]. We mostly use the term “model world“ for it.

We have implemented the model world in a software simulator called Virtual Laboratory. The program is not part of the thesis, however, all the particular simulations of biologically inspired situations described in the text have been created in this software. In the text, we refer the simulations as models, providing their definitions in terms of the primitives of the model world.

The first of the particular models in the next part of the thesis regards lumen formation. Lumen is a hollow cavity lined by collection of cells or being inside a single cell. Lumina or luminal tubes are parts of many organs including blood vessels, kidneys, or gut. There are several biologically observed mechanisms of how lumen arises. One of them is cavitation of solid multicellular mass. In-silico models capturing this kind of luminogenesis usually incorporate polarization within an individual cell and apoptosis as key elements of this process. We propose a theoretical scenario where none of these processes is necessary. In our model, chemical precursor of lumen arises in terms of concentration gradients. Polarisation then emerges on the level of multicellular structure. Directional growth together with cell migration are the key drivers of cavitation.

Next model deals with cancer onset. We name it Diversified tumour Model. It has been created and its preliminary version delivered within the project ContraCancrum. In this joint interdisciplinary effort, predictive multi-level modeling of development of selected particular types of cancer together with reactions on various treatment regimes was aimed [46], [47], [48]. Primary motivation for the Diversified tumour Model was non-imageable tumour growth in cancer onset. The model scenario starts from a single cell with a slight damage or increased susceptibility to oncogenic signaling. Progressive transformation in the progeny of

the cell is analyzed under various parameter combinations. The model suggests that gradual malignant transformation of a benign neoplasm on one side and fast onset of a highly aggressive tumour without any detectable precursor on the other hand may arise as consequences of various intensities of enzymatic activities on cell membranes and in the environment surrounding the cells.

Finally, difference between chronic inflammation and a physiological inflammatory response is modelled in terms of properties of migratory cells of the immune system. The model shows causal relationship between lack of membrane-based enzymatic activity towards a chemoattractant on the migratory cells and the chronic inflammatory behavior, suggesting this as an explanatory hypothesis for particular medical motivation.

Structure of the thesis. In chapter 1, brief outline of main cell-based modeling methodologies is provided. Chapter 2 contains the definition of the model world. We specify the reaction-diffusion component with regard to vax equilibrium, basic properties of the discrete cells, zygotic graph, cell division rules, apoptosis, and properties of flowaround. The chapter ends with the description of the overall simulation algorithm, putting the individual components together. In chapter 3, the model of lumen formation is provided. Chapter 4 contains the Model of Diversified tumour, in chapter 5 the model of cell migration in chronic and physiological inflammation is described. Chapter 6 contains concluding thoughts and remarks.

General description of an extension of the definition of the model world was published in [1]. Preliminary version of the Diversified Tumour Model became part of [114].

1. Cell-based modeling approaches

In this section we will briefly introduce main cell-based methodologies for modeling multicellular systems. The main sources of information are [6], [73], and [76].

Modeling of multicellular systems can be basically divided into two groups. Continuum approaches and cell-based approaches. In the first category, the system is represented in terms of continuous variables and its dynamics is usually defined by partial differential equations (PDE). The benefit of this approach is that the equations bring insights into the relationships among the components of the system. Emergent properties based on these components also arise. Disadvantage is that the discrete nature of the cells is not captured. Additionally, expressing more complicated local cell logic is clumsy.

In the cell-based models, cells are represented as discrete entities. Various kinds of behaviors and interactions of the individual cells are conceived by model definitions, leading to emergent properties when simulations are performed.

Combination of these approaches is hybrid modeling, where reaction-diffusion component is expressed in a form of PDE while cells are discrete. Hybrid modeling has the ability to step quite naturally across several scales (molecular / chemical, cellular, various temporal scales) while incorporating advantages of both of the individual approaches.

Cell-based (or hybrid) approaches can be categorized as lattice-based or lattice-free.

We will be further interested in four main kinds[1] of cell-based models[2]: Cellular automata (CA), agent-based models (ABM), cellular Potts model (CPM) as an extension of CA, and lattice-free models.

1.1 Cellular automata

In its basic definition [8], cellular automaton consists of a regular uniform grid with a discrete variable at each site. State of the automaton is completely specified by the values of the variables at every site. The automaton evolves in discrete steps. Value of a variable in given step is determined by the values of the variables in its neighborhood in the previous step. By neighborhood of a site the site alone is understood, plus the immediately adjacent sites. The update of all sites is synchronous, i. e. the variables at each site are updated simultaneously, based on the values of the variables in the neighborhood at the previous time step, according to a finite set of local rules [8]. One way of utilizing CA for cell-based modeling is using square (cubic) lattice with mutually exclusive space management, i. e. one site can be

1 Although not generally disjoint, these categories are widely used.
2 Including hybrid variants.

occupied by at most one cell [9], [14]. If a site is occupied, its state is composed of various properties of the cell, e. g. migration direction in terms of the grid topology (left, right, top, …, standing still) or counters until performing specified action like division or migration direction change [9]. Another variant are so called multi-compartment CA [73], where multiple cells are generally contained in a single lattice site. The sites have limited capacity for cells. When there are too many cells in a site, some of them shall be moved to neighboring sites. Algorithms solving this problem must be specified. In [10], [11], tumour growth has been modelled using multi-compartment CA. When going back to the mutually exclusive space management, hexagonal lattices have been also used [12], [13].

1.2 Agent-based models

Agent-based modeling, sometimes also referred as individual-based modeling [19], [20], is rather a paradigm than a notion being introduced by a formal definition. Referring [15], in ABM a system is modelled as a collection of autonomous entities making decisions, called agents. Each agent makes its individual assessment of the situation and decides based on a rule set. Agents may be capable of evolving. ABM paradigm describes a system from the perspective of its constituent units [15]. As mentioned in the introductory chapter, the main benefit of ABM is generating emergent results [16], [15], [5]. ABM and CA are similar in that the agents or cells are driven by the rules in their surroundings or environment and in generating emergent behaviors. Analysis of three ABM models with methodological elaboration is provided in [16]. ABM has been used in a wide range of domains outside of cell systems simulations, like social sciences, anthropology, or ecology [5], [20]. Various ABM software platforms are currently available [5].

1.3 Cellular Potts

Model definition. Cellular Potts model [42], [41] can be seen as a cellular automaton where single cell generally occupies multiple lattice sites. Assuming a 2D lattice, let's consider a spin $\sigma(i, j)$ defined at each lattice site (i, j), $\sigma \in \{1, ..., N\}$, where N is the number of cells in the scenario. The m-th cell is composed of all sites (i, j) where $\sigma(i, j) = m$. Every cell has an associated type $\tau(\sigma)$. We will define the total energy of the system (Hamiltonian) H as

$$H = \sum_{(i,j),(i',j') \text{ neighbors}} J\left(\tau\left(\sigma(i,j)\right), \tau\left(\sigma(i',j')\right)\right)\left(1-\delta_{\sigma(i,j),\sigma(i',j')}\right) + \lambda \sum_{\text{spins } \sigma} \left(a(\sigma) - A_{\tau(\sigma)}\right)^2 .$$

Here $J(\tau, \tau')$ is the surface energy between spins of type τ, τ'. Further $\delta_{\sigma,\sigma'}$ is Kronecker's delta, $a(\sigma)$ is the area of cell σ, A_τ is the target area for cells having type τ, λ determines the strength of the area constraint. The first sum specifies the total surface energy of "bonds" among cells. As we see, within a single cell

individual contributions are zero thus the surface energy of the inside of a cell is zero. J specifies the contact energy (per unit cell surface length) between various types of cells. In the second term, it is supposed that each cell type has its natural volume (area) A_τ. If a volume of particular cell differs from this value, this is connected with energy increase.

In each time step a site (i, j) is randomly chosen for update. In the update, the spin $\sigma(i, j)$ is changed to spin σ' of a randomly chosen neighbor of the site (i, j). There is a temperature parameter $T \geq 0$. The change is accepted with the following probability: For $T > 0$,

$$P(\sigma(i,j) \to \sigma'(i,j)) = e^{\frac{-\Delta H}{kT}} \quad if \ \Delta H > 0 ,$$

$$P(\sigma(i,j) \to \sigma'(i,j)) = 1 \quad if \ \Delta H \leq 0.$$

For $T = 0$, $P(\sigma(i, j) \to \sigma'(i, j)) = \{ 0 \text{ if } \Delta H > 0, \frac{1}{2} \text{ if } \Delta H = 0, 1 \text{ if } \Delta H < 0 \}$.
ΔH is the energy gain caused by the change, k plays the role of Boltzmann constant. Further, one monte carlo step (MCS) is defined as a chosen number of time steps. The MCS is a usual time measure in the model.

CPM characteristics. An advantage of cellular Potts model is its simplicity. It is not necessary to supply the position and diffusion of cell membrane in terms of an "artificial" dynamics. Relative contact energies and boundary curvature direct all the motion. Also, CPM is flexible and readily extensible. With regard to the "hybrid" direction, diffusion of chemicals is typically solved numerically on a grid matching with that one of the CPM. The response of the model cells to the chemical gradients is typically realized in a way that the cells are more likely to extend (or retract) pseudopods in the direction of given gradient [17], [18]. Extensions making it possible to model an effect of cell shape [21], persistent cell motion [22], or anisotropic differential adhesion [23] have been realized.

One of the disadvantages of CPM is limited speed of propagation of compression waves. If a cell aggregate is pushed on one side, it will be deformed instead of moving as a whole. Another drawback is that the model dynamics is nonlocal due to the volume constraint. Also, at nonzero temperatures, fragments of a cell can detach. Under higher temperatures, clusters of such particles can form, being longer lived than the small fragments. The clusters may grow to sizes comparable with the original cell, so that they can't be distinguished from the parent [41]. This is another case of nonlocality, kind of an "emergent" one. CPM is not particularly suitable for modeling plant tissue dynamics [7]. The plant cells have cell wall which maintains cell geometry and prevents cell motility, which is sort of incompatible with the CPM paradigm. Nevertheless, by a hybrid approach these incompatibilities have been tackled [24].

CPM with it's simplicity and physical transparency is popular and being widely utilized in cell-based modeling. It has been used to model various phenomena like blood vessel network formation [25], vascular sprouting [17], tumour growth [27], somite formation [26], or convergent extension [23]. Software toolkits implementing CPM are currently accessible [28], [29].

1.4 Lattice-free models

In the lattice-free models the cells can be generally placed at any position, without restrictions imposed by grid spacing. Cell positions are usually determined based on equations of motion, where forces acting on the cells are incorporated. The main benefit of the lattice-free models is the freedom to move a cell in any direction. The disadvantage is that a special algorithmic care must be taken in order to handle cell neighborhood. From the hybrid point of view, since chemical fields are usually computed on regular grids, some kind of interpolation techniques needs to be employed when interaction with these fields is determined. If a cell divides, nonoverlapping placement of the daughters has to be computed. Also, in migration there is a risk of cell collisions when the time step is "too big". Some types of Lattice-free models can be identified:

Spherical and ellipsoidal cell-centered. In the spherical cell-centered models [19], [30] the cells are represented as single points. Springs or energy potentials are used to maintain minimum predefined distances between neighboring cells. The ellipsoidal models [31], [32] are conceptually similar but two axes of different lengths are used to form elliptical shape.

Cell centered with Voronoi tessellation. In these models, neighbors of a cell are provided by Voronoi tessellation. In this way, the number of neighbors is obtained together with border length between two adjacent cells. This forms a base for computing of cell-cell interactions. These models have been used in modeling colorectal cancer [33] or multicellular tumour spheroids [34].

IBCell and related models. In the immersed boundary cell model (IBCell) [49], [50] a cell is modelled in a rather sophisticated way, as a body containing incompressible viscous fluid. The cell is bounded by elastic springs that define its shape together with the fluid contents. Simulation of cell shape changes is mostly based on appropriate spatio-temporal placing fluid sources and sinks on either side of cell membrane, where the fluid flow influences the membrane. This makes it possible to model cell geometrical adaptability. The elastic boundaries are discretized, points at the boundaries may be treated as receptors mediating various kinds of interaction of a cell with other cells or with the environment. In addition to modeling epithelial

acini [49], [50], this approach has been used to model various cancer conditions [36], [37].

1.5 Modeling techniques

Choices of rules or axioms within a modeling approach strongly influence characteristics of information that the following (emergent) results are bringing. In this section we will provide short summarization of some common choices used in literature in establishing rules axiomatizing basic cellular activities. Particularly, we will be interested in division, migration, differentiation, and apoptosis together with necrosis. Most of the information we provide is summed up in review [6].

Division. Cell division is often modeled as a probabilistic event. Cells can be set-up to divide after cell cycle time [9], [103], [107]. This time can be obtained experimentally [9], [107], [112] or assigned to each cell randomly based on normal distribution [9], [107]. In the latter case different times are assigned to different cells, the daughter cells can inherit the cell cycle time of the mother [107]. In time dependent simulations with step Δt probability P_{div} in particular step can be determined as $P_{div} = \Delta t / t_c$ where t_c is the cell cycle time [14]. Division probability can be also determined based on parameters like local nutrient concentration [11]. In case of cellular Potts division may be triggered when a cell reaches certain size [27] or volume-to surface ratio [110].

Within a division, positions of daughter cells have to be determined. One choice is to do this randomly, placing the daughters at the adjacent unoccupied sites [35], [9], [100]. When all neighboring sites are already filled, contact inhibition is commonly used to prevent cell division [98], [35], [107]. It may be desired to place the daughter cells away from each other with a free site inbetween [14] or it can be required that they are always adjacent to each other [108]. Alternatively, different probabilities to different available sites may be assigned. Another way is algorithmic simulation of pushing an adjacent cell by a daughter outwards in a model tumour until the edge of the conglomerate is reached where an empty space becomes filled [105]. As an alternative, daughters can be piled at the same site inside the tumour and replace a necrotic cell or fill a vacant place at the rim [11].

In CPM half of the lattice sites of the mother can become a new cell [97], [27]. In the lattice-free models the direction of the total force the cell experiences can determine the division orientation [101].

Migration. In random movement the new location of the moving cell can be selected randomly from one of the neighboring lattice sites [35], [100], [108]. If all the adjacent sites are occupied, contact inhibition is used as in the case of division [35], [100], [108]. Another mode is persistent random walk [9]. A cell moves in one

direction for some period of time and then the direction is changed. If the cell divides, random movement in the daughters is resumed after the division. Upon collision, the cells stop moving for some time and then the movement starts again with new directions being randomly chosen. [9]

In directed movement, the best location among the neighboring sites can be chosen based on factors like nutrient amounts, toxicity, and mechanical confinement [106], [113]. In the multi-compartment scenarios where multiple cells can reside in one lattice site, probability of migration may increase with the number of cells in the element [11]. Chemotactic displacement of a cell can be proportional to the difference between newly bounded receptors in the front and the back of the cell [104]. Migration based on relative concentrations of several particular chemical species has also been used [109].

Random and directed migration can be combined in various ways. One possibility is that a cell moves randomly until sufficient amount of a chemical is detected. Than the migration mode is changed, the cell follows given concentration gradient with the random compound substantially decreased [90].

In the lattice-free models cell movements are usually determined based on equations of motion where forces affecting given cell are incorporated [19], [111].

Differentiation. When a cell differentiates, its type in the lattice site can be simply changed. Rules for differentiation seem to be specific per concrete model. In [35], portion of mature mesenchymal stem cells differentiate based on mechanical stimulation and presence of vasculature, leading to three types of differentiated cells. Combination of the mechanical stimulus intensity in terms of “low / medium / high” with indication of presence or absence of nearby vasculature determines the differentiated cell type.

In [64] a cell assesses types and relative locations of components (extracellular matrix, free space) in its neighborhood in a hexagonal lattice. Based on this information type of the cell either changes or remains the same. Cell differentiation and dedifferentiation is possible in this way.

Apoptosis and necrosis. When simulating apoptosis the cell of concern is usually removed. Given place remains empty and can become occupied by another cell [102]. Apoptosis may be triggered when a (co)stimulus that caused its prior differentiation to current type changes [35]. Another possibility is to apoptose when (at least one) cell of specified type is present in the neighborhood [102]. Alternatively, apoptosis may occur when an area size the cell is in contact with the substrate gets below a treshold value (anoikis) [19], [101]. A cell is usually made necrotic when local concentration of oxygen or nutrients is under a treshold value

[27], [107]. Necrotic cells in tumour simulations are typically not removed, left to be participating in the composition of the neoplasm [99], [27].

2. Model world and Virtual Laboratory

Virtual Laboratory is a software simulation environment that implements model of cells together with (micro)environment they live in. The model uses Digital Biological Cell approach [1], instantiating many of its paradigms. Generally, our hybrid agent-based model consists of two logical parts: The environment and the cells. The environment is formed by discrete 2D lattice where discretized system of reaction-diffusion equations is being solved, describing spreading and other behavior of chemical substances present in the environment.

The cells are discrete entities occupying volume (space) in the environment. They are impermeable for the chemical substances. In agreement with biological intuition, boundary of a cell – which is part of the boundary of the environment – is called a membrane. Membrane of a cell is its main interface to interact with the surroundings. By means of their membranes the cells can secrete chemicals to the environment, sense their concentrations and cause their decay. Further, the cells can sense concentration gradients in their surroundings, migrate, divide and die. The inner decision logic of the cells is expressed by zygotic graph [1]. In the next paragraphs, detailed description of the cells and (our realization of) the zygotic graph will follow.

2.1 Chemical substances and reactions

In our modeling approach chemical substances will play a role of one kind of basic building blocks. We are not interested apriori in what particular real–world chemical species these represent. Our chemicals are rather placeholders, variables obeying kinetic and other rules within a model situation created in our model world. Defining or seeking correspondences with real–world chemical species is left to the modeller on the level of particular model situations. We will require that the system of substances and reactions among them will have sufficient expressing power. At the same time, we wish that the system is not too complex so that it can be rather easily understandable and usable to build constructions in connection with other parts of the model world. We also require reasonable level of chemical plausibility of reaction kinetics.

2.1.1 Reaction scenario

Chemical substances and vaxes. Let $A^{\vee} = \{A_1, ..., A_n\}$, $V^{\vee} = \{V_1, ..., V_n\}$ and $X^{\vee} = \{X_1, ..., X_n\}$ be nonempty mutually disjoint sets of chemical species. Let $Lv = A^{\vee} \cup V^{\vee}$. We will call elements of Lv ligands[3]. A triple (A_i, V_i, X_i) will be called the i-th vax, $1 \leq i \leq n$. If i is not important for us or if it is obvious from the context,

3 At some places we will use this term in order to stress that given substance from Lv binds to a receptor.

we will just use the term vax. Also, when X_i is not relevant for us, we will just be saying that A_i and V_i, or V_i and A_i, form a vax, or that they are complementary. For each $L \in Lv$, by $\lambda(L)$ we will denote substance $M \in Lv$ complementary to L and by $\chi(L)$ we will mean substance $X \in X^{\vee}$ such that (L, M, X) or (M, L, X) form a vax. Let *Vaxes* be the set of all vaxes (A_i, V_i, X_i), $i = 1, .., n$.

For each vax $(A, V, X) \in Vaxes$, let there be a chemical reaction $A + V \leftrightarrow X$. Such reaction will be called vax reaction.

Membrane anchoring and receptors. Substances from $Lv \cup X^{\vee}$ can be either freely diffusible in the environment or anchored to cell membranes. If we want to explicitly discern among individual forms regarding membrane anchoring within a vax $(A, V, X) \in Vaxes$, we will be using following notation: A^p, V^p, X^p for free diffusible forms, A^m for A anchored in a membrane, V^m for V anchored in a membrane, X^A for X anchored via its A part and not by its V part, X^V for X anchored by its V part and not by its A part, and X^{AV} for X anchored by its A part and V part. We state as a rule that A^m and V^m don't react together at the membrane of the same cell. Thus occurrence of X^{AV} means that X is anchored to different cells via A and V.

In many cases, the particular form of a substance regarding membrane anchoring will not be important for us, or it will be of interest only at some places. Thus we will often not be using the notation expressing the form, and specify it ad hoc.

In terms of biological context, receptors are proteins anchored in a cell membrane, capable to bind more or less specific substances from the outside of the cell and provide the information that the substance is bound to the cell interior [2][4]. In our model world, by receptor we will refer any substance $S \in Lv \cup X^{\vee}$ in membrane – anchored form.

If talking about S as about receptor, we will define kind of the receptor as follows: If $S \in Lv$ let kind of the receptor be S. If $S \in X^{\vee}$ kind of the receptor will be the substance $L \in Lv$ which is the part of complex S anchoring it to a membrane. If L is not unique (i. e. in case S is membrane-anchored by both its parts), regarded membrane, and thus L, will be either specified or obvious from context.

Alternatively, we will express receptor kind $H \in Lv$ when talking of $S \in Lv \cup X^{\vee}$ as of receptor by saying that the receptor is formed by H.

Further, if there is receptor S and $S \in Lv$, we will say that it is unoccupied. If $S \in X^{\vee}$, we will say that that it is occupied, or that it is occupied by $\lambda(H)$, where H is kind of S.

Decays. In addition to vax reactions there are reactions we will collectively call decays. These are spontaneous decay and membrane decays.

4 Chap. 1.

Let $L \in Lv \cup X^{\check{}}$ be a freely diffusible substance. Then let there be a reaction $L \rightarrow Z$. Here $Z \notin Lv \cup X^{\check{}}$ is a (are) symbolic or putative product(s) of decay of substance L. Z is unimportant for us, not being conceived by the model world. We simply state that diffusible substances in a model situation can undergo decay. This kind of reaction will be called **spontaneous decay**. The adjective spontaneous in the naming symbolizes the idea that the real world cause of the decay, whatever it is, is not important for us.

The other type of decays are membrane decays. These involve substances anchored to cell membranes. There are three kinds of membrane decays:

- **Membrane enzymatic activity**. It can be expressed as reaction $X \rightarrow R$, where $X \in X^{\check{}}$ is occupied receptor formed by $R \in Lv$. We assume that the ligand complementary to R is not membrane bound, i. e. X is regarded to be anchored in a cell membrane by its part corresponding to R. Membrane enzymatic activity is a way how cells can remove free diffusible ligands from their surroundings. Receptors are playing role of enzymes cleaving their (free diffusible) substrates.
- **Receptor internalization**[5]. It behaves in the same way as spontaneous decay, but the substance undergoing decay is membrane-anchored. Parameters (rate constants) of individual reactions are generally different from their spontaneous decay analogies. If receptor $X \in X^{\check{}}$ undergoes receptor internalization, we don't distinguish whether it is bound to membrane by its part belonging to $A \in A^{\check{}}$ or $V \in V^{\check{}}$. Generally, receptor internalization causes removal of ligands from cells' surroundings, cells are internalizing receptors together with ligands bound on them.
- **Raw receptor internalization**[5]. Raw receptor internalization is an analogy of receptor internalization but only substances from Lv forming the receptors are internalized. If $R \in Lv$ is an unoccupied receptor, the situation is the same as in receptor internalization. If receptor S of kind R is occupied by (originally) free ligand L, R is internalized and L "returns" to the free environment. If R is bound to receptor R' belonging to another cell, R and R' are internalized individually, each according to its own parameter (rate constant) of raw receptor internalization. Raw receptor internalization is a way how cells can remove receptors from their membranes without altering the outer environment.

In the model world, receptor internalization and raw receptor internalization are mutually exclusive. Let's have a Boolean parameter *UseReceptorInternalization*. If it is *true*, receptor internalization is to be used in particular model situation. If it is *false*, raw receptor internalization is to be used in given model.

5 In particular models presented later in this thesis, receptor internalization and raw receptor internalization are not being used.

2.1.2 Reaction kinetics and vax equilibrium

Vax reaction kinetics. Regarding vax reactions, we will assume these to be reactions where chemical bonds form and cease, obeying kinetic rules of covalent reactions[2]. As described in [2], such a reaction has a general form

$$aA + bB + \ldots \;\Leftrightarrow\; zZ + yY + \ldots ,$$

where capital letters represent particular molecules or atoms and lowercase letters represent the number of each in the reaction formula. For the rate of the forward reaction $Rate_{forward}$ we have

$$Rate_{forward} = k_f \cdot [A]^a [B]^b \cdot \ldots ,$$

similarly for the rate of the reverse reaction $Rate_{reverse}$ we have

$$Rate_{reverse} = k_r \cdot [Z]^z [Y]^y \cdot \ldots ,$$

where k_f is the rate constant of the forward reaction, k_r is the rate for the reverse reaction, and *[S]* denotes concentration of substance *S*.
At equilibrium the rate of the forward reaction equals that of the reverse reaction. Then we can write

$$k_f \cdot [A]^a [B]^b \ldots = k_r \cdot [Z]^z [Y]^y \ldots ,$$

$$\frac{k_r}{k_f} = \frac{[A]^a [B]^b \ldots}{[Z]^z [Y]^y \ldots} . \tag{2.1}$$

Let

$$K_{eq} = \frac{k_f}{k_r} , \; K_d = \frac{k_r}{k_f} . \tag{2.2}$$

Here K_{eq} is the equilibrium constant, K_d is the dissociation constant.

Vax equilibrium. Let $(A, V, X) \in Vaxes$ be a vax. Assuming the vax reaction $A + V \leftrightarrow X$ and equilibrium conditions, from (2.1) and (2.2) we have

$$\frac{[A][V]}{[X]} = K_d . \tag{2.3}$$

Let now $[A_0]$, $[V_0]$, $[X_0]$ be arbitrary concentrations of substances *A*, *V*, *X* respectively, let at least one of them be nonzero. Let $k_f > 0$, $k_r \geq 0$.[6] If the system is not at equilibrium, we will assume that after some time the equilibrium will be reached - we will be saying that the vax reaction passed, or shortly that the reaction passed. We will denote the corresponding equilibrium concentrations $[A_1]$, $[V_1]$, $[X_1]$.

6 For $k_r = 0$, K_{eq} in (2.2) is undefined. We are further using K_d only.

For substance $L \in Lv$, let T_L denote the total concentration of substance L in reacted and unreacted form with regard to the vax reaction L participates in. We will call T_L the r-concentration[7] of L. If L is unimportant or obvious, we will use shortly the term r-concentration. Due to mass conservation we have

$$[A_0] + [X_0] = T_A = [A_1] + [X_1], \tag{2.4}$$

$$[V_0] + [X_0] = T_V = [V_1] + [X_1]. \tag{2.5}$$

Since concentrations are nonnegative quantities, there must hold specially

$$[X_1] \leq T_A, T_V. \tag{2.6}$$

By expressing $[A_1]$ from (2.4), $[V_1]$ from (2.5), and substituting to (2.3) we get

$$\frac{(T_A - [X_1]) \cdot (T_V - [X_1])}{[X_1]} = K_d.$$

This can be arranged as

$$[X_1]^2 - [X_1](T_A + T_V + K_d) + T_A T_V = 0$$

and viewed as a quadratic equation in variable $[X_1]$.
It is not difficult to see that discriminant of this equation is nonnegative[8]. We get

$$[X_1]_{1,2} = \frac{T_A + T_V + K_d \pm \sqrt{(T_A + T_V + K_d)^2 - 4T_A T_V}}{2}.$$

It can be shown that the root

$$[X_1]_1 = \frac{1}{2}\left(T_A + T_V + K_d + \sqrt{(T_A + T_V + K_d)^2 - 4T_A T_V}\right)$$

doesn't fulfill (2.6), except of the case when the roots coincide. As a solution we get

$$[X_1] = [X_1]_2 = \frac{1}{2}\left(T_A + T_V + K_d - \sqrt{(T_A + T_V + K_d)^2 - 4T_A T_V}\right). \tag{2.7}$$

From (2.4) we have

$$[A_1] = T_A - [X_1] = \frac{1}{2}\left(T_A - T_V - K_d + \sqrt{(T_A + T_V + K_d)^2 - 4T_A T_V}\right) \tag{2.8}$$

7 As a shortcut for raw concentration.
8 Cf. proof of claim 2.1.2.

analogically (2.5) gives

$$[V_1] = T_V - [X_1] = \frac{1}{2}\left(T_V - T_A - K_d + \sqrt{(T_A + T_V + K_d)^2 - 4T_A T_V}\right) \quad (2.9)$$

Basic properties of vax equilibrium. We will now reformulate our thoughts in a slightly generalized way and make some simple practical observations.
Let $L \in Lv$, let's consider reaction

$$L + \lambda(L) \leftrightarrow \chi(L)\,. \quad (2.10)$$

From (2.4), (2.5)

$$T_L = [L] + [\chi(L)]\,.$$

Definition 2.1.1. Let

$$fxvax(u, v) = \frac{1}{2}\left(u + v + K_d - \sqrt{(u + v + K_d)^2 - 4uv}\right), \quad (2.11)$$

$$flvax(u, v) = u - fxvax(u, v), \quad (2.12)$$

be functions of u and v. We assume $u, v \geq 0$ and $K_d \geq 0$ to be a parameter.

Obviously

$$fxvax(u, v) = fxvax(v, u).$$

Claim 2.1.2. *For $u, v, K_d \in \mathbb{R}$, $K_d \geq 0$, fxvax(u, v) is a real valued function.*

Proof. It is immediately seen that for arbitrary $a, b \in \mathbb{R}$ there holds

$$(a + b)^2 - 4ab \geq 0,\ (a + b)^2 - 4ab > 0 \text{ for } a \neq b\,.$$

Thus the expression $(u + v + K_d)^2 - 4uv$ under the square root in (2.11) is always nonnegative. □

From (2.7) it follows that at equilibrium there holds

$$[\chi(L)] = fxvax(T_L, T_{\lambda(L)})\,, \quad (2.13)$$

and from (2.8), (2.9) at equilibrium there is

$$[L] = flvax(T_L, T_{\lambda(L)}),$$

when K_d in (2.11) is the dissociation constant of reaction (2.10).

Observation 2.1.3. *For u, v, $K_d \geq 0$*

$$fxvax(u, v) \leq u, v. \tag{2.14}$$

Observation 2.1.4. When $K_d = 0$, we have

$$fxvax(u,v) = \frac{1}{2}\left(u + v - |u-v|\right) = min(u, v). \tag{2.15}$$

In terms of substance concentrations and (2.13), in this situation the ligand which is present in lesser or equal total amount (reacted + unreacted form) than the other one will totally enter the reacted form. The (eventual) excess of the total amount of the other ligand will remain unreacted.

Observation 2.1.5. *Let's regard function fxvax(u, v) from definition 2.1.1 to be function of u, v, and K_d. Let's denote it F,*

$$F(u,v,K_d) = \frac{1}{2}\left(u + v + K_d - \sqrt{(u + v + K_d)^2 - 4uv}\right). \tag{2.16}$$

Let $c > 0$ be arbitrary constant. Then

$$F(c\cdot u, c\cdot v, c\cdot K_d) = c \cdot F(u, v, K_d).$$

This means that if we want to scale concentrations in our vax reaction scenario, we have to scale the dissociation constant as well. It is not surprising since based on (2.3) K_d has a dimension of concentration.

Proposition 2.1.6. *Let u, v > 0 be fixed values. Let's consider F defined in (2.16) to be function of K_d. Then F is decreasing on interval <0, +∞).*

Proof. Let's first assume $u \neq v$. We have

$$F'(K_d) = \frac{1}{2}\left(1 - \frac{u + v + K_d}{\sqrt{(u + v + K_d)^2 - 4uv}}\right).$$

By the proof of claim 2.1.2 in our setting we see that the expression under the square root in the denominator is always positive. Further,

$$\sqrt{(u + v + K_d)^2 - 4uv} < \sqrt{(u + v + K_d)^2} = |u+v+K_d| = u + v + K_d.$$

Thus the fraction is greater than one and the derivative is negative.

Let now $u = v$. In this case

$$F(K_d) = u + \frac{K_d}{2} - \frac{1}{2}\left(\sqrt{4uK_d + K_d^2}\right). \tag{2.17}$$

First we show that for each $K > 0$, $F(0) > F(K)$: From (2.17) we see that $F(0) = u$ and

$$F(0) - F(K) = \frac{1}{2}\left(-K + \sqrt{4uK + K^2}\right)$$

is obviously positive.
Next, F is decreasing on $(0, +\infty)$, from (2.17):

$$F'(K_d) = \frac{1}{2}\left(1 - \frac{2u + K_d}{\sqrt{4uK_d + K_d^2}}\right). \tag{2.18}$$

We have

$$2u + K_d = \sqrt{(2u+K_d)^2} = \sqrt{4u^2+4uK_d+K_d^{\,2}} > \sqrt{4uK_d+K_d^{\,2}}.$$

Thus we see that the fraction in (2.18) is greater than one and the derivative is negative. □

Summing up in terms of equilibrium (r-)concentrations, for $T_L,\ T_{\lambda(L)} > 0,\ K_d \geq 0$

$$[\chi(L)] \leq min(T_L, T_{\lambda(L)})$$

(which we already knew from (2.6)), the equality holds for $K_d = 0$ (2.15), and the sharp inequality is valid for $K_d > 0$. With increasing K_d the resulting concentration of the product $\chi[(L)]$ decreases, leaving more reactants L and $\lambda(L)$ in unreacted form. For the practice of creating particular models we can perceive the zero dissociation case as a kind of asymptotic scenario with regard to the dissociating reaction, an easily understandable and usable building block.

Kinetics of decays. Spontaneous decay and membrane decays are based on reaction of form $S \rightarrow H$, where S is a substance undergoing decay and H is a product of the decay. Rate of given individual reaction $Rate_{reac}$ will be

$$Rate_{reac} = k_{reac} \cdot [S],$$

where k_{reac} is the rate constant of the reaction, parameter from interval $\langle 0, 1)$. When $k_{reac} \in (0, 1)$ this gives an exponential decay of S. For $k_{reac} = 0$ the decay doesn't occur.

For spontaneous decay of freely diffusible substance L, we have reaction $L \rightarrow Z$. Let k_{sd} be the rate constant for the reaction. Each $L \in Lv \cup X^{\check{}}$ will have its own rate constant.

Let $(A, V, X) \in Vaxes$. Let A^p, V^p, A^m, V^m, X^A, X^V, X^{AV} be forms of A, V, X with regard to membrane anchoring as defined in paragraph Membrane anchoring and receptors in section 2.1.1.

Receptor internalization for A^m is seen as reaction $A^m \rightarrow W$, $W \notin Lv \cup X^{\check{}}$, having rate constant k_{ri}^A. Regarding V^m, we will understand this analogically as reaction $V^m \rightarrow W$ with rate constant k_{ri}^V. For substance X, we will have following reactions: $X^A \rightarrow W$, $X^V \rightarrow W$, $X^{AV} \rightarrow W$, all the three having the same rate constant k_{ri}^X.

Membrane enzymatic activity on A is a reaction $X^V \rightarrow V^m$, let it have rate constant k_{ma}^A. Membrane enzymatic activity on V is a reaction $X^A \rightarrow A^m$, let it have rate constant k_{ma}^V.

Let k_{rri}^A, k_{rri}^V be parameters of raw receptor internalization of A and V respectively, both being from interval $<0, 1)$. There will be following set of reactions: $A^m \rightarrow Z \notin Lv \cup X^{\check{}}$ with rate constant k_{rri}^A, $V^m \rightarrow Z$ with rate constant k_{rri}^V, $X^A \rightarrow V^p$ with rate constant k_{rri}^A, $X^V \rightarrow A^p$ with rate constant k_{rri}^V. Further there will be reaction $X^{AV} \rightarrow Z$ with rate constant $min(k_{rri}^A, k_{rri}^V)$. If $k_{rri}^A > k_{rri}^V$ then there will be reaction $X^{AV} \rightarrow V^m$ with rate constant $k_{rri}^A - k_{rri}^V$, otherwise there will be reaction $X^{AV} \rightarrow A^m$ with rate constant $k_{rri}^V - k_{rri}^A$.[9]

Reaction time scales. When comparing vax reactions and decays, we will suppose vax reactions to be "much faster" than decays and diffusion as well, assuming that equilibrium of a vax reaction is reached in negligible time. Based on this, we will not be considering rate constants k_f, k_r in our model world, but only dissociation constant K_d with regard to corresponding vax reaction. However, for membrane – environment interactions where a free diffusible ligand is bound to its receptor, we will still allow the ligand to take part in diffusion and undergo spontaneous decay. This will make it possible for our cells to be scanning concentrations in their surroundings without influencing these processes, and generally prevent the cells from cumulating ligands on their receptors.

Putting things together. We will synthesize reaction types and kinetics as follows: Let's denote the number of vaxes *NumVaxes* (= $|A^{\check{}}|$). Each vax reaction will have its own dissociation constant K_d^j, $j \in \{1, ..., NumVaxes\}$, $K_d^j \geq 0$. For each $L \in Lv$ there will be rate constant k_{ma}^L of membrane enzymatic activity on L, and parameter k_{rri}^L of raw receptor internalization of L if *UseReceptorInternalization* is *false*. If receptor

9 Products V^m, A^m of the last two reactions will be anchored to the membrane of the same cell as they were when being part of X^{AV}.

internalization is being used, we will have its rate constant k_{ri}^S for each $S \in Lv \cup X$. Finally, we will have rate of spontaneous decay k_{sd}^S for each $S \in Lv \cup X$.

2.2 Environment and discretization

2.2.1 Environment components

Lattice. As we have outlined in the beginning of the chapter, the space of the environment of the model world is formed by a 2D lattice. Panes of the lattice have square shape and the lattice is uniform, i. e. all panes have the same size. We will regard the length of the side of a pane to be unit of distance in the model world. The lattice has rectangular shape with its dimensions as parameters. By position in the lattice, or shortly position, we will mean a two-dimensional vector *(i, j)* with nonnegative integer components. The components denote indices of a pane in the lattice viewed as a matrix of panes where *i* denotes *i*-th column, *j* denotes *j*-th row, with both numberings starting from *0*. For a pane *P*, *LatticeIndices(P)* denotes position of *P* in the lattice. Let's consider panes not occupied by a cell (cf. next paragraph). We will think of such panes as being able to contain substances from $Lv \cup X$. Within a pane, concentration of every substance is regarded to be constant over the area of the pane. After we derive formulas for pane – membrane interactions, we will consider for each vax $(A, V, X) \in Vaxes$ the r-concentrations T_A and T_V (cf. (2.4), (2.5)) to be held in panes (being constant over the area of the pane), where individual concentrations of A, V and X are computed from T_A and T_V if (where) needed.

Cells in the lattice and membrane elements. Each cell in the model world has its shape occupying one or more panes in the lattice. Shapes of cells cannot change, however, cells can move. Formally, let *Sh* be a set of two-dimensional vectors with integer nonnegative components, which will represent a shape of a cell for us. Let *Pos* be a position in the lattice. Let $Oc = \{P \mid P \text{ is a pane in the lattice, } LatticeIndices(P) = Z + Pos,\ Z \in Sh\}$. *Oc* denotes a set of panes occupied by the cell. According to intuition, for a cell we will allow only such positions *Pos* that all its occupied panes are in the lattice. Also, a pane can be occupied by at most one cell, i. e. sets *Oc* for all cells must be mutually disjoint. Shapes of cells are parameters in particular models.

The interior of a cell is uninteresting for us from the point of view of the environment, there is no reaction-diffusion modeling there.

We will regard the boundary of a cell to form a membrane. Membrane is viewed as a set of membrane elements [1]. Membrane element consists of a border segment of a pane that is occupied by the cell, where the segment is either part of a side of the rectangle bounding the whole lattice, or it is part of boundary of another

pane that is not occupied by the same cell. Membrane elements can contain receptors. We understand receptor amounts as real quantities. We will define membrane element as a triple *(σ, v, R)*, where *σ* is a segment fulfilling the conditions given above, *v* is a unit normal to *σ* pointing outwards from the cell of concern, and *R* is a $|Lv|$ dimensional vector of amounts of receptors of individual kinds[10]. Existing membrane element in given time instant is uniquely determined by its segment and normal. We will assume that the distribution of membrane element receptors of each kind along the corresponding segment is uniform. In the following we will often use the term 'membrane element' in sense of the corresponding segment. Also, by telling that a pane is adjacent to a membrane element we will mean that the segment of the element forms one of the sides of the pane.

Cells can secrete ligands over membrane elements to neighboring unoccupied panes.

Environment boundary. Boundary of our environment consists of two logical partitions. The first are the four sides of the lattice rectangle minus their subsegments being (currently) parts of cell membranes. Let's call this partition a lattice boundary. The other partition are membrane elements facing the panes of the lattice unoccupied by cells.

On the lattice boundary the model world will allow either (only) homogeneous Dirichlet condition or (only) homogeneous Neumann condition for all substances in particular model. All of the models presented in this thesis use the zero-flux condition. We will further assume this one to hold without mentioning.

Membranes of cells are regarded impermeable for all substances, so we have the zero-flux condition on the boundary partition formed by membrane elements as a baseline. However, this is generally altered by production of ligands by cells and by membrane decays. As we will describe in detail later, the influence of receptors on the ligand composition of adjacent panes is reduced to membrane enzymatic activity and receptor internalization.

Time. We will call a time discretization quantum in our model world a step or a simulation step[11]. The simulation step is regarded to last for unit time. We will assume that arbitrary vax reaction reaches its equilibrium in time negligible in comparison with one step. The same holds for a vax reaction parallel on pane – membrane interface, that will be defined in the next paragraph.

10 Amount of receptors of particular kind is unterstood as the total amount disregarding receptor occupancy.

11 Simulation step corresponds to one step of the discrete simulation in the Virtual Laboratory.

2.2.2 Membrane interactions

Pane – membrane interactions. In this section we will define an analogy of vax reaction on a free pane surrounded by one or more membrane elements. If substances *A*, *V*, and *X* form a vax *(A, V, X) ∈ Vaxes,* we will distinguish whether *A* and *V* are in membrane anchored form or in a free diffusible form, as we did in paragraph Membrane anchoring and receptors in section 2.1.1. Regarding the forms of product *X*, we will only need three of them: Free, membrane-anchored by its *A* part, and membrane-anchored by its *V* part. Thus we have got in total seven kinds of substances. (Cf. Fig. 2.1.) A straightforward approach to build our interaction scenario would be to construct an overall reaction scheme involving all individual reactions, derive equations for equilibrium concentrations of individual substances and solve this system of equations. However, we will introduce kind of simplified setting which would be not too difficult to understand, follow our purposes, and which would be readily usable as an intermediary building block in our model world. Particularly we have following assumptions and requirements:

1. We will assume that *A* and *V* are not both present in a free diffusible form and as receptor kinds (disregarding reacted and unreacted forms) simultaneously in our pane and surrounding membrane elements. At least one of these substances is either only present as a receptor kind or it is only a free ligand or it is not present in the pane and its adjacent membrane elements at all.[12] We will see that using this assumption we don't have to construct a complex reaction scheme and we will be able to employ vax reactions in a nearly direct way.
2. If there are any occupied receptors of kind *A* or *V* before our reaction, we will assume them as unoccupied, making their receptor kinds counterparts bound in this way freely diffusible, capable to react with the freely diffusible *A*, *V,* and *X* that have been in the pane before. Now we will assume a vax reaction among the free diffusible substances, where the (now all unoccupied) receptors play a role of passive scanners that don't alter the resulting equilibrium concentrations of the free diffusible *A*, *V* and *X*.
3. The information about resulting receptor occupancy[13] must be provided as though the vax reaction in the pane and adjacent membrane elements passed without limitations. 1. still holds but we will not assume 2 when evaluating this information.

Generally, computation according to 3. will not provide equilibrium concentrations of *A*, *V*, and *X* fulfilling 2. When computing the resulting concentrations in our scenario, we will take free diffusible *A*, *V*, and *X* from a scheme obeying 2. and the

12 All models presented in this thesis fulfill this assumption and we will generally suppose that models obey this premise.
13 Amounts of occupied and unoccupied receptors of given kinds.

rest from another scheme obeying 3. In the model world, receptor occupancy provides information for cells, membrane enzymatic activity and receptor internalization. Environmental *A*, *V*, and *X* participate in spontaneous decay and diffusion, the first two can undergo membrane enzymatic activity and be targeted by receptor internalization. Thus the only points we have to resolve are membrane enzymatic activity and receptor internalization. This will be done later. Generally spoken, our setting separates measurements from processes, so that measurements don't influence processes. This will, among others, allow cell membranes to form relatively "nice" boundary conditions from the point of view of the environment. We will now specify the scenario.

Let *(A, V, X)* ∈ *Vaxes*. Let's consider a compartment containing solution of substances with uniform concentrations, bounded by a membrane containing receptors facing the compartment. Let A^p, V^p, X^p, A^m, V^m, X^A, X^V be forms of substances *A, V, X* defined in paragraph Kinetics of decays in section 2.1.2. The situation is sketched in Fig. 2.1. As we have by (2.7), after a vax reaction passed, the product concentration depends on only total amounts of reactant substances in reacted and unreacted form that entered the reaction. In analogy with (2.4), (2.5) we will introduce T_V^p as the total amount of *V* in reacted and unreacted form that is or may become freely diffusible, as

$$T_V^p = [V^p] + [X^p] + [X^A] .$$

Then we will denote T_V^m the total amount of *V* that must be anchored in the membrane,

$$T_V^m = [V^m] + [X^V] .$$

Analogically for *A* let

$$T_A^p = [A^p] + [X^p] + [X^V] ,$$

$$T_A^m = [A^m] + [X^A] .$$

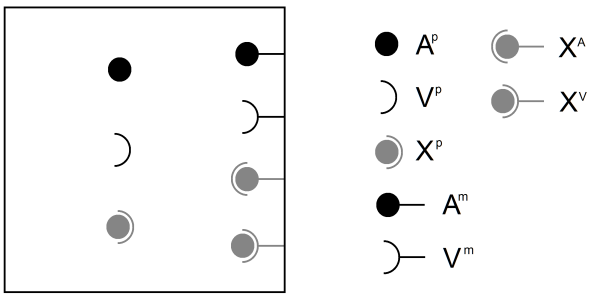

Figure 2.1: Vax substances in pane – membrane interactions.

In accord with section 2.1 let $[S_1]$ denote a concentration (amount) of substance S after our reaction it is involved in passed. Let us assume a pane not occupied by a cell, surrounded by one or more membrane elements.

First, we will describe computation of resulting concentrations of free diffusible A, V and X when considering requirement 2. and disregarding requirement 3. In this case, let $[A^p_{ps}]$, $[V^p_{ps}]$, and $[X^p_{ps}]$ be the resulting concentrations of free diffusible A, V, and X respectively[14]. We will define them as

$$[X^p_{ps}] = fxvax(T^p_A, T^p_V), \tag{2.19}$$

$$[A^p_{ps}] = T^p_A - [X^p_{ps}], \tag{2.20}$$

$$[V^p_{ps}] = T^p_V - [X^p_{ps}]. \tag{2.21}$$

Here expressions (2.19), (2.20), (2.21) are analogies of (2.7), (2.4), and (2.5) respectively. If we assume that before applying this scheme $[X^A] = [X^V] = 0$, i. e. there are no membrane-bound products, there is $[A^p_{ps}] \equiv [A^p_1]$, $[V^p_{ps}] \equiv [V^p_1]$, and $[X^p_{ps}] \equiv [X^p_1]$, when only considering reaction $A^p + V^p \leftrightarrow X^p$, taking $[X^p_1]$, $[A^p_1]$, and $[V^p_1]$ from (2.7), (2.4), and (2.5) respectively. We will call this method of determining free diffusible A, V and X *pane separation*.

Let now $L \in Lv$, $\Lambda = \lambda(L)$, $X = \chi(L)$. We will describe computation of occupancy of receptors formed by substance L, when considering requirement 3. and disregarding requirement 2. Let $[X^L_{rd(L)}]$ be the (resulting) occupancy of receptors formed by L under these considerations[15]. Let n be the number of membrane elements adjacent to to our pane. Let $[{}^iX^L_{rd(L)}]$ be the occupancy of the i-th membrane element, $i = 1, .., n$. We have

$$[X^L_{rd(L)}] = \sum_{i=1}^{n} [{}^iX^L_{rd(L)}]. \tag{2.22}$$

Let

$$[X_{rd(L)}] = fxvax(T^p_L + T^m_L, T^p_\Lambda). \tag{2.23}$$

Let's denote $T_{L,rd(L)} = T_L{}^p + T_L{}^m$ the total amount of L[16] entering the reaction considered by (2.23), let $T_{\Lambda,rd(L)} = T_\Lambda{}^p$. Seeing substances as in unreacted forms only, before the reaction, we are considering Λ^m not to participate in the reaction, as though its amount was zero. Let

14 The subscript *ps* stands as a scortcut for *pane separation* indicating this computation method – cf. end of paragraph.

15 Here *rd(L)* in the subscript indicates this our method of computation - reaction decoposition - where occupancy of receptors formed by L is of interest.

$$[X_{rd(L)}] = [X^{L}_{rd(L)}] + [X^{p}_{rd(L)}], \tag{2.24}$$

where $[X^{p}_{rd(L)}]$ is the concentration of diffusible X after the reaction considered by (2.23) passed. We assume that Λ reacts evenly with all L, regardless whether L is free or membrane bound, so that the product is distributed in the pane and in the individual membrane elements in the same rate as there was L[16] before the reaction[17]. Formally, we will put

$$[X^{p}_{rd(L)}] = [X_{rd(L)}] \cdot \frac{T^{p}_{L}}{T_{L,rd(L)}},$$

$$[{}^{i}X^{L}_{rd(L)}] = [X_{rd(L)}] \cdot \frac{{}^{i}T^{m}_{L}}{T_{L,rd(L)}}, \quad i = 1,..,n. \tag{2.25}$$

Here ${}^{i}T_{L}{}^{m}$ denotes the total amount of membrane-anchored L[18] in the i-th membrane element adjacent to the pane, ${}^{1}T_{L}{}^{m} + {}^{2}T_{L}{}^{m} + ... + {}^{n}T_{L}{}^{m} = T_{L}{}^{m}$. If $T_{L,rd(L)}$ is zero, then all the fractions in (2.25) are regarded to be zero. Let $[L^{m}{}_{rd(L)}]$ be the total amount of unoccupied receptors formed by L after reaction regarded by (2.23) passed. Let accordingly $[{}^{i}L^{m}{}_{rd(L)}]$ denote $[L^{m}{}_{rd(L)}]$ restricted to the i-th membrane element. We will put

$$[{}^{i}L^{m}_{rd(L)}] = {}^{i}T^{m}_{L} - [{}^{i}X^{L}_{rd(L)}], \quad i = 1,..,n.$$

We will call this method of computing $[X^{L}{}_{rd(L)}]$ and $[L^{m}{}_{rd(L)}]$ (i. e. $[X^{A}{}_{rd(A)}]$, $[A^{m}{}_{rd(A)}]$, $[X^{V}{}_{rd(V)}]$, and $[V^{m}{}_{rd(V)}]$ when considering vax *(A, V, X)*) a *reaction decomposition.*

We can check quite easily that under assumption in 1. *reaction decomposition* works correctly: For simplicity we will suppose that there is only one adjacent membrane element to the pane, having index *1* say. For more elements the extension is straightforward.

Let's consider computation of $[X^{L}{}_{rd(L)}]$. If receptors formed by L are missing, there can be nothing bound on it and $[{}^{1}X^{L}{}_{rd(L)}]$ should be zero. Indeed, if there is $[L^{m}] = [X^{L}] = 0$, then $T_{L}{}^{m} = 0$, which means that ${}^{1}T_{L}{}^{m} = 0$. According to the computation scheme $T_{L,rd(L)} = T_{L}{}^{p}$. If $T_{L,rd(L)}$ is zero, then (2.25) is by definition zero for all i, thus $[{}^{1}X^{L}{}_{rd(L)}] = 0$. If $T_{L,rd(L)}$ is nonzero, then $[{}^{1}X^{L}{}_{rd(L)}] = 0$ since ${}^{1}T_{L}{}^{m} = 0$. Let's now consider the case where receptors formed by Λ are missing. In this case Λ can be present only in diffusible form and binds to L which is in either form. But this is

16 In reacted and unreacted form.

17 It is easy to prove this intuitive assumption as a fact, for one membrane element starting with two reactions: $L^{p} + \Lambda^{p} \leftrightarrow X^{p}$ and $L^{m} + \Lambda^{p} \leftrightarrow X^{L}$, supposing both have the same dissociation constant.

18 In reacted and unreacted form.

exactly how our computation scheme was constructed, when we took $T_{L,rd(L)} = T_L^p + T_L^m$, $T_{\Lambda,rd(L)} = T_\Lambda^p$. We ignored $T_\Lambda^m = [\Lambda^m] + [X^\Lambda]$ and now $[\Lambda^m] = [X^\Lambda] = 0$. As a next case to check we make the assumption of L in free form generally missing. Here membrane-anchored Λ has no counterpart to react with thus there is only a reaction between free Λ and receptors formed by L there, meaning that there is either no product (if L is missing at all or Λ is missing in free ligand form), or the product is all anchored to membrane via its L part. In our scenario, by setting $T_{\Lambda,rd(L)} = T_\Lambda^p$ we are only taking the free Λ. No free L means $T_L^p = 0$ so $T_{L,rd(L)} = T_L^m$. We have also $T_L^{m1} = T_L^m$ by our assumption. If $T_{L,rd(L)} = 0$ then $[{}^1X^L_{rd(L)}] = 0$ since (2.25) is by definition zero for all i. If $T_{L,rd(L)} \neq 0$ then ${}^1T_L^m / T_{L,rd(L)} = 1$ giving $[{}^1X^L_{rd(L)}] = [X^L_{rd(L)}]$. The last case is the situation where Λ in free form is generally missing. In this case membrane-bound L has no counterpart to react with, so $[{}^1X^L_{rd(L)}]$ should be zero. In the scheme we have $[\Lambda^p] = [X^p] = [X^L] = 0$, thus $T_\Lambda^p = 0$, followingly $T_{\Lambda,rd(L)} = 0$. By (2.23) $[X_{rd(L)}] = 0$. If $T_{L,rd(L)} = 0$ then $[{}^1X^L_{rd(L)}] = 0$ by definition. Otherwise, $[{}^1X^L_{rd(L)}] = 0$ since $[X_{rd(L)}] = 0$.

Membrane – membrane interactions. In our environment two cells can touch each other. As in the previous paragraph, let substances A, V, X form a vax $(A, V, X) \in Vaxes$. Let Me^1, Me^2 be two distinct membrane elements sharing the same segment. In this case we will consider that the two cells containing these elements touch each other by these elements. Let A^1, V^1 be substances A and V respectively, anchored in Me^1. Let similarly A^2, V^2 be substances A and V respectively, anchored in Me^2. Then there will be two vax reactions: $A^1 + V^2 \leftrightarrow X^{1,2}$ and $A^2 + V^1 \leftrightarrow X^{2,1}$, both with dissociation constant K_d of reaction $A + V \leftrightarrow X$. By means of vax reactions on adjacent membrane elements touching cells can perceive substances bound in membranes of their neighbors. From the point of view of a cell scanning substances in its surroundings, it is insignificant whether a substance the cell feels via its receptors' occupancy is membrane-bound (receptors of another adjacent cell) or freely diffusible (ligand). The cell just feels the “signal”.

Discussion on design of pane-membrane interactions. When creating a model one must deal with making simplifications and assumptions. This is of course true in constructing our model world, which is sort of meta-model, a generic environment for creating various particular models motivated by different theoretical or biological impulses. Regarding the vax reactions, these play the role of a modeling tool for us, kind of a building block. At the entry level, as described in section 2.1, they represent particular parametrizable reaction scheme that can be easily understood. We want a pane (generally) surrounded by membrane elements to be another building block, not too difficult to understand and quite easily usable to construct other entities.

Although being built from simpler blocks, it should still be an expression unit with not too complicated behavior.

By means of receptors on membrane elements our cells (can) basically do two things on substances in the local surrounding environment: Scan their concentrations[19] and make them disappear. Also, the environmental substances can disappear by spontaneous decay and they can be transported by diffusion. By means of *pane separation* we make the membrane a "device" that neither accumulates ligands from the environment nor prevents them to participate in the environmental processes, as anticipated. If there are no membrane enzymatic activity and no receptor internalization, the process of concentration scanning by cells (via their receptors) doesn't alter the vax reaction in the pane.

If we think generally of a receptor–ligand interaction, we may consider freely diffusible ligand molecules to react with[20] membrane–anchored receptor molecules. (See Fig. 2.2 (a).) If we add the ligand substance to a membrane in a membrane–anchoring form and assume that this form will not react with the receptors, the original receptor–ligand interaction will remain unchanged. (Cf. Fig. 2.2 (b).) If we return to our starting receptor–ligand scenario and add the receptor (kind) substance in a free diffusing form, the ligand will be binding to both forms, as sketched in Fig. 2.2 (c). From the point of view of the original scenario, this setting may be viewed as a kind of inhibition. If we want to decrease the amount of receptor-bound ligand, we will add the receptor substance in a free form and it will attract part of the ligand, so that the resulting receptor occupancy will decrease.

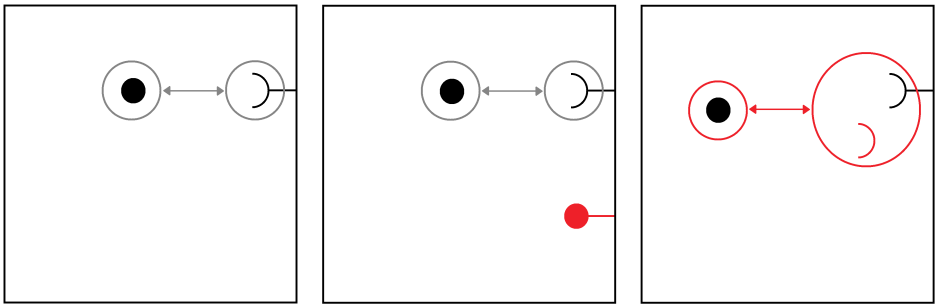

Figure 2.2: Supported extensions of basic receptor-ligand interaction: Basic interaction (a). Adding ligand substance in receptor form (b). Adding receptor substance in ligand form (c).

19 Concentration scanning in this sense is rather getting signal by cells from the occupancies of their receptors. E. g. receptor saturation may occur, where the real outer concetration is "beyond the measurable range". Interpretation of the receptor signal, if needed, is up to particular model.
20 initially unoccupied

There remains the general scenario where we add the receptor (kind) substance in a free form and the ligand substance in a membrane-bound form, thus getting both substances in both forms (scenario not shown). From the point of view of having simple receptor-ligand interaction there doesn't seem to be enough straightforward reasoning for such a scheme. By contrary, it looks to obfuscate this interaction and make things rather complicated. When constructing our model world, we have decided not to support this case.[21] We have limited the space of combinations within the conceptual unit of a pane surrounded by membrane elements, but left it relatively transparent.

2.2.3 Diffusion-reaction scheme

In our model world, all substances (elements of $Lv \cup X^{\smile}$) have the same diffusion coefficient $D \geq 0$. When focusing on the interior of the environment, there are three processes influencing concentrations of substances: vax reactions, diffusion and spontaneous decay. From what was said before it is obvious that all chemical interactions of a substance are defined on the substance alone or within the vax the substance belongs to. We will thus concentrate on a single vax.

Let $(A, V, X) \in Vaxes$. Let k_{sd}^{A}, k_{sd}^{V} and k_{sd}^{X} be rate constants of spontaneous decay of A, V, and X respectively. As we know, equilibrium concentrations of the vax components depend on r-concentrations T_A and T_V (cf. (2.7), (2.8), (2.9)). We will take the r-concentrations as basic notions, computing diffusion and decay for them. When determining concentrations in the environment, we will consider following couple of equations[22,23]:

$$\frac{\partial T_A}{\partial t} = D\Delta T_A - \alpha_T(A, T_A, T_V), \tag{2.26}$$

$$\frac{\partial T_V}{\partial t} = D\Delta T_V - \alpha_T(V, T_V, T_A), \tag{2.27}$$

where

$$\alpha_T(L, u, v) = k_{sd}^{L} \cdot flvax(u, v) + k_{sd}^{\chi(L)} \cdot fxvax(u, v)\,. \tag{2.28}$$

Here $T_A = T_A(x, t)$, $T_V = T_V(x, t)$, where x represents space variables, t represents time, Δ is Laplacian in space variables. Further, $\alpha_T(L, u, v)$ is the decay rate of T_L due to

21 In the Virtual Laboratory defining models that can lead to this scenario is not prevented by any checks. It is left upon the modeller to ensure adherence to this premise within particular models, or to have enough justification to break it, when accepting the setting of the model world.

22 Forming a base for discretization.

23 Boundary conditions for these equations will be given in the next paragraph. Initial conditions are not important for us here, we only assume that the initial T^{A}, T^{V} are nonnegative. Initial values of r-concentrations T^{A} and T^{V}, seen as "concentraions of unreacted ligands", are given in discrete form in the environment at the level of particular models.

spontaneous decays, $L \in Lv$, if $T_L = u$ and $T_{\lambda(L)} = v$. Functions *flvax* and *fxvax* are defined in (2.11), (2.12) respectively and we are considering dissociation constant K_d of reaction $L + \lambda(L) \leftrightarrow \chi(L)$ for them. As we see, our scheme doesn't hold individual vax-equilibrium concentrations of A, V, and X explicitly. When we want to determine spontaneous decay of any of regarded substances, we compute the actual "input" concentration "on the fly". Results of spontaneous decays are composed back to the (time) derivatives of the (cumulative) r-concentrations T_A and T_V.

Membrane decays and boundary conditions. We have been discussing the structure of boundary regarding our lattice in paragraph Environment boundary in section 2.2.1. In order to formulate boundary conditions for (2.26), (2.27), we will assume the environment boundary as a geometrical object, seeing receptor amounts in (the original) membrane elements as concentrations[24]. Discrete pane – membrane interactions we have established before will be then seen as part of discretization of our boundary conditions, as we will describe later.

Let C be a cell, let M be part of its membrane facing the free environment. Let $(A, V, X) \in Vaxes$, let T_A, T_V be the diffusing r-concentrations regarded in (2.26), (2.27). We will write the boundary conditions on the part of the boundary of our environment corresponding to M as

$$D \cdot \frac{\partial T_A(x,t)}{\partial v} = P(C,A,t) - (k_{ma}^A + k_{ri}^X) \cdot [X^V](T_A, T_V, [R^V]), \quad (2.29)$$

$$D \cdot \frac{\partial T_V(x,t)}{\partial v} = P(C,V,t) - (k_{ma}^V + k_{ri}^X) \cdot [X^A](T_A, T_V, [R^A]), \quad (2.30)$$

where

$$[X^V](T_A, T_V, [R^V]) = fxvax(T_A, T_V + [R^V]) \cdot \frac{[R^V]}{T_V + [R^V]}, \quad (2.31)$$

$$[X^A](T_A, T_V, [R^A]) = fxvax(T_V, T_A + [R^A]) \cdot \frac{[R^A]}{T_A + [R^A]}.$$

Here $x = (x_1, x_2)$ lays on M, $\partial T_A(x,t)/\partial v$ is spatial derivative of T_A in direction of the outer normal of M at x with regard to C in time t. $P(C, A, t)$ is production of substance A by cell C per unit membrane length in time t. Cell productions are determined based on zygotic graph, as it will be described later. Further, k_{ma}^A is rate constant of membrane enzymatic activity on A, k_{ri}^X is rate constant of receptor internalization of X. For the second relation analogically. Next, $[X^V]$ is local (membrane) concentration of receptors formed by substance V that are regarded as

24 Regarding all receptors as being unoccupied.

occupied by A for the purposes of determination of degradation / removal at membrane. I. e. $[X^V]$ represents local concentration of A regarded as bound to its receptors on the membrane, a quantity forming a "base" for degradation by membrane enzymatic activity and for removal by receptor internalization. Next, $[R^V]$ denotes membrane concentration of receptors formed by substance V. Function *fxvax* is defined in (2.11). The fraction on the right in (2.31) is the ratio of product being regarded in the bound receptor form. If the denominator were zero, we will regard the fraction to be zero. For $[X^A]$ the situation is analogical.

Diffusion – reaction discretization. In order to discretize (2.26) and (2.27) in our lattice, we will use finite volumes approach [3]. Let $L \in Lv$. We can rewrite (2.26), (2.27) as

$$\frac{\partial T_L(x,t)}{\partial t} - D \cdot \operatorname{div}(\nabla T_L) + \alpha_T(L, T_L, T_{\lambda(L)}) = 0,$$

$$\int_K \frac{\partial T_L(x,t)}{\partial t}\, dx - D \int_{\partial K} \nabla T_L \cdot v \; ds + \int_K \alpha_T(L, T_L, T_{\lambda(L)})\, dx = 0, \qquad (2.32)$$

where x represents the space variables, K is a control volume – a (unoccupied) pane of our lattice; v is the outer unit normal to ∂K. Let k be a constant time discretization step. Writing (2.32) at time $t_n = nk$, n is a nonnegative integer, and discretizing the time partial derivative by Euler explicit scheme we have a time discretized version (approximation) of T_L which fulfills:

$$\frac{1}{k}\int_K T_L^{(n+1)}(x) - T_L^{(n)}(x)\, dx - D \int_{\partial K} \nabla T_L^{(n)} \cdot v \; ds + \int_K \alpha_T(L, T_L^{(n)}, T_{\lambda(L)}^{(n)})\, dx = \qquad (2.33)$$

Regarding space discretization, we will consider cell-centered discrete unknowns ${}^K T_L^{(n)}$, where K belongs to the unoccupied panes of our lattice. Let E_K be the set of edges included in pane K. We can write the second integral from (2.33) as

$$-D \int_{\partial K} \nabla T_L^{(n)} \cdot v \; ds = -D \sum_{\sigma \in E_K} \int_\sigma \nabla T_L^{(n)} \cdot v \; ds.$$

We will approximate each flux from the sum

$$\int_\sigma \nabla T_L^{(n)} \cdot v \; ds$$

by finite difference approximation as

$$F_{L,K,\sigma}^{(n)} = h \cdot \frac{{}^Q T_L^{(n)} - {}^K T_L^{(n)}}{l}, \qquad (2.34)$$

where h is the length of segment σ and l is the distance between the centers of of the two adjacent panes K and Q that share σ as a common segment. As space discretization of (2.33) we have:

$$\frac{h^2}{k}\left({}^{K}T_L^{(n+1)} - {}^{K}T_L^{(n)}\right) - D\sum_{\sigma\in E_K} F_{L,K,\sigma}^{(n)} + h^2\cdot\alpha_T\left(L, {}^{K}T_L^{(n)}, {}^{K}T_{\lambda(L)}^{(n)}\right) = 0.$$

Since the panes in our model world are squares with unit side length, we have $l = h = 1$, k will correspond to one step, that is a unit time: $k = 1$. So we get explicit formula for our discretized T_L:

$${}^{K}T_L^{(n+1)} = {}^{K}T_L^{(n)} + D\sum_{\sigma\in E_K} F_{L,K,\sigma}^{(n)} - \alpha_T\left(L, {}^{K}T_L^{(n)}, {}^{K}T_{\lambda(L)}^{(n)}\right). \qquad (2.35)$$

Let's express the difference ${}^{K}T_L^{(n+1)} - {}^{K}T_L^{(n)} = \delta(L, K, n)$. By (2.35) we have:

$$\delta(L, K, n) = D\sum_{\sigma\in E_K} F_{L,K,\sigma}^{(n)} - \alpha_T\left(L, {}^{K}T_L^{(n)}, {}^{K}T_{\lambda(L)}^{(n)}\right). \qquad (2.36)$$

Discretization of boundary conditions. As described in paragraph Environment boundary in section 2.2.1, we can have either zero concentration condition or zero flux condition on the lattice boundary. The latter condition is also a baseline for cell membranes being part of the environment boundary, i. e. when membrane enzymatic activity, receptor internalization and cell production are not considered.

For the homogeneous Dirichlet and homogeneous Neumann conditions we will assume as though there are fictive neighbors on the opposite sides of corresponding edges of panes at the boundary. Concentration in the fictive neighbor will be zero for the zero concentration boundary and it will be the same as in the regarded real pane for the no-flux condition. Note that for the for the hom. Neumann condition concentrations at the fictive neighbors are generally not unique for given fictive pane, but they are unique for each boundary pane edge, i. e. for each “flux implemented”.

Let K be an unoccupied pane, let $M(K)$ be the set of membrane elements adjacent to K, let $M(K) \neq \emptyset$. Let's consider boundary conditions expressed by (2.29) and (2.30) at membrane elements of $M(K)$. Taking our vax (A, V, X), let ${}^{q}[X^V]^{(n)}$ be discretized $[X^V]$ from (2.29), (2.31), at time $t_n = n$, n is a nonnegative integer, and at $q \in M(K)$. We will compute ${}^{q}[X^V]^{(n)}$, for each $q \in M(K)$ via *reaction decomposition*. (Cf. paragraph Pane – membrane interactions in section 2.2.2.) Let's consider (2.23). We will put there $L = V$, $\Lambda = A$, $T_V^p = {}^{K}T_V^{(n)}$, $T_A^p = {}^{K}T_A^{(n)}$,

$$T_V^m = \sum_{(\sigma, v, R)\in M(K)} R_V,$$

where R_V is the component of R corresponding to (receptor kind) V. By (2.25) we get ${}^q[X^V]^{(n)}$ for q as the i-th membrane element adjacent to K in chosen numbering. For ${}^q[X^A]^{(n)}$ the situation is analogical. Let $\delta_b(L, K, n)$ be the change of ${}^K T_L^{(n)}$, $L \in Lv$, (cf. (2.35)) in the $(n+1)$th step due to boundary conditions on $M(K)$. We have

$$\delta_b(L, K, n) = P(C, L, n+1) + \delta_r(L, K, n) . \tag{2.37}$$

Without loss of generality, there is

$$\delta_r(L, K, n) = -\left(k_{ma}^V + k_{ri}^X\right) \cdot \sum_{q \in M(K)} {}^q[X^A]^{(n)} \tag{2.38}$$

if $L = V$ and

$$\delta_r(L, K, n) = -\left(k_{ma}^A + k_{ri}^X\right) \cdot \sum_{q \in M(K)} {}^q[X^V]^{(n)} \tag{2.39}$$

if $L = A$. In (2.37), $P(C, L, n)$ is production of substance L by cell C per unit membrane length in the n-th step.

Conditions for parameter values. Now we will focus on constraints that will be laid on the diffusion coefficient D, parameters of spontaneous decays and parameters of decays relevant to boundary conditions at cell membranes. We can write Fick's first law of diffusion [4] as

$$J = -D \nabla C ,$$

where J is diffusive flux, D is diffusion coefficient and C is concentration of of the diffusing substance. The expression states that the vector of diffusive flux has direction that is opposite to the direction of concentration gradient that causes it and that it is directly proportional to the magnitude of this gradient. In our discretization we will require that within each step, every diffusive flux has the opposite direction than the concentration gradient that is the cause of the flux at the beginning of the step. Particularly, we will want that the flux goes from a pane with (initially) higher concentration to a pane with (initially) lower concentration. Thus obviously D has to be nonnegative, we have stated this at the beginning of this section. Further, we will denote (the discretized) concentration of substance C in pane K at the beginning of a step $C(K)$, let then $C^D(K)$ be concentration of C in K at the end of the step, when supposing that only diffusion among K and its neighbors took place in the step. Let's consider pane K with its unoccupied neighbors $Q_1, ..., Q_n$, let $n \geq 1$. Let Q be one of these neighbors such that $C(Q) \leq C(Q_i)$, $i = 1, ..., n$. Let further $C(Q) \leq C(K)$. Then we will require that $C^D(Q) \leq C^D(K)$. Similarly, for an unoccupied neighbor Q' of K such that $C(Q') \geq C(Q_i)$, $i = 1, ..., n$, where $C(Q') \geq C(K)$, we will want that $C^D(Q') \geq C^D(K)$. We see that in order to fulfill these conditions in general case there has to be

$$D \leq \frac{1}{n+1} . \qquad (2.40)$$

(In the worst case, all the neighbors will have the same concentration.) We also see that if some of the neighbors $Q_1,\ldots, Q_n$ were the fictive ones implementing either the zero-concentration condition or the zero-flux condition, (2.40) would be (generally) the same. Thus in our lattice we put requirement $D \leq 1/5$.

Next, we require that after all processes influencing concentrations in an unoccupied pane K within a step are applied, the resulting concentration of every substance will be nonnegative. Let $(A, V, X) \in Vaxes$ be a vax.

Let's first consider K not to be adjacent to cell membrane. When looking at (2.28) and reminding (2.12), we see that for each $L \in Lv$

$$\alpha_T(L, T_L, T_{\lambda(L)}) \leq \max(k_{sd}^L, k_{sd}^{\chi(L)}) \cdot T_L .$$

From (2.34) clearly

$$F_{L,K,\sigma}^{(n)} \geq -{}^K T_L^{(n)} ,$$

thus (2.35) gives

$${}^K T_L^{(n+1)} \geq {}^K T_L^{(n)} \left(1 - 4D - \max(k_{sd}^L, k_{sd}^{\chi(L)})\right) . \qquad (2.41)$$

When assuming ${}^K T_L^{(n)} \geq 0$, in order to have ${}^K T_L^{(n+1)} \geq 0$ we get conditions for our vax

$$\max(k_{sd}^A, k_{sd}^X) + 4D \leq 1 ,$$

$$\max(k_{sd}^V, k_{sd}^X) + 4D \leq 1 .$$

Let's now regard K to be adjacent to a membrane. When looking at (2.38) and the paragraph above, considering computation of ${}^m[X^V]^{(n)}$ for $m \in M(K)$ for our K, from (2.23), (2.24), (2.22) (*reaction decomposition*), and (2.14) we have

$$\sum_{m \in M(K)} {}^m[X^V]^{(n)} \leq {}^K T_A^{(n)} .$$

Thus from (2.37), (2.38) we can see that

$$\delta_b(A, K, n) \geq -{}^K T_A^{(n)} \cdot (k_{ma}^A + k_{ri}^X) , \qquad (2.42)$$

since, as we will state later, cell productions are nonnegative. Because K is adjacent to the boundary formed by a cell (membrane), there will be zero diffusive flux with at least one neighbor of K. Let's look at (2.41), considering now our pane K there and substance A in place of L. Let $\delta_{\text{in}}({}^K T_A^{(n)})$ be the change of ${}^K T_A^{(n)}$ in the $(n+1)$th step due to diffusion, spontaneous decay and the (potential) boundary conditions on the edges of K being part of the lattice boundary. We have

$$\delta_{\text{in}}\left({}^{K}T_{A}^{(n)}\right) \geq - {}^{K}T_{A}^{(n)}\left(3D + max\left(k_{sd}^{A}, k_{sd}^{X}\right)\right). \qquad (2.43)$$

Adding (2.42) and (2.43), in analogy with (2.41) we can write:

$${}^{K}T_{A}^{(n+1)} \geq {}^{K}T_{A}^{(n)}\left(1 - \left(k_{ma}^{A} + k_{ri}^{X}\right) - max\left(k_{sd}^{A}, k_{sd}^{X}\right) - 3D\right),$$

getting condition

$$k_{ma}^{A} + k_{ri}^{X} + max\left(k_{sd}^{A}, k_{sd}^{X}\right) + 3D \leq 1.$$

Analogically based on ${}^{K}T_{V}^{(n)}$ we have

$$k_{ma}^{V} + k_{ri}^{X} + max\left(k_{sd}^{V}, k_{sd}^{X}\right) + 3D \leq 1.$$

2.2.4 Cell movement

When introducing diffusion-reaction computation scheme, we were supposing the situation boundary geometry to be unchanging in time. However, as stated beforehand, we wish our cells to be able to move. In this paragraph we will describe how cell movement is included to the environment.

Every cell in every particular model has a speed, zero or nonzero, that determines its movement. We regard cell speeds as real vectors. If a cell encounters an obstacle, only such component of the speed will apply where given direction is not blocked by the obstacle. An obstacle may be another cell or the lattice boundary. The unit of speed in our model world is the length of pane side per step. We will only allow cell speed magnitudes ≤ 1. For each cell we are tracking its real position, a grid coordinate is the largest integer $\leq$ real coordinate. According to our setting, cell location grid coordinate can change at most by one in one simulation step[25]. If exactly one grid coordinate changed within a step, the cell will move by one pane in the lattice in corresponding direction within that step. We will call this the elementary movement. If both grid coordinates changed within one step, we will regard this as two consecutive elementary movements within the step. We will have two basic approaches how to deal with r-concentrations T_L, $L \in Lv$, in the panes in the surroundings of a cell that has performed elementary movement: *Infilling* and *flowaround*. Whether the former or the latter is used for a cell in particular model is being a parameter for given cell, unchanging in time. If a cell divides, this parameter is inherited by the daughter cells.

Infilling. In infilling, we will only determine r-concentrations in the panes that were occupied by the cell before the elementary movement and became free after it. Let's call them receiving panes. Let *C* be a cell that performed elementary movement in an arbitrary step of interest. Let *Rec* be a set of receiving panes of *C* for that elementary

25 If we don't consider divisions.

movement. Let *Ms* be the set of membrane elements *m* adjacent to panes in *Rec* before the elementary movement, where there was an unoccupied pane Q_m forming the other neighbor of *m*. Let $L \in Lv$. Then after the elementary movement there will be the same r-concentration T_L for all $P \in Rec$,

$$T_L = \frac{1}{|Ms|} \sum_{m \in Ms} {}^{Q_m}T_L ,$$

where ${}^{H}T_L$ is T_L in pane *H* before the elementary movement. If *Ms* is empty, we will put $T_L = 0$.

Flowaround. In flowaround, we will simulate advection in a virtual surroundings of a cell *C* that has performed elementary movement. Roughly speaking, the virtual surroundings will have rectangular shape of constant size, with stationary flow velocities provided as parameters, having these zero over the boundary of the rectangle. Cell *C* will be in the middle of the rectangle and there will be no other cells there, despite there might be some in the real surroundings. It is also possible that part of the virtual surroundings would be outside the environment grid. In places of the "real" objects and in the "outside" zones, we will set "hypothetical" concentrations of substances, based on known concentrations in the rest of the virtual surroundings. Then we will simulate advection. After advection is computed, resulting concentrations will be "copied" to the "real" surroundings, where corresponding panes exist and are not occupied by any cell. Situation is sketched in Fig. 2.4 (a).

Advection in flowaround. In this paragraph we will provide discrete formula describing advection for our flowaround. Let's start with linear transport equation with velocities $\boldsymbol{w}$:

$$\frac{\partial u(x,t)}{\partial t} + \operatorname{div}(\boldsymbol{w}u)(x,t) = 0,\ x \in \Omega,\ t > 0 \qquad (2.44)$$

$$u(x,0) = u_0(x),\ x \in \Omega,$$

where

$$\boldsymbol{w} \in C^1(\bar{\Omega},\bar{\Omega}),\ \boldsymbol{w} = 0 \ \ on \ \ \partial\,\Omega,\ u_0 \in L^{\infty}(\Omega).$$

We will consider Ω to be an interior of a rectangle formed by union of nonempty set of panes, seeing the panes as closed squares. Discretizing by finite volumes, proceeding in analogy with paragraph Diffusion – reaction discretization in section 2.2.3 and with introduction in [3], we have

$$\int_K \frac{\partial u(x,t)}{\partial t}\,dx + \int_{\partial K} \boldsymbol{w}(x,t)u(x,t)\cdot v\,ds = 0, \qquad (2.45)$$

for each K belonging to the panes forming $\bar{\Omega}$; v is the outer unit normal to ∂K.
For k being a constant time discretization step, writing (2.45) at time $t_n = nk$, n is a nonnegative integer, and discretizing the time partial derivative by Euler explicit scheme we have a time discretized version of u:

$$\frac{1}{k}\int_K u^{(n+1)}(x) - u^{(n)}(x)\,dx + \sum_{\sigma\in E_K}\int_\sigma \boldsymbol{w}(x, t_n)\, u^{(n)}(x)\cdot v\; ds = 0, \qquad (2.46)$$

where E_K is the set of edges included in pane K. For $\sigma \in E_K$ let

$$w_{K,\sigma}^{(n)} = \int_\sigma \boldsymbol{w}(x, t_n)\cdot v\; ds.$$

Let $u_K^{(n)}$ be cell-centered discrete unknowns of space discretization, where K belongs to the panes forming $\bar{\Omega}$. We will discretize each term of the sum in (2.46) as

$$F_{K,\sigma}^{(n)} = w_{K,\sigma}^{(n)}\, u_K^{(n)} \quad for \quad w_{K,\sigma}^{(n)} \geq 0\ ,$$

$$F_{K,\sigma}^{(n)} = w_{K,\sigma}^{(n)}\, u_Q^{(n)} \quad for \quad w_{K,\sigma}^{(n)} < 0\ .$$

Here Q is a neighboring pane to K with common edge σ. So we have a discretization scheme

$$\frac{h^2}{k}\left(u_K^{(n+1)} - u_K^{(n)}\right) + \sum_{\sigma\in E_K} F_{K,\sigma}^{(n)} = 0\ , \qquad (2.47)$$

$$u_K^{(0)} = \int_K u_0(x)\,dx$$

for each pane K being part of $\bar{\Omega}$ and for each nonnegative integer n. Further, h is the length of σ which is *1*. We will rewrite (2.47) as

$$u_K^{(n+1)} = u_K^{(n)} - k\cdot\sum_{\sigma\in E_K} F_{K,\sigma}^{(n)}\ . \qquad (2.48)$$

Relation (2.48) will form a base for computation of advection within an algorithm computing flowaround.

Flowaround algorithm. We will first introduce preliminary concepts. Let C be a cell. Let *Sh(C)* be shape of C as introduced in paragraph Cells in the lattice and membrane elements in section 2.2.1. Let

$$a_{lo} = \min_{(a,b)\in Sh(C)} a\ ,\ a_{hi} = \max_{(a,b)\in Sh(C)} a,\ b_{lo} = \min_{(a,b)\in Sh(C)} b\ ,\ b_{hi} = \max_{(a,b)\in Sh(C)} b\ .$$

Let $Width(C) = a_{hi} - a_{lo}$, $Height(C) = b_{hi} - b_{lo}$. We can see *Width(C)* and *Height(C)* as width and height of the bounding rectangle[26] of *C*. Let

$$Sh_0(C) = \{(a - a_{lo},\ b - b_{lo}) \mid (a,b) \in Sh(C)\}.$$

Let G_C be a rectangular lattice consisting of square panes of unit side length, with width $W_{GC} = Width(C) + 2a$ and height $H_{GC} = Height(C) + 2b$, where *a* and *b* are nonnegative integers, parameters of (the flowaround of) cell *C*. Let's assume $Sh_0(C)$ as the shape of *C*. Let *C* be placed at position[27] $Pos = (a, b)$ in G_C. G_C is thus a grid having *C* "placed in its center", more precisely, the center of the bounding rectangle of *C* is in the center of G_C. Let $Pan(G_C)$ be the set of all panes in G_C. Let U_d be the set of possible directions of unit movement, $U_d = \{(0, 1), (1, 0), (0, -1), (-1, 0)\}$. Let $Edg(G_C)$ be the set of all edges of all panes in G_C. Let $Ng(G_C) = \{(K, Q, \sigma) \mid K, Q$ *are neighboring panes in* G_C *sharing common edge* $\sigma\}$. We will be denoting (K, Q, σ) as $K|_\sigma Q$. Let $Nedg(G_C) = \{\sigma \mid \exists\ K|_\sigma Q \in Ng(G_C)\}$. Let μ be a mapping $\mu : Edg(G_C) \times U_d \to \mathbb{R}^2$, $\mu(\sigma, Sm)$ represents flow velocity across σ when *C* performs elementary movement in direction *Sm*. We will require that $\mu(\sigma, Sm)$ must be orthogonal to σ. Also, for all $\sigma \in Edg(G_C) \setminus Nedg(G_C)$ there must be $\mu(\sigma, Sm) = 0$ for each $Sm \in U_d$. Mapping μ is a parameter of each cell for particular model in the model world. The triple of parameters (a, b, μ) defines flowaround for a cell in concern. It is unchanging in time. As stated beforehand, if a cell divides (as it will be described later), its definition of flowaround is inherited by daughters.

Now we will define special kinds of panes in G_C. Let's assume $a, b \geq 1$, let *C* perform unit movement in G_C in direction $Sm \in U_d$. Let M_0^{Sm} be the set of panes in G_C occupied by *C* before the movement, let M_1^{Sm} be the set of panes in G_C occupied by *C* after the movement. Let $Rec^{Sm} = M_0^{Sm} \setminus M_1^{Sm}$. *Rec* is the set of panes that have been uncovered by the movement. In accord with paragraph Infilling we will refer them as receiving panes. Let $Em^{Sm} = M_1^{Sm} \setminus M_0^{Sm}$. These are the panes that have become covered by the cell, we will refer them as emitting panes.
Let $v_{K,\sigma}$ denote outer unit normal of pane *K* at (the interior of) its edge σ. We will pose constraints on μ, for each $Sm \in U_d$ we will require:

1. $K \in Em^{Sm} \Rightarrow \mu(\sigma, Sm) \cdot v_{K,\sigma} \geq 0$ for all $\sigma \in E_K$. I. e. there can be only outfluxes from emitting panes.
2. $K \in Rec^{Sm} \Rightarrow \mu(\sigma, Sm) \cdot v_{K,\sigma} \leq 0$ for all $\sigma \in E_K$. I. e. there can be only influxes to receiving panes.
3. $K \in M_0^{Sm} \cap M_1^{Sm} \Rightarrow \mu(\sigma, Sm) = 0$ for all $\sigma \in E_K$. I. e. there can be no flux from or to panes that remain covered during the movement.

26 The smallest (area) rectangle with horizontal and vertical sides containig given cell.
27 As described in paragraphs Lattice and Cells in the lattice and membrane elements in the first two paragraphs of section 2.2.1.

4.

$$K \in Em^{Sm} \Rightarrow \sum_{\sigma \in E_K} \mu(\sigma, Sm) \cdot v_{K,\sigma} \leq 1 . \tag{2.49}$$

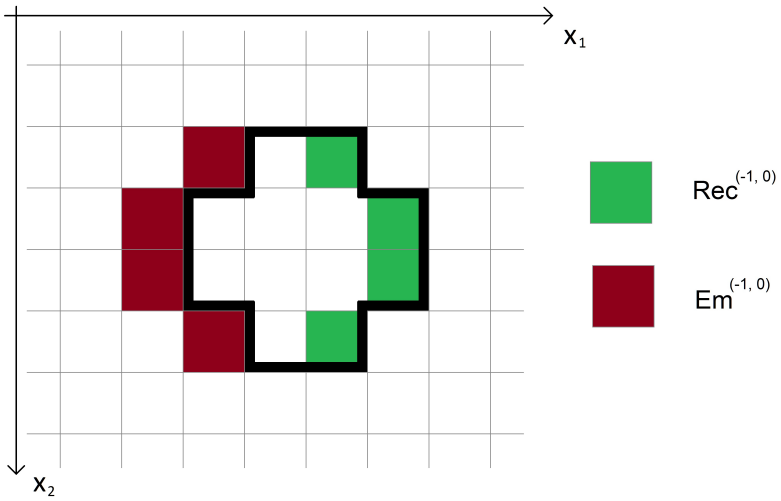

Figure 2.3: Example of receiving and emitting panes. Unit movement in direction (x_1, x_2) = (-1, 0), situation before the movement.

Let's denote G the environment lattice, let C be located at position Pos_G in G. Let Pos_{GC} be the position of C in G_C. As stated before, $Pos_{GC} = (a, b)$. We will say that panes K in G and K' in G_C correspond (or that they are corresponding), if $LatticeIndices_G(K) - Pos_G = LatticeIndices_{GC}(K') - Pos_{GC}$. As expected, $LatticeIndices_H(P)$ denotes indices of pane P in lattice H (cf. paragraph Cells in the lattice and membrane elements in section 2.2.1). Let $K \in Pan(G_C)$. For $\sigma \in E_K$, $Sm \in U_d$, let $Ein(K, \sigma) = max(-\mu(\sigma, Sm) \cdot v_{K,\sigma}, 0)$, $Eout(K, \sigma) = max(\mu(\sigma, Sm) \cdot v_{K,\sigma}, 0)$. Let

$$Vin(K) = \sum_{\sigma \in E_K} Ein(K, \sigma), \quad Vout(K) = \sum_{\sigma \in E_K} Eout(K, \sigma).$$

Let $Vm(K) = max(Vin(K), Vout(K))$.

Let's suppose that in step k C performs elementary movement from position Pos_G in G in direction $Sm \in U_d$. We will simulate advection in panes of G that have corresponding panes in G_C, assuming as though C does elementary movement in G_C from Pos_{GC} in direction Sm, by following algorithm performed within step k:

1. For each pane K in G that is not occupied by a cell, considering the situation before the elementary movement of C, if there is pane K' in G_C corresponding to K, set r-concentrations of all substances in K' as they are in K.

2. For each pane K in G_C such that $K \in Rec^{Sm}$ set r-concentrations of all substances in K to *0*.
3. Let *Spec* be a set of panes K in G_C, such that when considering the situation before the elementary movement, a pane corresponding to K in G does not exist (it would be "out of G"), or it is occupied there by a cell other than C. We will refer set *Spec* as special panes.
4. **Perform procedure** <u>*SetupInitialConcentrations(Spec)*</u>, it will set initial concentrations of all substances in all panes in *Spec*.
5. Determine number of internal steps n for computation of advection:

$$n \leftarrow \lceil \max_{K \in Pan(G_C)} Vm(K) \rceil .$$

6. $i \leftarrow 0$
7. **Repeat** n times
8. **Foreach** (pane K in G_C)
9. **If** ($K \notin Em^{Sm}$)
10. **Foreach** ($L \in Lv$)
11. $${}^{K}_{(i+1)}T_L \leftarrow {}^{K}_{(i)}T_L - \frac{1}{n} \sum_{\sigma \in E_K} f_{K,\sigma} ,$$

$f_{K,\sigma} = \mu(\sigma, Sm) \cdot v_{K,\sigma} \cdot {}_{(i)}{}^{K}T_L$ for $\mu(\sigma, Sm) \cdot v_{K,\sigma} \geq 0$,
$f_{K,\sigma} = \mu(\sigma, Sm) \cdot v_{K,\sigma} \cdot {}_{(i)}{}^{Q}T_L$ for $\mu(\sigma, Sm) \cdot v_{K,\sigma} < 0$,
where Q is a pane such that $K|_{\sigma}Q \in Ng(G_C)$. By ${}_{(j)}{}^{P}T_L$ we understand r-concentration of L in pane P in the j-th internal step of our advection computation, ${}_{(0)}{}^{P}T_L$ is r-concentration of L in pane P at the beginning of the k-th step of the main simulation.

12. **EndForeach**
13. **EndIf**
14. **EndForeach**
15. $i \leftarrow i + 1$
16. **EndRepeat**
17. For each pane K in G_C such that $K \notin M_I^{Sm}$, if there is a pane K' in G corresponding to K that is not covered by a cell in G, considering the situation after the elementary movement of C, set all r-concentrations in K' as they are in K. We regard r-concentration of substance L in K to be ${}_{(n)}{}^{K}T_L$ for all $L \in Lv$.

Procedure <u>*SetupInitialConcentrations*</u>*(Spec)*

1. Let $Free_C$ be a set of panes in G unoccupied by a cell, that have corresponding panes in G_C, assuming situation before the elementary movement of C. For each pane $K \in Spec$, for each substance $L \in Lv$ we will set r-concentration T_L in K to the average value of T_L computed over all panes

in $Free_C$. If $Free_C$ is empty, r-concentrations of all substances in K will be set to zero.

2. We will perform St iterations[28] of computation of discretized diffusion equation on panes in $Spec$ for r-concentration T_L of each substance $L \in Lv$, using values set in step 1. as initial condition. By computing the diffusion, we get approximation of Laplace equation on panes in $Spec$. Boundary conditions will be following: For each pane $K \in Spec$, for each σ being an edge of K such that σ is not part of any other pane from $Spec$:
   - If there is a pane Q such that $K|_\sigma Q \in Ng(G_C)$ and there is a pane Q' in G corresponding to Q, where Q' is free before the elementary movement of C, we will assume Dirichlet boundary condition on σ for r-concentration of each substance in Lv, taking concentration in Q' as boundary concentration on σ.
   - In all other cases (Q doesn't exist, it hasn't corresponding pane in G or the corresponding pane is occupied before the elementary movement of C), there will be zero flow condition over σ as boundary condition.

Sample situation of boundary conditions from step 2. of procedure SetupInitialConcentrations is sketched in Fig. 2.4. Computation of step 2. of the procedure will be done as following: Parameter St is an internal parameter determined as $St = n \cdot max(W_{GC}, H_{GC})$, where n is the number of steps the own simulation of flows is split to, determined in step 5. of the algorithm. Regarding computation of diffusion, let ${}^{K,(m)}T_L$ be r-concentration of substance $L \in Lv$ in pane $K \in Spec$ at the end of the m-th step of our computation, $1 \leq m \leq St$, ${}^{K,(0)}T_L$ *denotes* the initial r-concentration of L in K. We will employ (2.35), using ${}^{K,(m)}T_L$ in place of ${}^{K}T_L^{(n)}$, where n in the latter corresponds to m in the former, with $D = 1/5$ and $\alpha_T \equiv 0$. Boundary conditions will be implemented by fictive neighbors.

When approximating Laplace equation in step 2. of procedure SetupInitialConcentrations, we are determining the number St of iterations of the relaxation step so that it keeps computational costs low rather than it would regard achieving reasonable convergence. Since elementary movement of a cell is only by one pane, we anticipate that maximum advection velocities will be ~ 1. Thus, if n from step 5. is small, the contents of only those panes in $Spec$ that are close to the "boundary" with regions of real panes will be generally transported by advection to the real panes. From this point of view, we may see procedure SetupInitialConcentrations as setting average r-concentration to the panes of $Spec$ and "shifting" this average in the panes that are expected to influence r-concentrations in nearby real panes towards r-concentrations in these real panes.

28 More explanation regarding this parameter and related computation will follow.

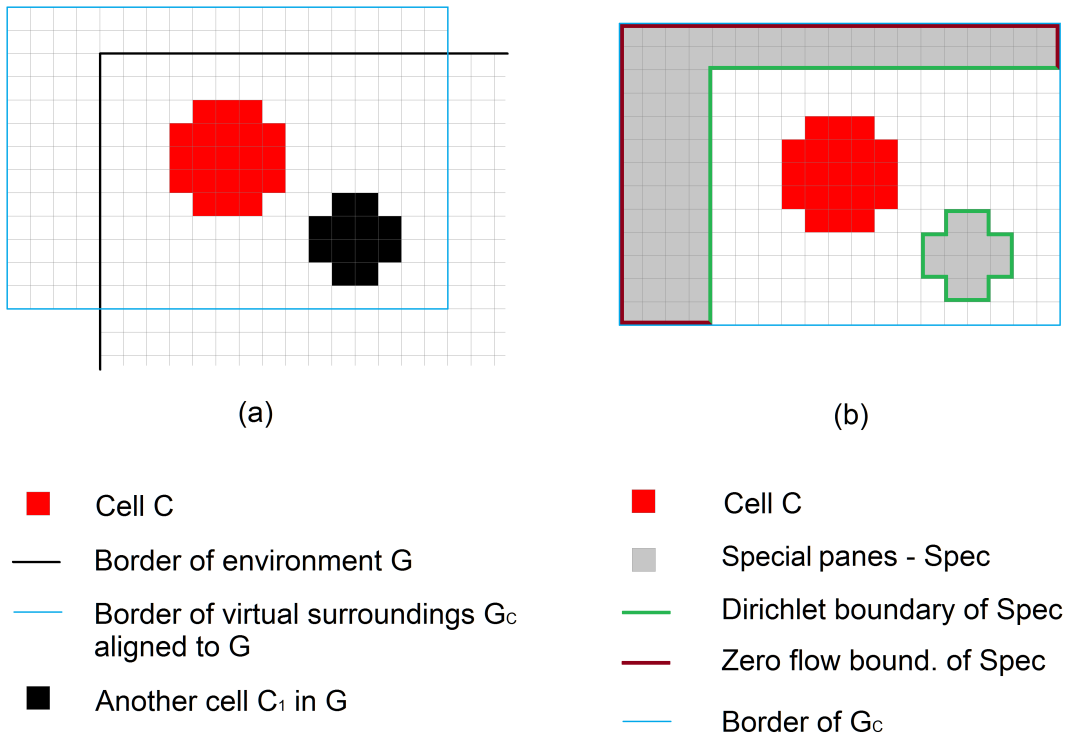

Figure 2.4: Example of virtual surroundings of a cell: Alignment of environment lattice and the lattice of the virtual surroundings (a). Boundary types for regions of special panes in the virtual surroundings in procedure SetupInitialConcentrations (b).

Within the flowaround algorithm, r-concentrations in panes are updated by the expression in step 11. which corresponds to advection discretization (2.48).

By splitting the computation into *n* iterations in step 7. and by choice of *n* in step 5. we limit the total outflux from a pane and the total influx to a pane in single iteration by *1*, which is a volume of a pane.

In the nested loops in step 7. and following, emitting panes are neglected from r-concentration update. In (2.49) we limited total outflux from emitting panes for elementary cell movement by one. Since these panes get covered by the moving cell, we only allow at most the whole contents of these panes to flow to neighboring (nonemitting) panes. Due to (2.49) we know that flow velocities from these panes don't cause (require) splitting the computation into more than one step based on step 5. If the computation is split, we assume as though the cell in each iteration makes an area of an emitting pane covered, where this area has the size corresponding to the volume that has flown out from the pane.[29] Thus we regard the r-concentration to be unchanged by all iterations except of the last one. Since the r-concentration in the

29 Justifying setup of outfluxes where this size is different, i. e. when for an emitting pane *K* *Vout(K) < 1,* is left to the modeller on the level of particular models.

pane after it got covered is unimportant, we don't need to update the r-concentration at all. Regarding receiving panes, due to setting r-concentrations in them to zero in step 2. and by allowing no outfluxes there, we can interpret inflowing concentrations as amounts that accumulate, while the cell gradually leaves the pane. At the end of the flowaround computation, the "uncovered area" of the receiving pane equals to one, so we can interpret the accumulated sum as r-concentration.

Discussion on Flowaround. In our model world, we wish to have a possibility to express (r-)concentration changes happening due to advection caused by movement of cells. However, we consider it beyond the scope of our work to implement physically realistic dynamic computation of advection velocities. Instead, we decided to use a model with stationary velocities in chosen surroundings of moving cells. We didn't want to determine or automatically generate the velocity field for cells (cell shapes) apriori from within the model world for particular models but we wanted this to be provided by the modeller, so that a wide range of conditions could be expressed. Our flowaround algorithm is defined in a way that it relevantly captures advection in surroundings of a cell in situations where there are no obstacles there and the surroundings is fully contained in the environment lattice. In this case, when advection velocities provided by the modeller are realistic, we may expect realistic results as well. On the other hand, presence of obstacles or interference with environment boundary brings geometry that is unreflected by the advection model, together with concentration substitutes in the special zones (panes), that generally flow to the regular panes. Thus, for models with high density of cells, small sizes of surroundings for flowaround or usage of infilling instead may be an appropriate choice.

Generally, we didn't require divergence-free velocity field in (2.44), although this might seem appropriate for modeling of liquid environment around the cells. We didn't want to restrict flexibility of the model world.

2.2.5 Apoptosis

When a cell performs apoptosis, it disappears from the environment within a single step. Panes that were occupied by the cell became free, we will want to set r-concentrations of substances in these panes. This will be similar as in infilling. Let C be a cell that undergoes apoptosis in particular step, let's consider C just before being removed from the environment in that step. Let M be the set of membrane elements of C. Let $Nseg = \{\sigma$: *There is* $(\sigma, v, R) \in M$, *there is unoccupied pane* K *where* σ *is edge of* $K\}$. For $\sigma \in Nseg$ let K_σ be the unoccupied pane where σ is an edge of K_σ. For each substance $L \in Lv$, let ${}^{K}T_L$ be T_L in pane K and

$$W_L = \frac{1}{|Nseg|} \sum_{\sigma \in Nseg} {}^{K_\sigma}T_L .$$

If *Nseg* is empty then let $W_L = 0$. After *C* is removed from the environment lattice, in each pane that became unoccupied, r-concentration of *L* will be set to W_L.

2.3 Cell logic

In the previous section we have described our model cell from the point of view of the environment, providing interaction interface between the cell and its outside. Now we will define the decision logic of a cell, together with a mechanism that controls whether a cell will perform division. In our internal model of cell we are not trying to mimic inner parts of biological cells and their interactions. Throughout the section, ways how cell membrane receptor composition changes will be also described.

2.3.1 Cummulative state and concentration gradient

Cummulative state. Cummulative state represents an internal state of model cell. Cummulative states correspond in one-to-one relationship to substances from the set *Lv*. At each time instant (step) a cell is in exactly one cummulative state. Let $L \in Lv$. We will say that a cell is in cummulative state on *L*, or shortly that it is in cummulative state *L*, if, freely spoken, *L* is the most seen substance by the cell via its receptors in given step. Formally, we will understand cummulative state as a map *Ks* assigning to each cell *C* and time $t_n = n$, $n \in \{-1, 0, 1, ...\}$, a substance $L \in Lv$ as follows: For $t_n = -1$, *Ks* is provided as initial condition for all cells present in given model situation in time *0*. For $t_n \geq 0$, let *M* be the set of all membrane elements of *C* in time t_n. For $Me \in M$ let S_{Me} be the vector of occupancies of individual kinds of receptors on *Me*, computed in the *(n+1)*th step[30] according to pane – membrane or membrane – membrane interactions, depending on whether *Me* is adjacent to a free pane or to a membrane element of another cell, respectively. If *Me* is adjacent to the lattice boundary, S_{Me} is zero. Let

$$S_M = \sum_{Me \in M} S_{Me}$$

be the vector of total occupancies of all kinds of receptors on the cell membrane. Let $\overline{K}_M \subseteq Lv$ be the set of substances for which corresponding components of S_M attain maximum over all components of S_M. Let $K_M \subseteq Lv$ be the set of substances complementary[31] to those in $\overline{K}_M$. We will first determine a candidate value of *Ks* *L′*. If K_M contains exactly one element, then *L′* is this element. Otherwise, let L_0 be the value of *Ks* for *C* in the previous simulation step or the one specified as an initial condition, if current step is the first one. If $L_0 \in K_M$ then $L' = L_0$. Otherwise, *L′* is

30 We regard steps to begin from 1, assuming the n-th step to "start" at time t_{n-1} and "end" at time t_n, providing output values that regard time t_n. More details will follow in section 2.4.
31 In sense of vax reactions.

arbitrarily chosen element of K_M.[32] We will allow a change of value of *Ks* from L_0 only if the new signal is "strong enough" in comparison with the one telling *C* to stay for L_0: Let *Ks change threshold* be a positive parameter. Let $S_M(Z)$ denote component of S_M corresponding to the amount of occupied receptors formed by substance *Z*. If $S_M(\lambda(L')) - S_M(\lambda(L_0)) \geq$ *Ks change threshold*, we will put $L = L'$, otherwise $L = L_0$.[33]

Concentration gradient. We want our cells to be able to perceive concentration gradients in their surroundings. Let $L \in Lv$ be a substance. If cell *C* wants to detect concentration gradient G_L of *L*, this will be computed as follows: If *C* has zero amount of receptors on *L*, (i. e. if the total amount of receptors formed by $\lambda(L)$ on the membrane of *C* is zero), G_L will be zero. Otherwise: Let *M* be the set of all membrane elements of *C*. We will put

$$G_L = \frac{1}{|M|} \sum_{(\sigma, \nu, R) \in M} W_{(\sigma,\nu)} \cdot \nu \ , \qquad (2.50)$$

where $W_{(\sigma, \nu)}$ is

- T_L in the pane *K* adjacent to segment σ on its side in direction of ν, if such pane exists and is unoccupied[34]; otherwise it is
- the amount of receptors formed by *L* on membrane element of another cell adjacent to (σ, ν, R), if such membrane element exists, or
- zero otherwise.

As we see, G_L takes into account r-concentrations or amounts of kinds of receptors on adjacent membrane elements rather than values that would be measured by receptors of *C*. Although the second variant is more realistic, we would have to pay attention regarding the behavior of our measurement system. Particularly, if receptors get (nearly) saturated, we could get (nearly) zero measured gradients although the real gradients might have been "big". When designing our model world, we will favour the ease of creation of models when having "ready to use realistic information" regarding pericellular gradient, before the more realistic model of "not always working" measurement system that generally needs special attention. Similarly as in the case of vax reactions analogy on pane-membrane interface, the by-cell perceived gradient is rather a building block for us, than a primary target of exploration and detailed modeling. For getting the external gradient, we require that the cell has nonzero amount of receptors that (can) sense given substance. Otherwise we assume that the cell doesn't recognize the substance and our gradient is zero.

32 In the implementation in Virtual Laboratory, *Ks* in this case is the substance in K_M with the lowest index in internal ligand numbering.

33 Introducing *Ks change treshold* (also) hinders random fluctuations of cummulative states in the simulations in Virtual Laboratory if a cell sees multiple signals with nearly identical strengths.

34 I. e. ${}^{K}T_L^{(n)}$ from (2.35) in time *n*.

From (2.50) we also see that when computing G_L we are not taking into account particular shape of the cell. From the point of view of size and shape, we are just assuming a very simple model of cell gradient sensing, which, however, works well for regular cell shapes and uniform sizes.

In given time instant for a cell we are only interested in concentration gradient of a substance the cell is in cummulative state on. Gradients of the other substances are not important for us here.

2.3.2 Zygotic graph and cell division

Zygotic graph. Now we are ready to define the core of the internal functionality of our cells. It plays a conceptual role of DNA in the model world. It is the same for all cells in given particular model situation and can be seen as a common program, where each cell generally executes different part of it; meaning of the program relates to the whole scenario including cells, environment and their interplay rather that to individual cell.

Let zygotic graph be a quadruple (G_P, G_R, G_M, G_A), where:

G_P is oriented weighted graph whose vertices are elements of the set Lv and weights are nonnegative. An edge from vertex A to vertex B with weight w means that if a cell is in cummulative state on substance A, it will secrete amount w of substance B to its surroundings. More precisely w is divided by the number of membrane elements of the cell. For each membrane element, if it neighbors with an unoccupied pane, this fraction of ligand B will be secreted to the pane. Otherwise, nothing will be done. We will call G_P a production graph.

G_R is oriented weighted graph with vertices being elements of Lv and nonnegative weights. An edge from A to B with weight w means that if a cell is in cummulative state on substance A, it will add amount w of [35]receptors formed by $\lambda(B)$ to its membrane. I. e. the cell is adding receptors by means of which substance B is being perceived. The amount w is divided by the number of membrane elements of the cell and this fraction is added to the amount of given receptors in each membrane element. G_R is called a receptor graph.

G_M is a mapping from the set Lv to interval $<-1, 1>$. If a cell is in cummulative state to substance A:

$$Spd = \frac{G_A}{\| G_A \|} \cdot G_M(A), \text{ if } \|G_A\| \geq Min\,gradient,$$

$$Spd = 0, \text{ if } \|G_A\| < Min\,gradient.$$

Here Spd is the cell speed. (Cf. the first paragraph in section 2.2.4.) G_A is the concentration gradient perceived by the cell (cf. (2.50)), $\|G_A\|$ is the Euclidean norm of G_A. $Min\,gradient > 0$ is a threshold parameter stating the minimum detectable

35 unoccupied

gradient magnitude for a cell, it is the same for all cummulative states (substances from *Lv*) and for all cells. In line with our naming so far we will call G_M a movement graph. We can still see it as a weighted graph where the only allowed kind of edges is the one from a vertex to itself.

G_A is called an apoptotic graph, it is a mapping $G_A: Lv \rightarrow \{0, 1\}$. If a cell is in cummulative state *S* and $G_A(S) = 1$, the cell will perform apoptosis. (Cf. paragraph 2.2.5).

Cell Division. For a cell, we will now see its membrane as a compartment. The compartment will serve us as a base for determining, if the cell should divide. Let *Mo* be the sum of amounts of all receptors in all membrane elements of the cell. Let *Dt* be a positive parameter, let's call it division threshold. If $Mo \geq Dt$ in given simulation step, we will say that the cell *wants to divide*. If a cell *wants to divide* and it is not a daughter cell of one that did divide in current step, we will try to find locations for two daughter cells with regard to free place in the proximity of the cell and respecting other constraints. If the locations are found, the cell will divide within given simulation step. Both of the daughter cells will have the same shape as the mother cell. Membrane elements in the daughters will contain each half of the original amount of receptors of each kind in comparison with the membrane elements of the mother cell.

Regarding the placement for daughter cells, the cell can choose a direction of its division. When determining the places for the daughters, we are trying to find locations that respect this direction as much as possible. We will introduce parameter *Division direction*, that can have following values: *Parallel to gradient*, *Perpendicular to gradient* and *Random*. For the value *Parallel to gradient*, we are trying to follow the direction of the concentration gradient of the substance the cell is in cummulative state to, if the magnitude of the concentration gradient is $\geq$ *Min gradient*. Otherwise, the division direction will be random. For the value *Perpendicular to gradient* the situation is the same, but the preferred division direction is perpendicular to the concentration gradient. For *Random* the direction is randomly chosen.

After we got the actual desired division direction, we will use it as an input for an algorithm that determines the locations for daughter cells. Detailed formalized description of the algorithm will not be provided. We will sketch the main idea together with substantial features and omit details:

- We require that after the division:
  - Both of the daughter cells may only occupy panes that were either empty or occupied by the mother cell before the division. Basic assumptions about the cells in the environment must hold, i. e. each of the daughter

cells must be whole in the lattice and every pane in the lattice must be occupied by at most one cell.
    - Both daughter cells must be close to each other: Let R be the bounding rectangle[36] of the mother cell in the environment lattice. Let R have width w and height h. Then the bounding rectangle of the pair of the daughter cells R_d must have width at most $2w$ and height at most $2h$.
    - The daughter cells must be close to the original position of the mother cell: Let P_0 be the real location of the upper left corner of R, let P_1 and P_2 be real locations of the upper left corners of the lattice bounding rectangles of the daughter cells. Then P_0 must lie on the segment P_1P_2.
- We will proceed as follows: Among the location pairs for daughter cells fulfilling the above conditions we are first trying to find those that match most the actual desired division direction. (There can be more pairs of locations with the same (best) direction match.) From the subset of location pairs matching best the direction, we are searching one, where the original location of the mother cell is closest to the center of the (daughter) locations in the pair. If there exists no location pair fulfilling the conditions in the previous points, the cell will not divide. In this case we will say that the cell *couldn't divide*.

We may wish to modify the algorithm in order to force the daughter cells to touch each other. This is useful when we want the cells after division to be in mutual contact by area (part of cell boundary) of defined size. We will introduce parameters: *Touching required*, *Min common elements*, and *Max common elements*. The first one has Boolean value, the others are nonnegative integers. When *Touching required* is true, we restrict the set of possible locations of the daughter cells in the algorithm only on those where the number of (pairs of) membrane elements by which the cells touch each other is in range <*Min common elements*, *Max common elements*>. This may lead to (greater) deviation of the division direction from the required one, in comparison with the case when we don't require touching of cells. If our restricted set is empty, we will regard that the cell *couldn't divide*.

When we have the locations for daughter cells, we will model the course of the division in the environment in a following way: For our purpose we will temporarily allow that cells can partially or wholly cover each other, i. e. there can be more cells occupying one pane.

- At the beginning, both daughter cells will be placed at the position of the mother cell, fully covering each other.
- Each of the daughters will migrate to its destination position. Both cells will have internal speeds for this movement such that they will run their paths during the same time. Both of the daughters will be running simultaneously,

36 The smallest (area) rectangle with horizontal and vertical sides containig regarded object(s).

movement of each will be a sequence of elementary movements from the starting position to the destination one, forming a discretization of a segment between these positions respecting the lattice. On their paths, the cells will go "through" possible obstacles. For each elementary movement of each of the daughters, either flowaround or infilling will be computed, depending on the setup of the mother cell (that has been inherited to the daughters). This whole movement of the daughters will be simulated within one step of the main simulation.

2.3.3 Receptor treatment

Receptor normalization. If a cell *wanted to divide* in particular simulation step but some of the conditions for division, as described in the previous paragraph, were not fulfilled, then the cell *couldn't divide*. In this case we will generally restrict the total amount of receptors on cell membrane. We will introduce parameter *Membrane capacity*[37], requiring $Dt \leq Membrane\ capacity$. Assuming Mo to be the sum of amounts of all receptors in all membrane elements of our cell, if $Mo > Membrane\ capacity$ we will change amounts of receptors in membrane elements so that after the change there will be $Mo = Membrane\ capacity$. Let M be the set of all membrane elements of the cell. For each membrane element $(\sigma, v, R) \in M$ we will change R to R' putting

$$R' = R \cdot \frac{Membrane\ capacity}{Mo} . \tag{2.51}$$

Receptor decays. Under receptor decays we will understand receptor internalization and raw receptor internalization, defined in chapter 2.1. We remind here that the former and the latter are mutually exclusive on the level of model in the model world. Receptor internalization influences membrane receptor composition and (r-)concentrations in the surroundings of a cell. Raw receptor internalization only alters membrane receptor composition. Membranes of our cells are homogeneous, i. e. the amount of receptors of each kind in every membrane element of given cell is the same.

If $q = (\sigma, v, R)$ is a membrane element, for $L \in Lv$ we will denote by q_L the component of R representing receptor amount of kind L. Let's consider cell C with the set of its membrane elements $M(C)$ in time n, where n is a nonnegative integer. Let $\Lambda = \lambda(L)$, let $X = \chi(L)$.

In order to compute receptor internalization of receptors formed by L on the membrane of C, we will first determine quantity ${}^0\delta_{ri}(q, L)$ for each $q \in M(C)$, distinguishing three cases:

37 This parameter doesn't mean a limit for the total amount of all receptors on cell membrane that can't be exceeded in any case. E. g. receptor normalization is performed only on cells that didn't divide in given step.

(a) There exists an unoccupied pane K adjacent to q. Let ${}^{q}[X^{L}]^{(n)}$ be the amount of occupied receptors formed by L in q in time n, computed by reaction decomposition in pane K and its adjacent membrane elements in computation of discretized boundary conditions in step $n+1$. (We use ${}^{q}[X^{V}]^{(n)}$ from the paragraph above (2.37) for $L = V$.) Further, let ${}^{q}[L^{m}]^{(n)}$ be the amount of unoccupied receptors formed by L in q in time n, computed by the reaction decomposition. Thus there holds $q_L = {}^{q}[X^{L}]^{(n)} + {}^{q}[L^{m}]^{(n)}$. Let

$$ {}^{0}\delta_{ri}(q, L) = -k_{ri}^{X} \cdot {}^{q}[X^{L}]^{(n)} - k_{ri}^{L} \cdot {}^{q}[L^{m}]^{(n)}, \quad \textit{if there is pane } K \textit{ adjacent to } q . $$

(b) There exists membrane element q^2 adjacent to q. Let $[X^{2,1}]^{(n)}$ denote amount of substance X anchored in q by L and in q^2 by Λ, in time n, computed by vax reaction in step $n+1$, i. e. $[X^{2,1}]^{(n)} = fxvax(q^2{}_{\Lambda}, q_L)$. (Cf. paragraph Membrane – membrane interactions in section 2.2.2.) Denoting $[L^{1}]^{(n)}$ the amount of L anchored in q in time n computed by the vax reaction, that is $[L^{1}]^{(n)} = q_L - [X^{2,1}]^{(n)}$, we lay

$$ {}^{0}\delta_{ri}(q, L) = -k_{ri}^{X} \cdot [X^{2,1}]^{(n)} - k_{ri}^{L} \cdot [L^{1}]^{(n)}, \quad \textit{if there is membrane element } q^2 \textit{ adjacent to } q . $$

(c) q is adjacent neither to a pane nor to another membrane element. (*) We will put

$$ {}^{0}\delta_{ri}(q, L) = -k_{ri}^{L} \cdot q_L , \quad \textit{if } (*) \textit{ holds}. $$

We will now define the change $\delta_{ri}(C, L)$ of q_L due to receptor internalization in the $(n+1)$th step, that will be the same for all $q \in M(C)$, as

$$ \delta_{ri}(C, L) = \frac{1}{|M(C)|} \sum_{q' \in M} {}^{0}\delta_{ri}(q', L) . \tag{2.52} $$

We wanted to preserve membrane homogeneity, so we didn't use ${}^{0}\delta_{ri}(q, L)$ directly in membrane elements, since in cases (a) and (b) ${}^{0}\delta_{ri}(q, L)$ depends on receptor occupation, that is generally different for every membrane element of C.

Regarding raw receptor internalization, for each $q \in M(C)$ we will define the change ${}^{0}\delta_{rri}(q, L)$ of q_L due to raw receptor internalization in the $(n+1)$th step as

$$ {}^{0}\delta_{rri}(q, L) = -k_{rri}^{L} \cdot q_L . $$

Since we suppose the membrane of C homogeneous, we can introduce the change $\delta_{rri}(C, L)$ of q_L due to raw receptor internalization in the $(n+1)$th step that will be the same for all $q \in M(C)$:

$$ \delta_{rri}(C, L) = -k_{rri}^{L} \cdot q_L^{0} , \tag{2.53} $$

where $q^0{}_L$ is arbitrary membrane element of C.

2.4 Simulation algorithm

In the sections above we have described individual components of the model world including chemical reactions, properties of the environment, and behavior of cells. Now we will put these parts together and formulate the algorithm expressing the whole scenario.

Let's call particular model in the model world a situation. Suppose that we have a situation with width W and height H, understanding width and height as the number of columns and rows of the environment lattice respectively. According to the last paragraph in section 2.1.2 we further assume that there is number of vaxes *NumVaxes* and we consider diffusion coefficient D in our situation.

Initial conditions. Concerning the environment, these are initial locations of cells and values of r-concentrations T^A and T^V for each vax $(A, V, X) \in Vaxes$ in every unoccupied pane. Specially, if T^V is zero in a pane, then T^A specifies initial concentration of A there and vice versa. For every cell we specify its initial cummulative state and initial amounts of [38]receptors of every kind. (In accord with cell membrane homogeneity, each of this amounts is uniformly distributed in all the membrane elements of the cell.)

Own algorithm. Let N be the number of simulation steps of our computation, let *Lat* denote the environment lattice. Let ${}^K T_A^{(n)}$, ${}^K T_V^{(n)}$ denote values of T^A, T^V respectively in pane K in time n, with ${}^K T_A^{(0)}$, ${}^K T_V^{(0)}$ being initial conditions, for vax $(A, V, X) \in Vaxes$. Let Γ be the set of all cells in the situation. The algorithm will proceed as follows:

1. $n \leftarrow 0$
2. **Repeat** N times
3. **Perform procedure** *ReactionDiffusion(n)*
4. **Foreach** (C in Γ)
5. Compute cummulative state *Ks(C, n)* of C and time n as described in paragraph Cummulative state in section 2.3.1. When determining receptor occupancy at membrane elements adjacent to free panes, r-concentrations T_A, T_V of time n will be used for each $(A, V, X) \in Vaxes$. Particularly, in each membrane element *Me* of C adjacent to a free pane, K say, ${}^K T_A^{(n)}$ and ${}^K T_V^{(n)}$ will be used[39] as inputs regarding K in places of T_L^p and T_A^p respectively in (2.23) when occupancy of receptors of kind A is computed. If occupancy of receptors of kind V is desired, we will use ${}^K T_V^{(n)}$, ${}^K T_A^{(n)}$ in places of T_L^p and T_A^p respectively in (2.23).

38 unoccupied
39 Cf. procedure *ReactionDiffusion*.

6. Determine gradient G_{Ks} of the cummulative state substance *Ks*, perceived by *C*, as described in paragraph Concentration gradient in section 2.3.1. Values T_{Ks} of time *n* will be used within computation.
7. Determine cell speed *Spd* of *C* using movement graph G_M, based on *Ks* and G_{Ks}, as described in paragraph Zygotic graph in section 2.3.2.
8. **EndForeach**
9. Perform changes of amounts of receptors on cell membranes due to either receptor internalization or raw receptor internalization in dependence on parameter *UseReceptorInternalization.* When receptor internalization is being computed, first determine contributions $\delta_{ri}(C, L)$ defined in (2.52) for each cell $C \in \Gamma$, and for each substance $L \in Lv$. In panes adjacent to membrane elements of *C*, use r-concentrations T_L, T_Λ, of time *n* for computation, where $\Lambda = \lambda(L)$. After the contributions are computed, walk through the cells and substances again and add precomputed $\delta_{ri}(C, L)$ to amount q_L for each membrane element *q* of *C*. For raw receptor internalization, we will update the receptor amounts directly, for each cell $C \in \Gamma$, for each substance $L \in Lv$ and for each membrane element *q* of *C*, setting $q_L \leftarrow q_L + \delta_{rri}(C, L)$, where $\delta_{rri}(C, L)$ is defined in (2.53).
10. **Foreach** (*C* in Γ)
11. Produce ligands by *C* to free panes adjacent to *C* using production graph G_P, based on cummulative state *Ks* of *C*, as described in paragraph Zygotic graph in section 2.3.2[40]. R-concentrations T_A, T_V of time $n+1$ computed in step 3. will be updated for regarded vaxes *(A, V, X)*.
12. Add receptors to membrane elements of *C* using receptor graph G_R, based on cummulative state *Ks* of *C*, as described in paragraph Zygotic graph in section 2.3.2.
13. **EndForeach**
14. For every cell *C* in Γ, if *C* should undergo apoptosis according to its cummulative state *Ks* and apoptotic graph G_A, perform apoptosis on *C* as described in section 2.2.5 and remove *C* from Γ. r-concentrations of time $n+1$ are used to determine r-concentrations in the panes that became unoccupied.
15. $\Gamma \leftarrow$ **Perform procedure** Divisions(Γ)
R-concentrations of time $n+1$ are being updated in flowaround or via infilling in internal movements within divisions, as described in paragraph Cell Division in section 2.3.2.
16. **Foreach** (*C* in Γ)

40 Note that production of ligand *L* per each membrane element *Me* of *C* adjacent to a free pane is $P(C, L, n+1)$ for the quantity *P* used in (2.37).

17. Update real location of *C* based on its speed *Spd* and obstacles in its surroundings, as described in the first paragraph in section 2.2.4. Perform elementary movement(s) of *C* if needed, together with Infilling or Flowaround[41], using or updating r-concentrations of time *n+1*.
18. **EndForeach**
19. $n \leftarrow n + 1$
20. **EndRepeat**

Procedure *ReactionDiffusion(n)* *//n is the zero based index of step*

1. **Foreach** (pane *K* in *Lat*)
2. **If** (*K* is not occupied)
3. $i \leftarrow 1$
4. **Repeat** *NumVaxes* times
5. $A \leftarrow A_i,\ V \leftarrow V_i$
6. ${}^{K}T_{A}^{(n+1)} \leftarrow {}^{K}T_{A}^{(n)} + \delta(A, K, n) + \delta_r(A, K, n),$
7. ${}^{K}T_{V}^{(n+1)} \leftarrow {}^{K}T_{V}^{(n)} + \delta(V, K, n) + \delta_r(V, K, n).$

   $\delta(A, K, n)$ expressed in (2.36) is the change of ${}^{K}T_{A}^{(n)}$ due to reaction-diffusion, $\delta_r(A, K, n)$ defined in (2.39) is contribution of membrane enzymatic activity and receptor internalization from membrane elements adjacent to *K*[42]. Similarly for ${}^{K}T_{V}^{(n)}$, $\delta_r(V, K, n)$ is defined in (2.38).
8. $i \leftarrow i + 1$
9. **EndRepeat**
10. **EndIf**
11. **EndForeach**

Procedure *Divisions(Γ)* // Γ is a set of cells

1. $\Gamma_1 \leftarrow \varnothing$
2. **Foreach** (*C* in Γ)
3. Evaluate *wants to divide* flag of *C* as described in paragraph Cell division in section 2.3.2.
4. **If** (*wants to divide* flag is *true* in *C)*
5. **If** (conditions for division of *C*[43] are fulfilled)
6. Perform cell division for *C*[43].
7. $\Gamma_1 \leftarrow \Gamma_1 \cup \{C_a, C_b\}$, where C_a, C_b are daughter cells of *C*.
8. **Else**

41 As described in the first paragraph of section 2.2.4.

42 Boundary conditions on lattice boundary and baseline zero flow over cell membranes is realized by fictive neighbors.

43 As described in paragraph Cell division in section 2.3.2.

9. $\Gamma_1 \leftarrow \Gamma_1 \cup \{C\}$
10. Perform receptor normalization for C if needed, as described in paragraph Receptor normalization in section 2.3.3.
11. **EndIf**
12. **Else**
13. $\Gamma_1 \leftarrow \Gamma_1 \cup \{C\}$
14. **EndIf**
15. **EndForeach**
16. **Return** (Γ_1)

Summary of the algorithm. In each iteration corresponding to a step, we first compute reaction-diffusion in free panes, applying all the boundary conditions except of cell productions. We also still remember the original r-concentrations for all ligands. These are used to compute cummulative states and gradients for cells, and later for receptor internalization on membrane elements. After we have cummulative states and gradients for cells, we are able to determine cell speeds. We proceed with receptor decays. When computing receptor internalization, we use two stages. First, differences caused by receptor internalization are determined for all membrane elements of all cells. Then these are applied in a separate pass. We are preserving input information on adjacent membrane elements so that both in each adjacent pair are updated correctly. Raw receptor internalization doesn't have this dependency, it can be done inplace.
Next, production of ligands and receptors follows. Now we have all the information necessary to decide, whether a cell wants to divide. We first perform apoptoses, then divisions and finally cell movements.

Generally, as we see, the cummulative state a cell enters in a step determines its behavior “immediately” in given step.

3. Model of lumen formation

3.1 Biological background

Lumen is understood as the space in the interior of a hollow tubular structure [67]. Important cell types exhibiting lumen formation are epithelial cells, including endothelial cells especially. Epithelial tubes are important part of many organs including kidneys [56], [58], gut [57], or trachea [58]. Epithelial tissues consist of polarised cells whose plasma membranes are divided into apical and basolateral domains [59]. While some epithelial lumens form from preexisting polarised epithelial structures, de novo lumen formation from nonpolarised cells is recognized as an important driver of epithelial tissue morphogenesis, especially in formation of small epithelial tubules [60]. The lumen of all blood vessels in vertebrates is lined and formed by endothelial cells [61]. Unlike other epithelial cells, endothelial cells form lumens as they invade tissues [62]. Although most vertebrate vessels exhibit specialized apical and basal domains, nonpolarised early vessels have been observed [63].

As described in [38], in angiogenesis, one way of lumen formation starts by development of intracellular vacuoles in endothelial cells. The vacuoles enlarge and coalesce. Union of adjacent cellular lumens in multiple cells leads to formation of a continuous tube. Another way is forming intercellular lumen by creating a bud via protrusion and migration of neighboring endothelial cells in newly formed or established vessels. These budding cells maintain their polarity and junctional contacts. An intercellular lumen is already formed at the start of bud formation.

Generally, tubes can be also formed by wrapping, cavitation, and cell hollowing [39]. In wrapping, part of epithelial sheet invaginates and curls, until the edges of the invaginated region meet and seal. In this way, a tube is formed that separates from the sheet and that is parallel to its plane. In cavitation, there is a solid cylindrical multicellular mass first. The central cells are eliminated, converting the object into a tube. In cell hollowing, there is a lumen formed within a cytoplasm of a single cell, spanning the length of the cell.

Special form of cavitation can be seen in lumen onset mediated by prior formation of polarised transient epithelial structure called rosette [43]. In a rosette five or more cells interface at a central point. Further cell rearrangements lead to organ development. In various contexts, rosettes open to form (micro)lumens in their apical centers. Microlumens can connect and form continuous lumen [44].

3.1 Cell-based models of lumen formation

One kind of agent-based models of lumen formation uses axiomatic algorithmic rules to define how cells interact with local components; the rules are

partially custom for given motivations, comming out and adopting basic notions from observations of these experimental in-vitro situations [64], [65], [45]. In [45], a 3D agent-based model of epithelial acinus formation is introduced. Lumen is formed by apoptotic cavitation and maintained by keeping equilibrium between cell proliferation and apoptosis. Cell polarisation is preserving physiological epithelium morphology. Apoptosis in the model is necessary and sufficient for initiating lumen formation.

Another approach is using cellular Potts [41], [42]. In [40], such kind of agent-based computer model was employed when studying two mechanisms of lumen formation: Vacuolation (1) and cell-cell repulsion of adjacent cells with cell shape changes (2). In addition to vacuolation and cell – cell repulsion, the model simulates cell motility and cell surface polarisation. As an underlying biological motivation, angiogenesis is used, lumen development in an originally cavity-free branched sprout is simulated. Within the model setting it is demonstrated that each of the principles (1) and (2) can produce lumen on its own. Combination of both improves lumen formation with regard to robustness to parameter values. Apical-basolateral cell surface polarisation is necessary for lumen formation.

Other strategies based on Mote Carlo approach [52], more or less similar to cellular Potts, are being used as well. In the context of modeling self-assembly of cells and the cellular aggregate fusion process for predicting and optimizing postprinting structure formation in organ bioprinting technology [66], coalescing and forming of 3D bi-layered lumina is modelled in [51]. Kinetic Mote Carlo approach [52] is employed. Sorting of cells based on different adhesivities makes the core of the lumen formation and coalescing processes. Initially, there are conveniently arranged sets of mutually touching spherical clusters in the simulation. The clusters consist of two kinds of cells and hydrogel. As a result, luminal tubes are formed. The cells have no special properties in addition to different adhesivities (like apoptosis or polarisation), the process is kind of self-organization. In [53], in-vitro fusion of uniluminal vascular spheroids together with alike variant of Monte Carlo computer model is described.

In [49], [50], IBCell model is employed to simulate 2D acinus formation. The acinus model uses cell polarisation and apoptosis as key components of a cavitation scenario. A cell has receptors on its membrane, sensing signals from extracellular matrix and adjacent cells. Under wide range of tested parameter values the model provides resulting monolayer of polarised cells surrounding hollow cavity. Apoptosis is necessary for lumen formation.

3.2 Our lumen formation model

In [54], experimental in-vitro scenario is described where beads coated with endothelial cells from human umbilical vein were put to fibrin gel. Sprouting and cell

migration from the beads occurred but no formation of patent lumens has been observed. When skin fibroblasts were plated on the top of the gel, tip cells with multicellular lumens behind appeared, where the lumens were not formed by coalescing vacuoles. From this observation we make a hypothesis that the fibroblasts may have secreted a substance to the environment, where nonzero concentration of the substance was necessary for intercellular lumen formation in the setting. In [39] similar consideration is made when a common pathway of tubulogenesis is being proposed, starting with initial signal for polarisation for a cell or group of cells that may be in a form of a uniformly distributed component of extracellular matrix surrounding the cells.

Situation setting. Our model will start with a single cell and uniform concentration of one ligand in the surrounding environment. We will use two vaxes (A_i, V_i, X_i), $i = 1, 2$. Zygotic graph is as follows in Fig. 3.1.

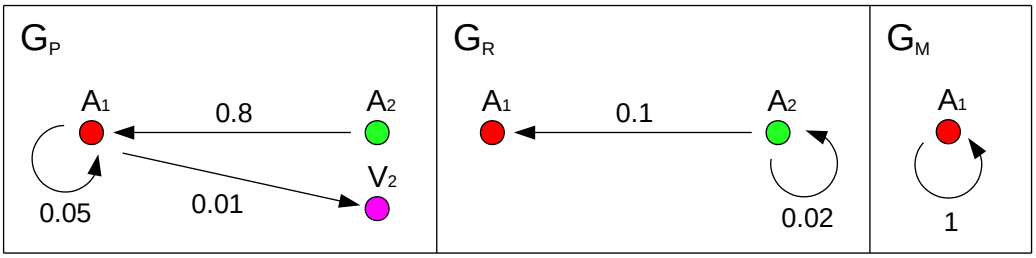

Figure 3.1: Zygotic graph for model of lumen formation. Colors represent given ligands. Apoptosis is not used.

We use square environment lattice with 160 × 160 panes. At the beginning, one cell is placed in the center of the lattice, being in cummulative state on A_2 and having total amount of receptors on A_2 (i. e. formed by V_2) equal to *2*. Detail of the initial cell is shown in Fig. 3.2.

Ligand A_2 is initially uniformly distributed in the environment. Infilling is used to resolve surrounding concentrations when cells move.

Important parameters of the situation are following: *Division direction = Parallel to gradient*, $k_{sd}^{A_1} = 0.01$, $k_{sd}^{X_2} = 0.15$. Other spontaneous decays are zero. For membrane enzymatic activity $k_{ma}^{A_1} = k_{ma}^{A_2} = 0.25$. Other membrane enzymatic activities are irrelevant since, as it is seen from the receptor graph and initial cell receptors, only receptors on A_1 and A_2 are possible in the scenario. Further, there is $D = 0.2$ and *Touching required = false*, which means that there are no constraints on the numbers of touching membrane elements after cell divisions. Further, *Division threshold = 14*, *Membrane capacity = 14.1*, *Min gradient = 0.001*, *Ks change threshold = 1E-6*, $K_d = 0$ for each vax. Note that from the zygotic graph and

initial conditions it follows that in our situation $T_{A1} = [A_1]$. The simulation was run for 900 steps.

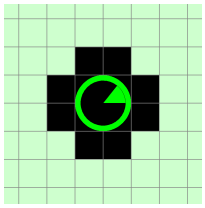

Figure 3.2: Initial cell for model of lumen formation. The cell is in cummulative state on A_2 (denoted by the green color of the outer rim of the pie graph) and has total amount 2 of receptors on A_2. (Denoted by the green sector in the pie graph. The full angle corresponds to Division treshold which is 14 here.) Initial concetration of A_2 in all unoccupied panes is 2.

Results. Development of the situation is coarsely sampled in Fig. 3.3 and Fig. 3.4. At the beginning, the initial cell starts in cummulative state (CS) to A_2. Reminding the zygotic graph (Fig. 3.1), cells in A_2 are producing A_1 and adding receptors. During some time this leads to divisions. Due to membrane enzymatic activity, A_2 is being removed by the cells in their vicinity. Also, A_2 is not being produced in any CS. Thus concentration decrease of A_2 (decrease of T_{A2}) occurs in the area of the initial cluster (Fig. 3.3 (c1); Fig. 3.4 (a1).) Lack of A_2 (T_{A2}) in the area of the center of the cluster causes that A_1 is typically the most seen ligand there by the cells rather than A_2. (Cf. Fig. 3.3 (c3), Fig. 3.4 (a3).) In CS to A_1, this ligand is being produced, but no receptors are being added. Thus the cells staying in CS to A_1 don't divide, divisions occur rather on the rim of the cluster where the influence of A_2 is greater. The gradient of A_2 goes roughly radially from the center of the cluster to the outside. The cells on the rim are dividing in direction parallel to this gradient. At the same time, there is free space in direction outside from the cluster rather than inside it in the local surroundings of these rim cells. Thus, after a division one daughter remains roughly at the position of the mother while the other daughter is located in direction outside from the cluster in the proximity of the mother. The outer daughter is dominantly influenced by A_2 and tends towards another division. The inner daughter is rather influenced by A_1 and stays quiescent with regard to divisions. Production of A_1 in CS to A_2 is by one order of magnitude more intensive than its production in CS to A_1. Thus there is concentration gradient mostly towards the cells on the rim which are in CS to A_2, leading to migration of the inner cells to the outer cells. Summed up, the cells on the edge “proceed outwards“by directed divisions while the cells in the inside move towards these edge cells from the inside, leaving the space there hollow. This leads to formation of a ring of cells that further grows.

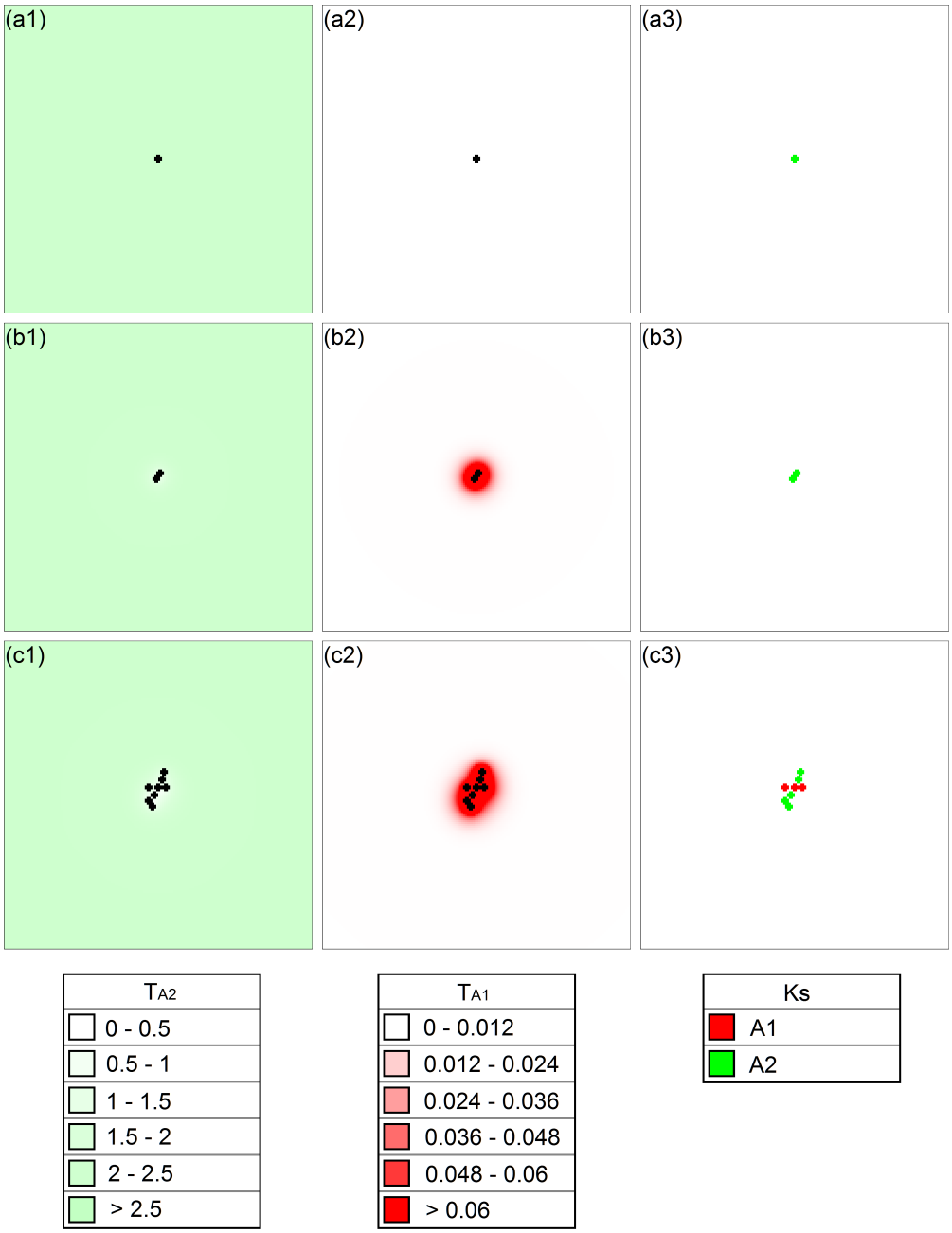

Figure 3.3: Lumen formation – initial cluster. Cells and r-concentration of A_2 (1). Cells and (r-)concentration of A_1 (2) . Cells colored by cummulative states (3). Step 0 - initial conditions (a). Step 150 (b). Step 300 (c).

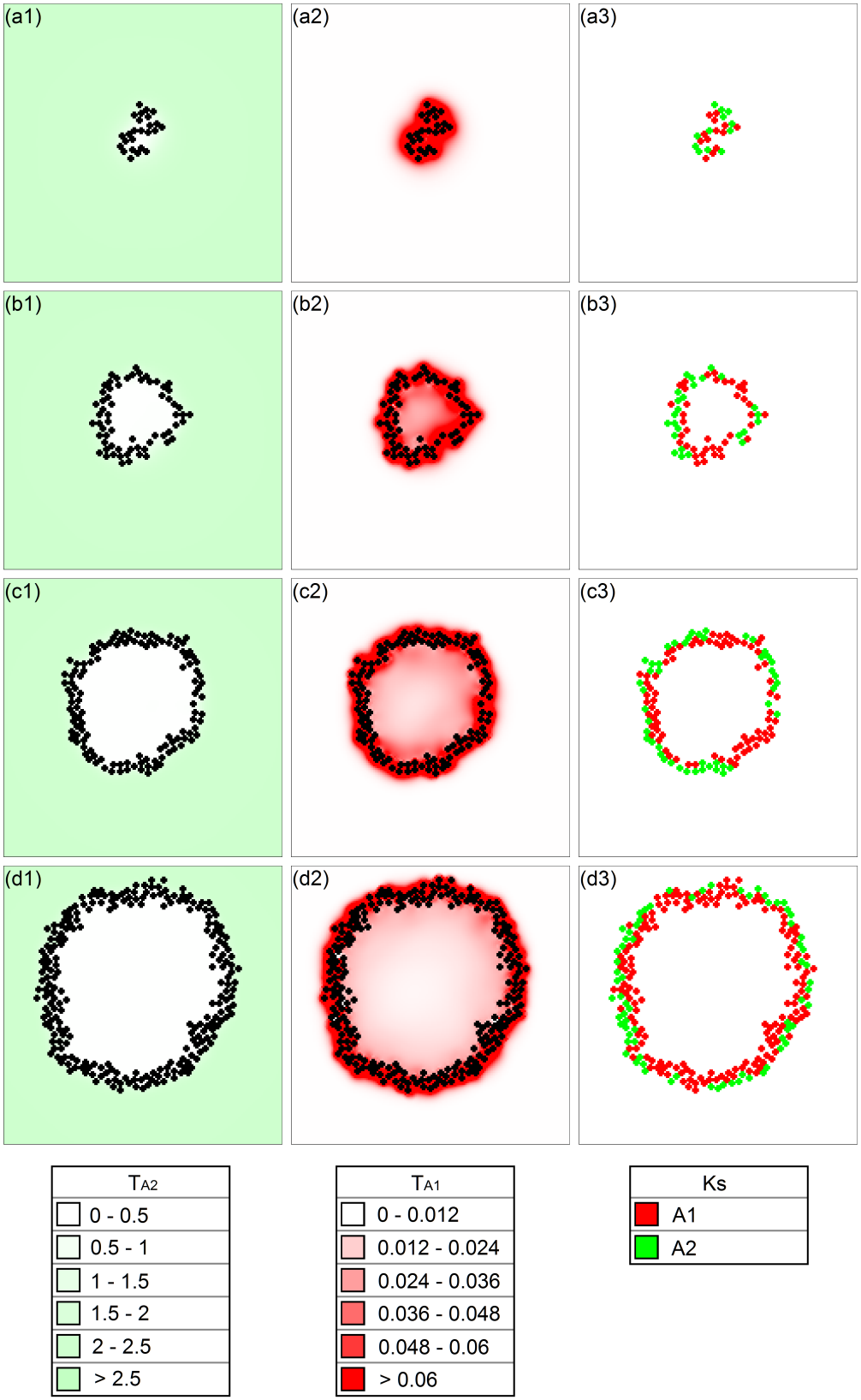

Figure 3.4: Lumen formation – continuation, cavity emergence. Cells and r-concs. of A_2 (1). Cells and (r-)concs. of A_1 (2). Cells colored by cum. states (3). Step 450 (a). Step 600 (b). Step 750 (c). Step 900 (d).

Production of V_2 in CS to A_1 causes removal of (residual) A_2 inside the lumen. Product X_2 undergoes fast spontaneous decay. V_2 is mostly produced by the cells on the inner side of the ring, acting in their proximity and diffusing rather to the inside than to the outside of the ring due to the natural barrier formed by the cells nearer to (at) the outer edge of the ring. V_2 also "remains"in the (inside) location of its production when the cells producing it progressively move away.

Two seeds. We are further interested in how two lumens growing in mutual proximity interact, especially whether coalescing occurs. We have taken a situation with the height being twice the height of the original scenario, having initial concentration of A_2 set to *2* in all panes, keeping all the other parameters the same as in the original setting but using two initial cells (each with properties as in Fig. 3.2) instead of one, located at the vertical axis of the situation rectangle, and being symmetric around the situation center. We have been testing range of initial distances between the cells from 4 (cells touching) to 84. Each time the scenario was run for 900 steps. Results for selected initial cell distances are shown in fig. 3.5. For cell distances between *4* and *16*, single lumen develops. The cells form one cluster during first 300 steps, which is vertically elongated with increasing initial cell distance (data not shown). Around step 450, small lumen is formed, preserving elongation in cases of more distant initial cells. (Cf. Fig. 3.5 (b1).) The lumen further grows, becoming markedly more symmetric than the initial phase if elongation had occurred. (Cf. Fig. 3.5 (c1).)

For distances of initial cells between *17* and *24* the situation is similar. Either one cluster or two clusters containing roughly units of cells form and (nearly) merge within first 300 steps (data not shown). In next 150 steps small elongated lumen forms (cf. Fig. 3.5 (b2)), which further grows. Previous asymmetry is reduced but not so much as in the previous cases (Fig. 3.5 (c2)).

If the distance between initial cells is further increased, being between 25 and 44, separate or nearly separate small lumens form from each initial cell during the first 450 steps, as exemplified in Fig. 3.5 (b3). The small lumens further coalesce into one vertically elongated, where the wall is typically thickened in the places of the vertical center. This thickening remains or grows together with the lumen, generally it is preserved (cf. Fig. 3.5 (c3)). In the growing system, in most cases when the two lumens contacted and started coalescing, the cells in the area near to the contact further redistributed only "partially", this was leading to the irregular thickness of the lumen wall.

When the initial cells are more distant from each other, in range between 45 and 80, initial lumens grow greater before the walls contact, which happens after step 450.

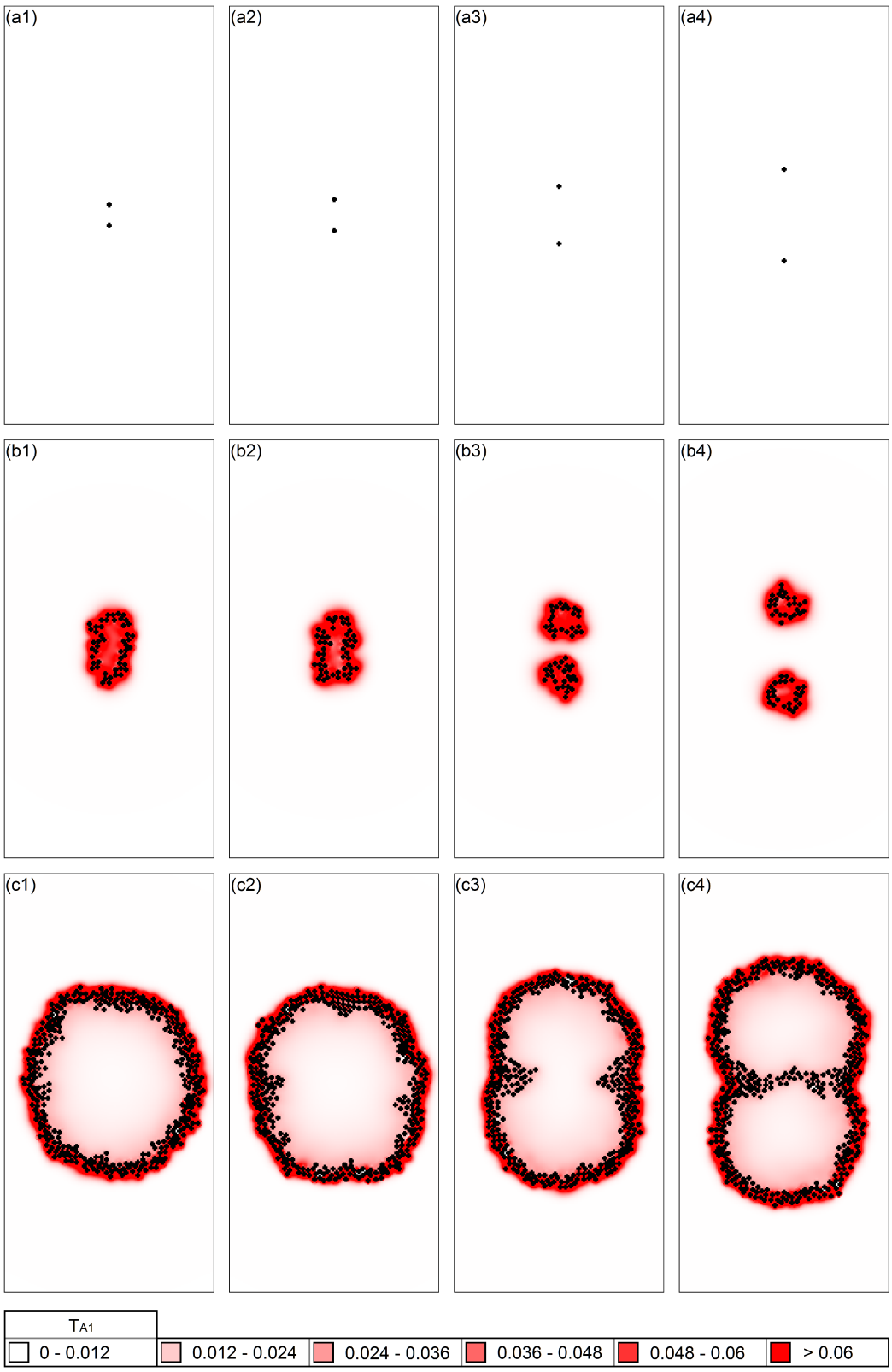

Figure 3.5: Lumen formation from two seeds; cells and (r-)concs. for A_1. Step 0 (a). Step 450 (b). Step 900 (c). Distance of initial cells: 16 (1), 24 (2), 44 (3), 70 (4).

For smaller initial cell distances the lumens coalesce partially, having protrusions from the walls into the inside. Isolated isles of cells in the interior sometimes appear as well, being located along the horizontal axis in the vertically central area of the situation. For more distant initial cells the lumens are fully segregated, as demonstrated in Fig. 3.5 (c4).

We see that putting two initial cells close enough to each other leads to formation of a single lumen. When there are more initial cells in a line with distances between neighbors sufficiently small, the situation is analogical, leading to formation of a single tubular lumen (data not shown).

Larger timescales. Biological tubes can represent a transient phase of organ development. Simple columnar epithelium can give rise to complex architecture [55]. Our model exhibits kind of post-luminal pattern formation, although this was not an intention during its design. When turning back to the original situation, as described in paragraph Situation setting, the simulation was performed for 900 steps. If putting the initial cell to larger area (containing given initial concentration of A_2 in all unoccupied panes), leaving enough space around the cell and letting the situation evolve for longer times, around step 1200 the lumen wall starts having irregular thickness. The outer edge of the growing ring has still roughly circular shape but the inner edge becomes slightly lobular. Further, the lobes extend in the area of attachment to the growing outer rim, which leaves cells in them as moving outwards. Some of the lobes separate and form individual isles, others stay attached to the rim and get elongated. In this way the process continues. The growing rim has still roughly the same thickness while leaving “excessive“ cells in the lobes and isles behind.

From the point of view of lumen formation this growth phase is uninteresting for us. We didn't strive to “code” additional mechanism to the zygotic graph that would stop the process of growing before the formation of lobes starts or that would otherwise fixate the luminal structure, although this might be interesting. We understand our model with its relatively simple zygotic graph as a standalone unit, where only part of it is usable for lumen formation, without handling how to extract this phase or switch the whole process to another “path“. We regard these questions not to be in our current scope.

3.3 Discussion

We have created model of lumen formation starting from a single individual cell.

In [40], cell polarisation is necessary for lumen development, in [45], [49], [50] it is an important component. In our approach polarisation occurs as well but in different senses. In the early phases, membrane enzymatic activity of the initial cell

and its descendants causes polarisation of the environment with regard to (r-)concentration of A_2. A chemical precursor of the lumen arises. Inside is where A_2 is in low (r-)concentration, outside is where it is abundant. Further on, the cells start recognizing the inside, since the A_2 signal is attenuated there and they can switch to A_1. In this way the "chemical polarisation" is transferred to a "cell system polarisation" embodied by cummulative states – a cell in CS on A_1 is "at the luminal edge", a cell in CS on A_2 is at the "outer edge".

In, [45], [49], [50], apoptosis causes cavitation. Our model achieves and maintains cavitation[44] by means of cell rearrangements. In [51], cell rearrangements based on different cell adhesivities are used without requiring an organized behavior on the level of individual cell. We employ chemotaxis as the underlying concept behind rearrangements, which are necessary for formation and maintenance of the cavity.

From physical point of view our model doesn't provide means or conditions regarding mechanical development and maintenance of the hollow structure, which is naturally supported by cell lateral adhesions and basal anchoring. Our approach seems to be suitable for a gelous environment where cells can migrate and stay naturally at their locations without need for mechanical support.

Generally, the model offers a hypothesis concerning the role of cell migration in the early phases of lumen formation. We have shown a context where chemotaxis is sufficient for lumen formation, without need of either apoptosis or cell polarisation.

44 In given timescale, cf. paragraph Larger timescales in section 3.2.

4. Model of Diversified tumour

In this section we will describe a model that tries to enlighten the question of onset of tumour growth starting from an almost healthy cell. By exploring the behavior of the progeny of such cell we will identify various growth phases of the emerging in-silico neoplasm. Parametric analysis will be then carried out, offering explanatory hypotheses for existence of progressive benign-to-malignant transformations on one hand and for occurrence of aggressive phenotypes without apparent observable precursors on the other hand. We call our model the Diversified tumour Model (DTM), stressing relative diversity of cell types and behaviors the model exhibits with regard to simplicity of zygotic graph and initial conditions it is based on.

4.1 Introduction

Cancer is understood as a family of diseases characterized by uncontrolled invasive cell growth. As initial cause of abnormal cancer growth genetic mutations are being considered [68]. However, changes in tissue microenvironment can also initiate and drive cancer formation [69]. In [72], finer structuring into five partially overlapping biological models of carcinogenesis is offered: (1) “Mutational” in sense of point DNA mutations where given gene product directly influences cell proliferation or other neoplastic phenotypes. (2) Genome instability, where mutations in some genes severely weaken genome integrity protection mechanisms. Changes in given genes substantially increase frequency of mutations downstream. (3) Non-genotoxic mechanisms where DNA is not changed structurally but rather functionally, including epigenetic modifications. (4) Somatic cellular selection that concentrates on the role of micro and macro environment in selection of cells that have gained some “advantage”. (5) Tissue organization, focusing on the role of local (micro)environment around the pre-cancerous cells and also incorporates theory of microstatic fields that maintain normal cell behavior and tissue microarchitecture in adult organism.

There are six hallmarks of cancer introduced in [71]: Self-sufficiency in growth signals, insensitivity to anti-growth signals, tissue invasion and metastasis, limitless replicative potential, sustained angiogenesis and evading apoptosis.

In this section we will be only interested in modeling of nonangiogenic tumours. Basic cancerous growth is often simulated by avascular tumour spheroids. With formation of three layered structure of the model tumour microenvironment – proliferating outer rim, sublayer of quiescent cells, and necrotic core – these have been reproduced by practically any modeling approach [73], [74]. There are diffusible nutrients present in the environment, being consumed by the growing cell conglomerate. Due to nutrient depletion in the inner parts of the model neoplasm, the

cells there are becoming quiescent (usually not dividing but alive) and necrotic. In cell-based models the three kinds of states or cell types corresponding to the tumour layers are often incorporated axiomatically or rather explicitly in given model definition.

Another approach to biological explanation and followingly modeling of internal tumour structuring is the cancer stem cell (CSC) hypothesis [75], [68], [76]. tumour is viewed as a composition of two kinds of cells: CSCs and the rest. CSCs have unlimited proliferation capacity while the other cells have only limited replication potential. A CSC can divide either into two CSCs or into one CSC and one differentiated cell. In [77], [78], tumour growth with CSCs has been modelled using cellular Potts and cellular automata respectively. The models show that when only proliferative cells (CSCs) are present, spherical shapes are produced. If asymmetric CSC divisions are allowed, tumours with irregular borders arise. In the latter case, the whole tumour turns out to be a composition of smaller rather spherical conglomerates, where each arises from a single CSC. These conglomerates can be viewed as "self-metastases" [79], [80]. When killing part of the cells in growing neoplasm in certain time in [77], as a model of therapy, inner properties of the followingly repopulated tumour differ for the only-CSC and differentiating scenarios. In the latter case, relatively few CSCs remaining after the therapy undergo "many" divisions during the repopulation, leading to greater accumulation of mutations in comparison with the former case where all cells divide evenly in the renewal of the tumour. The differentiating scenario thus leads to more aggressive regrown phenotype after therapy than the only-CSC (undifferentiating) case.

One way of modeling tumour growth onset is by disruption of tissue homeostasis [76]. Another approach is focusing on mutations: In [70] a 3D agent-based stochastic model is used to simulate transformation of normal cells to tumour cells within a growing conglomerate starting from one normal cell. The six hallmarks of cancer stated in [71] are incorporated in the scenario as phenotypical mutations, which occur with selected probabilities during cell divisions. Other kinds of probabilistic events like competition for cell survival with a neighboring cell or elimination of a cell due to mutation are also included. It has been observed within the model that early-onset cancers proceed through a different sequence of mutations than late-onset cancers.

4.2 Diversified tumour Model

Situation setting. We use two vaxes (A_i, V_i, X_i), $i = 1, 2$. The environment lattice is a square 250×250 panes. At the beginning there is one cell in the middle of the situation. There is a rectangular area surrounding the initial cell containing A_1 in concentration 3. In the rest of the situation the initial concentration of A_1 is zero. Other substances don't participate in the situation in free diffusible form. The initial

conditions regarding the starting cell and its proximity are shown in Fig. 4.1. Pie graphs, if displayed on cells in figures (e. g. Fig 4.1 (b)), will have the general semantics as follows: Color of the outer annulus is the color representing the substance the cell is in cummulative state on. Full angle of the circle inside represents membrane capacity. Individual colored sectors stand for amounts of receptors on ligands denoted with corresponding colors. If there is an arrow emanating from the center of the pie graph, it represents gradient of the ligand the cell is in CS on, perceived by the cell. In our DTM scenario, A_1 will be marked by red color, A_2 and V_2 will be both marked by green color since conceptually they have the same function.

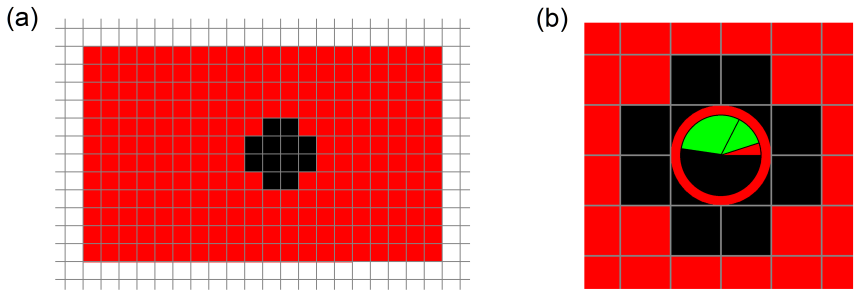

Figure 4.1: Initial cell and its proximity. The rectangle surrounding the initial cell contains concentration 3 of A_1 (red), it is horizontally asymmetric and vertically symmetric around the cell (a). Initial setup (detail) of the starting cell (b): The cell is in cummulative state on A_1 (red annulus) and contains following amounts of receptors: 40 on A_1 (the small red sector), 100 on A_2 (the smaller green sector) and 240 on V_2 (the larger green sector). The cell has no receptors on A_2. Ligands A_2 and V_2 are both marked with green color since semantically they play the same role. Division treshold is 800 (the full circle of the pie graph).

Zygotic graph follows in Fig. 4.2.

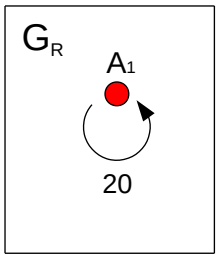

Figure 4.2: Zygotic graph. $G_P = G_M = G_A = \emptyset$.

We prescribe that if a cell divides, the daughters must be touching by exactly one membrane element. I. e. we have *Touching required = true* and *Min common*

elements = *Max common elements* = *1*. Regarding decays, there is $k_{sd}^{A_1} = 0.001$, $k_{ma}^{A_1} = 0.3$. Further, there is *Division direction* = *Parallel to gradient* and *Min gradient* = *0.001*, *D* = *0.2*, *Division threshold* = *800*, *Membrane capacity* = *801*, *Ks change threshold* = *1E-5*. $K_d = 0$ for both vaxes. Infilling is used for treatment of surrounding concentrations in cell movements within internal simulation of cell divisions.

As we can see from the scenario definition, the only diffusible ligand in the situation is A_1. Thus there is $T_{A1} = [A_1]$. Ligands A_2 and V_2 are present solely in receptor form. They perform signaling between adjacent cells. Adjacency of daughter cells just after division is forced.[45] V_1 is present in receptor form only, mediating perception of A_1 by the cells. Conceptually, ligand A_1 plays the role of a pathological "oncogenic" signal, its initial concentration in the surroundings of the cell represents exposition of the cell to that signal. Ligands A_2 and V_2 model (contact-mediated) physiological signal, in corresponding cummulative states a cell "stays quiet". The initial cell is slightly "damaged", or "little" sensitive to the pathological signal, by means of the initial presence of receptors on A_1. However, in CS on A_1 the cell adds receptors on A_1 (only). If the cell stays in this cummulative state long enough, this will send the cell to division. It applies for the daughters as well. The situation is schematically sketched in Fig. 4.3.

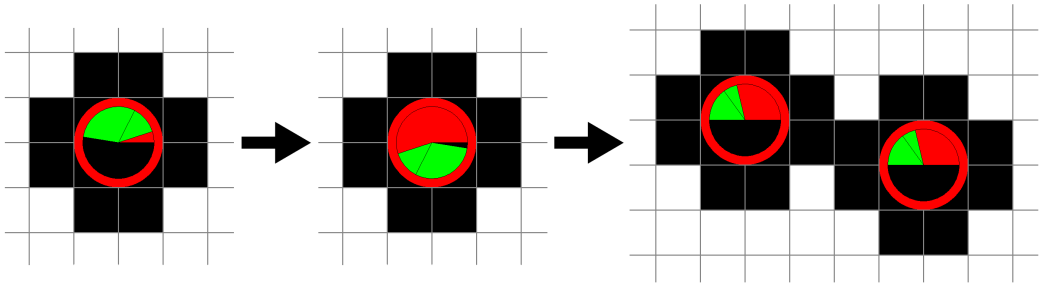

Figure 4.3: Staying in the cummulative state on A_1 (red annulus) for the initial cell throughout multiple steps leads to adding receptors on A_1 (red sector) and followingly to division. Relative amount of receptors on A_1 increases, relative amount of receptors on A_2 and V_2 (green sectors) decreases. Free diffusible A_1 concentraions are not shown.

Cell health and divisions. Let's assume that every cell divides whenever it *wants to divide.* From whence it follows that at the end of computation of every step the total amount of receptors is less than *Membrane capacity*. Let's further suppose that a cell is always in CS on A_1, including its progeny. If a cell divides, number of receptors on every ligand is halved in the daughters while *Membrane capacity* (and *Division threshold)* are the same in the mother and in each daughter. Let $[V_2^m]^0$, $[A_2^m]^0$, be the

45 Adjacenecy in particular cell pairs is generally not preserved due to changes of cell amount and locations caused by further divisions.

initial amounts of receptors of the initial cell on A_2, V_2 respectively. We can easily see that

$$[V_2^m] = \frac{1}{2^d} \cdot [V_2^m]^0 ,$$

where d is the number of divisions the cell has undergone and $[V_2^m]$ is the amount of receptors on the cell in time of concern. For $[A_2^m]$ the situation is analogical. Further, for a cell between any two divisions we have

$$\frac{1}{2} Dt - \left([A_2^m] + [V_2^m]\right) \leq [V_1^m] \leq Dt - \left([A_2^m] + [V_2^m]\right) ,$$

where Dt is *Division threshold*, and $[V_1^m]$ is the amount of receptors on A_1 in time of interest. Summed up, we see that $[V_2^m]$ and $[A_2^m]$ on individual cell membrane are decreasing exponentially with the number of divisions the cell went through while $[V_1^m]$ is bounded between two (positive) constants. Let's now assume that the sum of all receptors on a cell is Mc = *Membrane capacity* in discrete time $n > 0$. Let the cell be in CS on A_1 in the $(n+1)$th step and let receptor normalization occur. (I. e. the cell *couldn't divide*.) According to (2.51) we have

$$[V_2^m]^{(n+1)} = [V_2^m]^{(n)} \cdot \frac{Mc}{Mc + \delta(V_1^m)} , \tag{4.1}$$

where $[V_2^m]^{(n)}$ is the amount of receptors on A_2 in discrete time n and $\delta(V_1^m)$ is the amount of receptors on A_1 the cell adds to its membrane when being in CS on A_1. For receptors on V_2 the situation is analogical. Obviously,

$$[V_1^m]^{(n+1)} = Mc - \left([V_2^m]^{(n+1)} + [A_2^m]^{(n+1)}\right) .$$

Thus we see that if a cell remains in CS on A_1 and it *wants to divide* but can't, the evolution of membrane receptor composition is structurally analogical to the case when the cell is in CS on A_1 and (its progeny) undergoes divisions. Since the fraction in (4.1) is positive and less than one, amounts of receptors on A_2 and V_2 both decay exponentially. At the same time, $[V_1^m]$ is bounded between two (positive) constants. Since a cell in cummulative state on a ligand other than A_1 is quiescent, we see that the structural influence of staying in state on A_1 is “cummulative”, being only interrupted by staying in other cum. states. Stated otherwise, if the amount of receptors on A_2 and V_2 is understood as a degree of health of a cell, the cell has a “memory for disruption”. If the process of losing this health is interrupted at some time (by switching to another state), when it restores, it continues at the stage it was before the interruption. For our particular setting, assuming cells can divide, time between two divisions (i. e. the time after which $[V_2^m]$, $[A_2^m]$ are halved, when

starting to count at a division) needed to be spent in CS on A_1 is 20 steps. Halving time for $[V_2^m]$, $[A_2^m]$ if receptor normalization is used is approx. 28 steps in CS on A_1.

Physiology-reminiscent growth. The phases shortly after starting simulation of our scenario are shown in Fig. 4.4.

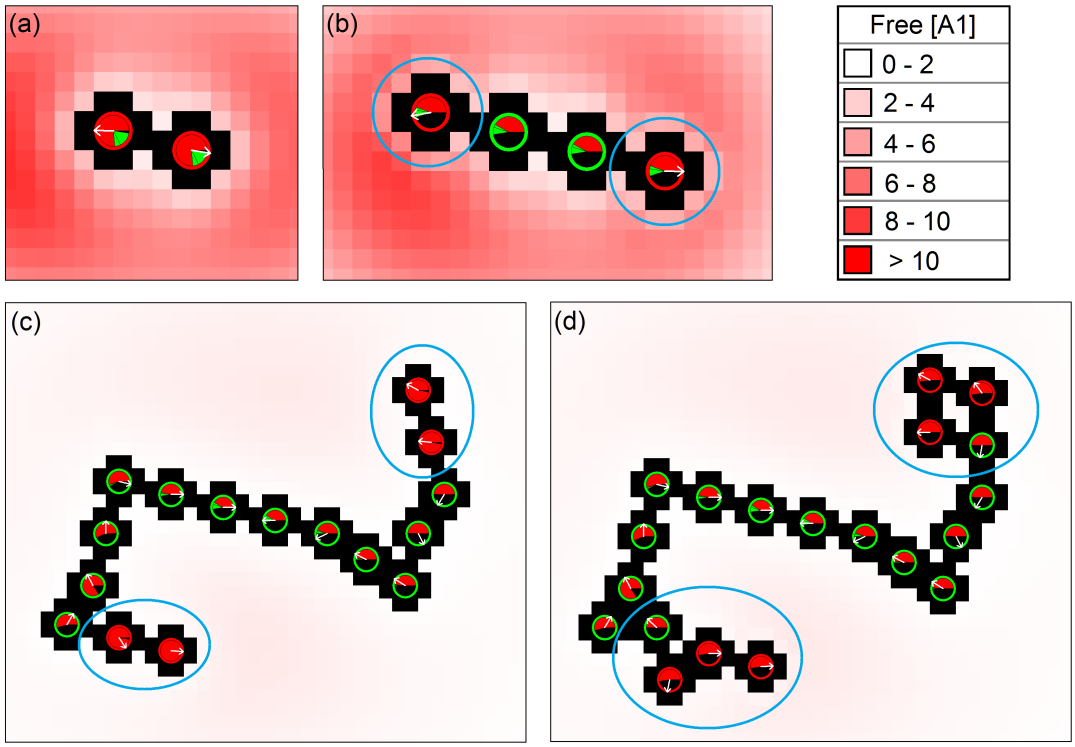

Figure 4.4: Physiology-reminiscent growth. White arrows denote gradient of cummulative state perceived by individual cells, missing arrow means that gradient magnitude is < Min gradient. (a): Step 40. Situation just before the second division. (b): Step 43. Differentiation of tip cells (denoted by circles) and quiescent inner cells. (c) Step 180: Correct differentiation to tip / quiescent cell stops working, all 4 marked cells will divide. (d): Step 182: End of physiology-reminiscent growth. Marked cells are daughters of those marked in case (c). Only one cell in each quadruple gets quiescent.

After the division of the initial cell, its daughters are most influenced by ligand A_1 in the surroundings and remain in cummulative state on it. Due to membrane enzymatic activity the ligand is being cleaved in the surroundings of the cells, its concentration lowers most near the center of the two-cell conglomerate. Since the cells see no A_1 by the membrane elements they are touching each other and by contribution of given A_1 concentration lowering, the perceived gradient direction in the cells is roughly perpendicular to the axis of symmetry between them, heading away from the center of mass of the conglomerate in each cell. The situation is shown in Fig. 4.4 (a). When

these two cells divide in the opposing directions described above, after a short time the inner cells of the nascent "thread" turn to CS on A_2 or V_2 (Fig.4.4 (b)) since concentration of A_1 in their surroundings is lowered, each of them feels the physiological signal (A_2, V_2) by two membrane elements and the membrane "area" of each of these cells capable of feeling A_1 is decreased by given two membrane elements that are touching the neighbors. On the other hand the outer cells feel the physiological signals only by one membrane element each, concentration of A_1 in their surroundings is higher than in the center of the situation and only one membrane element in each outer cell is "blocked" from feeling A_1 by touching a neighbor cell. The outer cells remain in CS on A_1. This kind of scenario recurs throughout several following divisions. Cells on the edges are remaining in CS on A_1 while the inner cells are getting quiescent some time after division. Phenomenologically, we can understand this as "differentiation", where one daughter remains a tip cell while the other becomes the "quiescent nondividing cell". This can be regarded as kind of physiological behavior at first sight, part of "normal functionality of the tissue the cells originally belong to". However, despite being "morphologically correct", internally, the sensitivity to physiological signals in the cells decreases over divisions. In Fig.4.4 (c) the penultimate cells have too little receptors on A_2 and V_2 so that the A_1 signal prevails in them and they go to division before the A_1 signal would be "lowered enough" by membrane enzymatic activity, diffusion, and spontaneous decay, allowing them to switch to some of the quiescent states. Both pairs of cells at each end divide, as it is seen in Fig. 4.4 (d).

Pathological differentiated growth. As we can see in Fig. 4.4 (d), one cell in each marked quadruple has become quiescent.

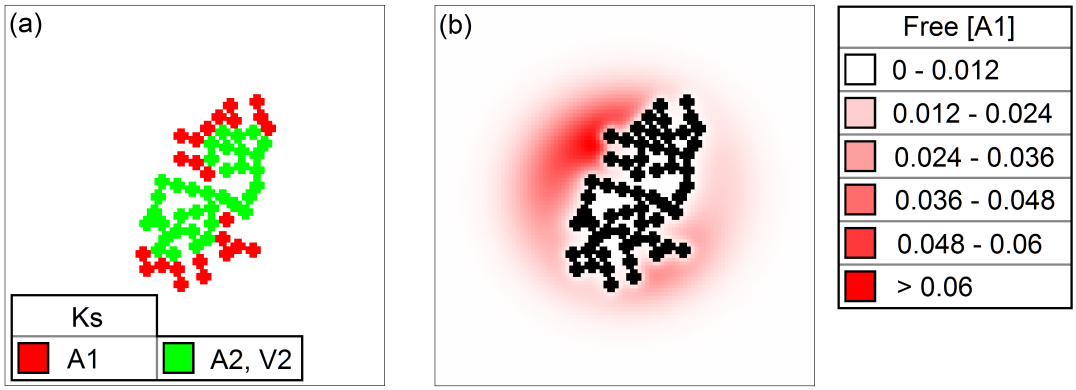

Figure 4.5: Pathological differentiated growth; step 270. Rim of dividing cells (in cum. state on A_1) forms, cells in the inside of the forming conglomerate differentiate (a). Concentration of A_1 is being reduced inside of the conglomerate in comparison with its outer surroundings due to membrane enzymatic activity (b).

In this phase, differentiation to the quiescent states still occurs, but only in cells being more surrounded by other cells than in the previous phase and with a delay after division. A rim of growing cells forms, leaving quiescent differentiated cells behind. The situation is shown in Fig. 4.5. Ligand A_1 is being progressively cleaved inside the forming conglomerate. This leads to switching of the inner cells to CS on A_2 or V_2 some time after division, when concentration of A_1 becomes low enough. Further progression of the growth with the rim fully surrounding the conglomerate is shown in Fig. 4.6 (a).

Pathological undifferentiated growth. After some time the amount of receptors

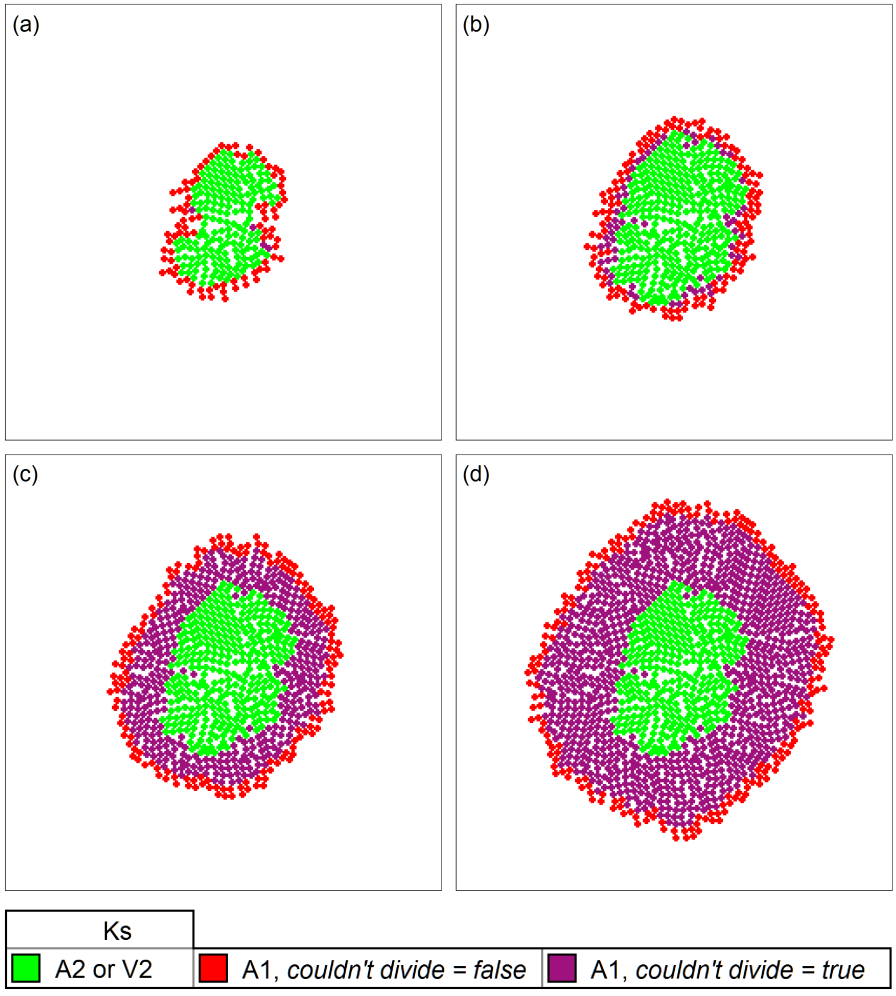

Figure 4.6: Pathological undifferentiated growth – transition and progress. Step 393: Pathological differentiated growth occurs, cells behind the growing rim are differentiating (a). Step 480: Cells adjacent to the rim stop differentiating, staying in CS on A_1; they want to divide but due to lack of space they cannot (b). Step 580 (c), step 700 (d): The coglomerate is growing on the rim. No new differentiation occurs, the previously differentiated quiescent core (cells in CS on A_2 or V_2) remains conserved.

on A_2 (and V_2) in the cells in CS on A_1 on the rim and in its proximity goes below the value of parameter *Ks change threshold.* If a cell wants to change the cummulative state, this threshold is the smallest difference between the signal for the new CS and for the current one (i. e. A_1) that must be exceeded in order to perform the CS change. Since the amount of receptors on A_2 (and V_2), that is the maximum possible strength of the signal "generated" by these receptors, is under the threshold, even if the total signal for staying in CS on A_1 is zero, the cell is not able to change its cummulative state. We will call such cells totally transformed. A totally transformed cell either progressively goes to division producing totally transformed daughters or it has the *Couldn't divide* flag set, meaning that it wants to divide but due to (spatial or geometrical) constraints it cannot. Totally transformed cells are not able to hear (process) any physiological signals from the environment.

Progress of our scenario is shown in Fig. 4.6. After a period of continuation of the pathological differentiated growth (Fig. 4.6 (a)), totally transformed cells start to occur and followingly all the cells in CS on A_1 become totally transformed. Small layer of cells with *couldn't divide* flag in CS on A_1 not going to differentiation any more forms (Fig. 4.6 (b)). Further on the layer grows in thickness by proliferation of the rim cells (Fig. 4.6 (c), (d)).

Summary. By means of rather simple initial conditions and zygotic graph, together with appropriate setting of situation parameters, we have constructed model of progressively transforming tumour. Starting from a single partially damaged cell getting an "oncogenic", "stressing" impulse, process of tumour growth started and three phases have been observed: Physiology-reminiscent growth, pathological differentiated growth and pathological undifferentiated growth. We can see this process as a competition of two influences or other processes: The physiological one, leading to formation of a "structured" fibre in the first phase, and the pathological one, leading to uncontrolled cell divisions, which has fully burst in the third phase in totally transformed cells. The second phase can be interpreted as an intermediate stage.

4.3 Parametric analysis of DTM

We will examine the behavior of our scenario in dependence on two parameters: $k_{sd}^{A_1}$ and $k_{ma}^{A_1}$, also referring them as spontaneous decay and membrane enzymatic activity respectively in this section, assuming A_1 is always in concern.

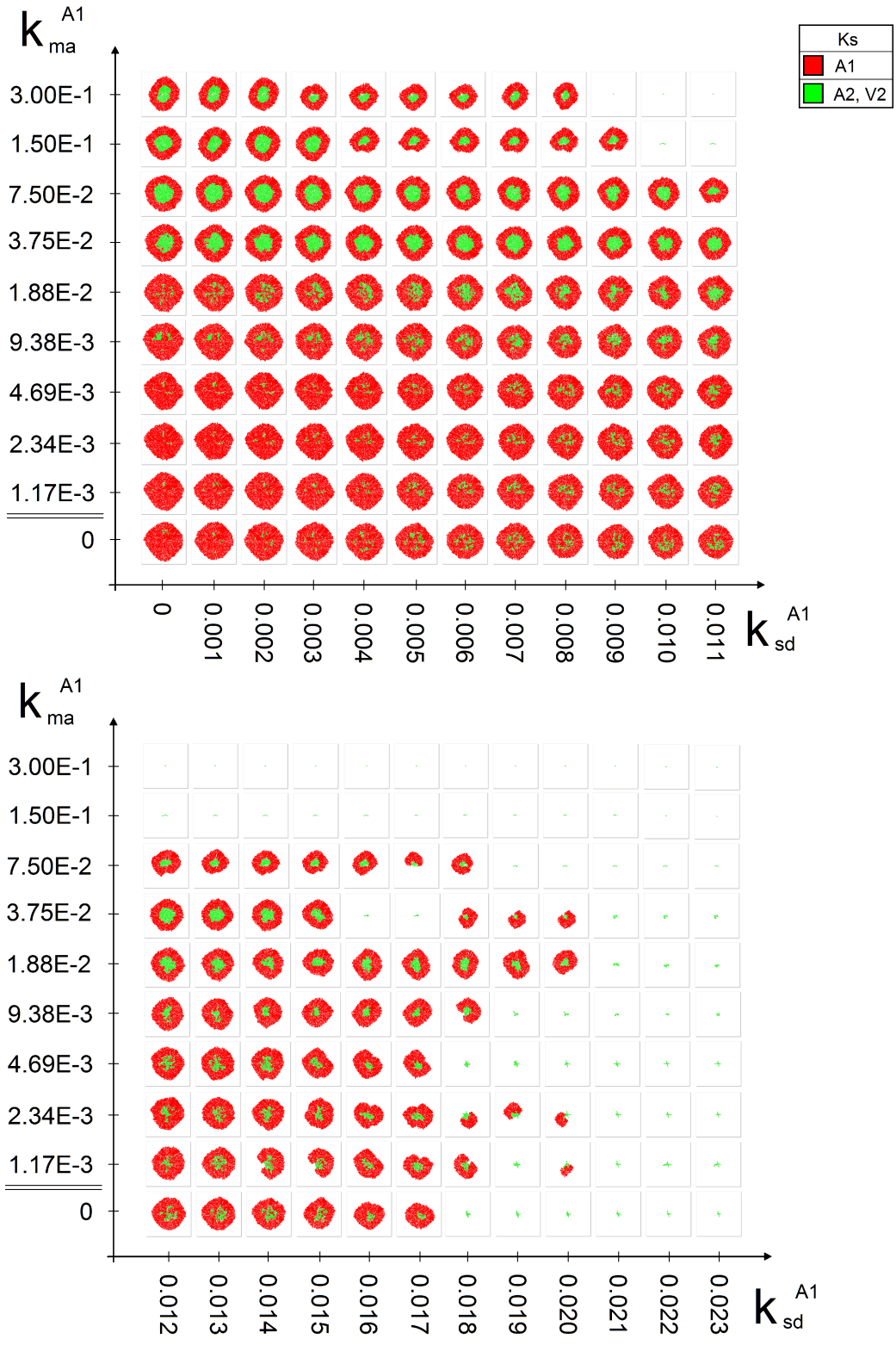

Figure 4.7: DTM parametric analysis overview. Each scenario has been run for 700 steps. Situations containing cells in CS on A_1 reached pathological undifferentiated growth. In the others, growth of the conglomerate stopped with all cells being quiescent.

For $k_{sd}^{A_1}$ we will be sampling interval $<0,\ 0.023>$ with constant step 0.001. Regarding $k_{ma}^{A_1}$, we will examine values $0{,}3 \cdot 2^i,\ i = -8, -7, \ldots, 0$ and case $k_{ma}^{A_1} = 0$. All the other parameters will be the same as in section 4.2, running each simulation for 700 steps. Overview of results is shown in Fig. 4.7.

Basic findings. There are two kinds of resulting scenarios. In the first one uncontrollably growing totally transformed cells arose. In the other, all cells became quiescent entering CS on A_2 or V_2, growth of the conglomerate stopped. We can divide the sampled parameter space into three categories along the $k_{sd}^{A_1}$ axis (cf. Fig. 4.7): For "small" values in interval $<0,\ 0.008>$ all the situations are of the uncontrollably growing kind regardless of the value of $k_{ma}^{A_1}$. When the values of $k_{sd}^{A_1}$ are "large", in interval $<0.021,\ 0.23>$ (and greater, data not shown), stopping growth is the case for every situation, for all values of $k_{ma}^{A_1}$. In the "middle", for $k_{sd}^{A_1}$ in $<0.009,\ 0.020>$, either uncontrollably dividing or stopping growth occurs in dependence on $k_{ma}^{A_1}$. For intensive membrane enzymatic activity ($k_{ma}^{A_1} = 0.3,\ 0.15$), stopping growth starts to occur for smaller values of spontaneous decay than for the less intensive membrane enzymatic activities, where sometimes fluctuations between final conglomerate types appear for constant $k_{ma}^{A_1}$ with growing $k_{sd}^{A_1}$.

Based on these findings we conclude that spontaneous decay plays substantial role in inducing the scenario where all cells become quiescent (after some time). For sufficiently large values of $k_{sd}^{A_1}$ this type of situation occurs independently on $k_{ma}^{A_1}$. On the other hand, membrane enzymatic activity has only limited potential to create growth-stopping scenario, unable to achieve this without synergy with spontaneous decay.

Dedifferentiation. For small values of both parameters, roughly for $k_{sd}^{A_1} < 0.06$, $k_{ma}^{A_1} \leq 4.69\text{E-}3$, the quiescent core in the middle of the conglomerate is strongly reduced or nearly missing. (Cf. Fig. 4.7.) Due to low decay and cleavage, concentration of A_1 remains high in the center of the situation for a long time. Most of the cells in the central area are strongly influenced by A_1 for this long period and never switch to a quiescent state. Some cells do become quiescent, but only transiently, dedifferentiation occurs after a while: When such a cell first switches to CS on A_2 or V_2 it must be receiving sufficiently strong signal from its neighbors at that moment. If the neighbors are staying in CS on A_1, after a while they want to divide but they can't. Receptor normalization takes place in these cells, progressively decreasing the amounts of A_2 and V_2 on their membranes. Thus the signal that the receptors of given cells are exerting on the quiescent cell is weakening. Since A_1 is still present in the microenvironment in considerable concentration, the quiescent cell switches back to CS on A_1. Staying there leads to receptor normalization after some time, continuing transformation of the switched-back cell. In some cases this

scenario occurs inductively for islands of cells in CS on A_2 or V_2 surrounded by couldn't-divide cells in CS on A_1. The cells on the rim of the island dedifferentiate. After some time the signal they are sending to their inner neighbors ceases due to receptor normalization and followingly the inner neighbors dedifferentiate as well, etc. Finally, the whole island disappears and all its original cells are turned to CS on A_1.

Another reason for dedifferentiation, not necessarily observed for values of $k_{sd}^{A_1}$ and $k_{ma}^{A_1}$ as specified above, is cell translocation due to division. Let there be a cell sending the "quiescing" signal to its adjacent neighbor. If the cell divides, none of the daughters now touches the cell the mother was adjacent to. Thus the original neighbor of the mother now gets less of the "quiescing signal" and dedifferentiates.

Transition prefix. We will be further interested in conglomerate size in uncontrollably growing scenarios just before totally transformed cell(s) appear, in dependency on $k_{sd}^{A_1}$ and $k_{ma}^{A_1}$. We will regard a cell to be totally transformed if it is in CS on A_1 and the amount of receptors on V_2 is less than *Ks change threshold.* Obviously for any totally transformed cell the amount of receptors on A_2 is below the threshold. as well since the amount of receptors on A_2 on the initial cell is less than its amount of receptors on V_2 and this inequality is preserved throughout divisions and in receptor normalization. We will assume that in the uncontrollably growing scenario in any simulation step there is a cell C that has been uninterruptedly in CS on A_1 since the first step and receptor normalization never occurred in the history of C. For our particular scenario setting we can compute in a straightforward way that the last step before C gets totally transformed is step 500 and C went through 24 divisions. We have run the scenario for each parameter combination in our sampling for 500 steps. Total numbers of cells in resulting conglomerates are shown in Fig. 4.8.

We will call the number of cells in a scenario just before the first occurrence of a totally transformed cell a *transition prefix*. From our data (Fig. 4.8) we see that transition prefix is basically decreasing with increasing spontaneous decay. Only large values of membrane enzymatic activity cause transition prefix decrease for wider range of values of $k_{sd}^{A_1}$. For $k_{ma}^{A_1} = 1.5E\text{-}1$ there is a relatively patent "jump"between $k_{sd}^{A_1} = 0.03$ and $k_{sd}^{A_1} = 0.04$, similarly for $k_{ma}^{A_1} = 3.0E\text{-}1$ there is a jump between $k_{sd}^{A_1} = 0.02$ and $k_{sd}^{A_1} = 0.03$. In both cases for the larger $k_{sd}^{A_1}$ there is a linear tip cell growth with a single tip cell in the whole situation for some time shortly after the scenario simulation starts. Further massive growth "begins" from this single tip cell. For smaller $k_{sd}^{A_1}$ two or more tip cells arise in the early stage, performing linear "thread" growths for some time. Then the massive growth "starts" from these multiple "seeds" in parallel, leading to greater conglomerate in comparison with the first case at the time the simulation is stopped.

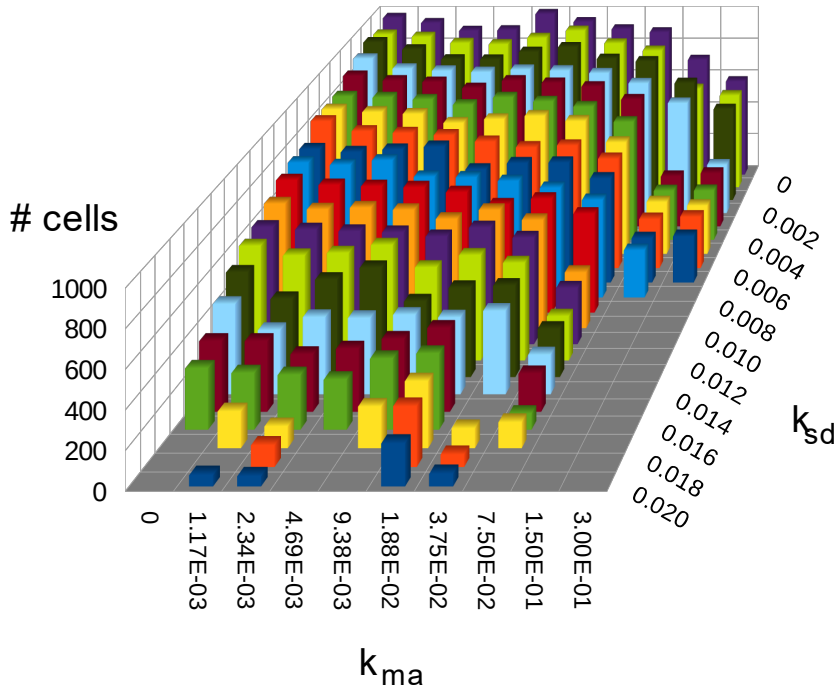

Figure 4.8: Cell counts in step 500 for uncontrollably growing scenarios; k_{sd} and k_{ma} relate to A_1. Zero values (no bars) indicate growth-stopping scenario for given parameter combinations.

Majority of the smallest transition prefixes occur roughly for $k_{sd}^{A_1}$ in $\langle 0.018, 0.020 \rangle$. In most of these situations there is a period where only one or two tip cells are growing for longer time leaving quiescent strings behind. On the other hand, in situations where the largest conglomerates form, a growing rim of rather circular shape forms shortly after the beginning, having proliferating cells along whole its perimeter nearly all the time.

Theoretically, there are two limiting growth modes (see. Fig. 4.9). Firstly, the "linear"one with a single tip or stem cell, producing one further nondividing cell and one stem cell that divides again, etc. This leads to linear dependency of the number of cells on the (maximum) number of divisions in a history of a single cell. After n divisions of the "stem cell" we have totally $n+1$ cells. In the other mode each daughter further divides, and so forth. This leads to exponential dependency. After n divisions in a history of one cell we have 2^n cells in the whole conglomerate when assuming that the time between two divisions is the same for every cell.

In our scenarios, some of them approached the limit linear growth quite effectively. The smallest conglomerate had 50 cells, with the maximum number of divisions in a history of a single cell 24.

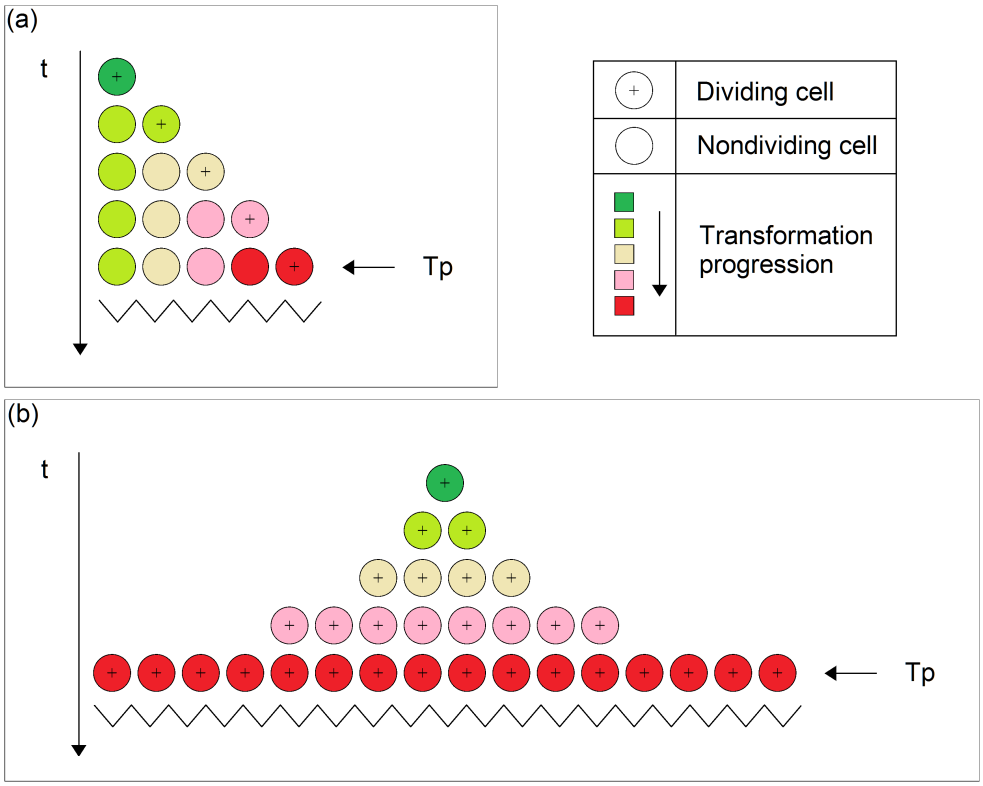

Figure 4.9: Transition prefix (Tp) under theoretical limiting growth modes. Linear growth (a). Exponential growth (b).

The largest tumour in our 500 steps scenario had something less than 1000 cells, making the distinction in final conglomerate sizes not smaller than one order of magnitude upon entering the uncontrollably dividing growth mode.

Detectability. There are grading systems for various kinds of cancer including, astrocytomas [82], breast cancer [81] or ovarian cancer [83]. Generally, grades are bound with degree of cell differentiation in the tumour. Lower grades mean well or moderately differentiated cells, higher grades mean poorly differentiated or undifferentiated cells [84]. If there is evidence of more than one grade or differentiation in a tumour, the least differentiated is regarded as the histopathological grade. Increasing grades are connected with increasing malignancy. Lower grade tumours grow slower, high grade tumours are strongly aggressive and infiltrative. While some kinds of high grade tumours form rapidly as de novo neoplasms without clinical or histological evidence of lower grade precursor lesions, others develop progressively from lower grade tumours [85]. The theoretical limiting growth modes (cf. Fig. 4.9) until the totally transformed cells occur offer a hypothesis for these two kinds of emergence of high grade tumours. We will assume that totally transformed cells divide always into two further dividing daughters. In the case of the linear growth mode (Fig. 4.9 (a)), this exponential growth starts from

two totally transformed cells. There is a precursor “benign” or “less malignant” tumour containing number of cells linear with respect to the number of divisions a totally transformed cell has undergone. On the other hand, the precursor of the totally transformed tumour in the exponential growth mode (Fig. 4.9 (b)) has exponential number of cells in dependency on the number of divisions in a single line. After the total transformation occurs, the growth has the same character as it had before. The linear transition prefix is “small” in comparison with the exponential one and in our hypothesis we interpret this in terms of detectability: There are so little cells in the precursor neoplasm that it is impossible or unlikely to be detected by (the state of the art) medical cancer diagnostic methods. The smallest detectable size is generated nearly exclusively by the exponentially growing progeny of the (two) totally transformed cells. Thus the detected tumour is a highly aggressive one, composed almost solely of the totally transformed cells. When looking at the exponential transition prefix, neoplasm of this size is big enough to be detected. Even before total transformation is reached, the “benign“ or “moderately malign“ neoplasm can be discovered by the diagnostic tools.

We have demonstrated that in terms of DTM a good approximation of the linear growth before reaching total transformation can be achieved. Further, within the spatial constraints given by the model definition, faster growth modes, although not exponential, are possible. Each of these growth kinds is a consequence of different values of $k_{sd}^{A_1}$ and $k_{ma}^{A_1}$, where all the other parameters are the same in both “kinds“ of scenarios. More particularly, linear growth modes, modelling aggressive tumours without apparent precursors, tend to occur in the areas of the space of these parameters where changes or fluctuations between stopping and unstopping growth occur.

4.4 Discussion

In this chapter we have introduced Model of Diversified tumour. Starting from uncomplicated initial conditions and having simple zygotic graph, together with appropriate setting of other model parameters we got a tumour with three distinct growth phases generating corresponding parts of the neoplasm: Physiology-reminiscent growth, pathological differentiated growth and pathological undifferentiated growth. Unlike classical avascular spheroid models generating proliferating outer rim, sublayer of quiescent cells and necrotic core [73], [74], despite some similarities our growth phases rather resemble generation of structures used in histopathological classification of tumour grades [84] based basically on degree of differentiation. Since differentiation is realized in quite a simple way, morphologically distinctive structures are observed in physiology-reminiscent growth only. Tissues generated by pathological differentiated growth and pathological undifferentiated growth are distinguished based on cell cummulative

states, without obvious morphological distinctions. Another feature our model differs in from classical avascular spheroid simulations, bound to the design of the model world, is the level of axiomatization. More precisely, the distinction is in the motivational level captured. In agent-based modeling, often entities closely related to observed phenomena, like oxygen or nutrient concentration and depletion or cell necrosis, are axiomatized. Other kinds of such entities are conceptual biological explanations, theories, or hypotheses, as cancer stem cells [77], [78]. In DTM, we have inherited the axiomatizing primitives as vaxes, spontaneous decay, membrane enzymatic activity, cell division direction or cell touching after division. Rather than attempting to implement the conceptual hypotheses to the particular DTM scenario definition, we only did basic usage of the axiomatizing apparatus. As results we obtained more or less emergent properties, that might have been tempting to be axiomatized instead. Let's take the notion of cancer stem cells. We did not put rules encoding symmetric or asymmetric "stem cell" divisions into the model. This concept, realized by the change of cummulative state of one daughter while preserving cummulative state of the other one, was present as a consequence of the local interplay of the cells and the microenvironment in the tip cell thread forming growth in the physiology-reminiscent phase. Then this concept was present in the pathological differentiated growth, where a rim of dividing cells formed while the inner daughters were switching to be quiescent. The microenvironment conditions were different than in the previous case and so was the resulting morphology. Further, these two different "CSC" modalities got a next new meaning in the detectability hypothesis. The thread forming tip cell growth is basically responsible for generating the linear transition prefix that we connect with de-novo formation of aggressive neoplasms. On the other hand, the pathological differentiating modality is responsible for large less aggressive conglomerates we connect with highly malignant tumour development from a lower less malignant grade. We got a two - tiered conceptual structure as a result. If willing to use the notion of CSCs, these are strongly implicit for the model, appearing and disappearing under various local spatio – temporal conditions. However, "driving" them kind of indirectly to form particular behavior in given conceptual tier turns out to be matter of quantitative parameter combinations, how it was disclosed by the parametric analysis. Instead of coding phenomenologically bound rules or concepts axiomatically, we got the "formulation" of (un)expected higher level behaviors in terms of locations or regions in the parameter space of our original axiomatization.

Focusing now on the other particular results, we have observed dedifferentiation in some parametrizations, identifying its two distinct local causes: Receptor normalization in neighboring cells and loss of contact with an adjacent cell due to its division. The former seems to be bound to low membrane enzymatic activity and low spontaneous decay acting simultaneously.

Finally, we have observed that spontaneous decay is the major factor influencing the overall behavior in terms of appearance or preventing the uncontrollably dividing growth. Large spontaneous decays lead to stopping growth while small spontaneous decays cause unstopping growth proceeding to occurrence and proliferation of totally transformed cells. For values of spontaneous decay inbetween, both types of growth occur, in dependence on membrane enzymatic activity. Connecting our observations together, the general role of membrane enzymatic activity seems to be rather local and morphogenic, constituting tip cell formation and thread growth under suitable conditions.

5. Model of cell migration in chronic inflammation

In this chapter we will focus on the role of membrane enzymatic activity in inflammatory response mediated by migrating cells. Taking rheumatoid arthritis as a motivating source of biological information we will construct a scenario showing different properties of collection of migratory cells based on membrane-associated chemoattractant cleavage. It will be demonstrated that membrane enzymatic activity can transform group of individually responding chemotactic cells into an organized community exhibiting response to inflammatory chemotactic cue that is adequate to the intensity of the stimulus.

5.1 Biological motivation

As a motivation for our model we took observations and results presented in [86]. In this study the role of proteolytic enzyme dipeptidyl peptidase-IV (DPP-IV) [87] in a free soluble form as well as in membrane-bound form in rheumatoid arthritis (RA) has been assessed. Particularly, specimen of synovial fluid (SF) [89] from patients with RA and osteoarthritis (OA) have been comparatively analyzed. While RA is a chronic inflammatory disease [88], OA possesses substantially lower inflammatory component. In [86] it has been observed that activity of free diffusible DPP-IV in SF does not substantially differ between OA and RA. However, there was significantly lower activity and expression of the membrane-bound DPP-IV in synovial fluid mononuclear cells (FMNC) in RA than in OA. As further reviewed in the study, stromal-cell derived factor-1α (SDF), chemokine and substrate of DPP-IV, is mostly synthesized and secreted into synovial environment by synoviocytes, reaches higher concentrations in synovial fluid in RA than in OA, and FMNC contain receptor on SDF. Also, abundant presence of activated immune cells containing membrane-bound DPP-IV has been observed in synovial tissue, associated with migratory phenotype and a tendency to infiltrate the rheumatoid synovium.

5.2 Cell-based modeling of migration of immune cells

In [90] agent-based model of migration of T cells and dendritic cells (DCs) in lymph node was introduced. It was analyzed how antigen-specific T cells locate DCs. In a 2D lattice-based model T cell occupies one pane while DC has action radius over several panes. Random motion vs. chemotaxis are compared. Direction choices in the random motion for both types of cells are influenced by short term persistence, i. e. by giving a (greater) likelihood of preserving the motion direction from one simulation step to the following. In the chemotaxis scenario, chemotactic navigation complements random motion of T cells only in the vicinity of DCs. In this case every DC has a prescribed stationary chemoattractant gradient in its local surroundings. If a nearby T cell feels the gradient, it gets attracted. Some time after starting being

attracted the T cell cell becomes chemoattractant-insensitive, turning back to persistence – driven random motion. This period (desensitization time) is a parameter. Further, resensitization period is also parametrically provided. Within the rule set, binding of T cells and DCs after contact is also treated. As a result, in the model random motion turns out to be sufficient for effective T cell scanning. Chemotaxis was causing crowding of T cells in DCs' vicinity, decreasing unique T cell DC contacts, thus having inhibitory effect on the scanning process.

On the other hand, later study [93] regarding the same biological motivation, that uses cellular Potts model, concludes that chemoattraction of T cells enhances the DC scanning efficiency. The reason for the distinctive results in comparison with the prior work resides in different formalisms of the methods. In the cellular Potts model, the space of interest in the model lymph node is fully filled with the cells. For each T cell that has migrated to a DC another T cell had to “free the space”. Thus a DC doesn't get blocked by the T cells that have migrated to its vicinity. Instead, the T cells “regularly compete” for that space. This effect is strengthened by desensitization. While the sensitive “chemotacting” T cells opt more likely to proceed towards the DC, the desensitized ones do not. Consequently, the insensitive cells are being effectively repelled from the DCs. Actually, microstreams of T cells going to the DCs and away from them are observed, where pushing the insensitive cells by the sensitive chemotacting ones also plays a role. In the agent-based model formalism, cells can't move to already occupied positions. This was leading to chemotactic T cell crowding at the DCs in [90]. In the cellular Potts model, absence of this requirement together with the model dynamics made it possible for cells to escape from the chemokine attraction field.

Another model involving cell migration in lymph node is provided in [94]. Hybrid agent-based approach is used there and lymph node function in healthy and infected states is addressed.

An agent-based model of clearance of early infection with fungal spores was presented in [91]. The model is implemented in agent-modeling software tool NetLogo [92]. In a 2D grid there are migrating neutrophil agents striving to hunt and phagocyte static conidial agents (fungal spores). In the model it has been observed that for initial random distribution of conidia, random walk with short term persistence was more effective than without it. Chemoattraction where conidia were sources of diffusing chemoattractant was even more efficient. If neutrophils that phagocyte a conidium produce the chemoattractant, thus sending a “signal” to other neutrophils, this leads to their accumulation in areas where conidia have been already eliminated, impairing effectivity. If the conidia are initially located in clusters, sending the chemotactic signal by successful neutrophils is a better strategy in comparison with random walk. There was an upper threshold parameter introduced in the model, turning off chemotaxis when exceeded. For high values of this

threshold, the attracted neutrophils migrate and reach the attracting ones, being effective at the beginning of the search process, but not in the later phase, when the conidia in the surroundings of the attractors are already removed. In this later phase, lower thresholds are more effective.

5.3 Model of chemotaxis in chronic inflammation

Situation setting. The model uses two vaxes (A_i, V_i, X_i), $i = 1, 2$. Situation with initial conditions is shown in Fig. 5.1.

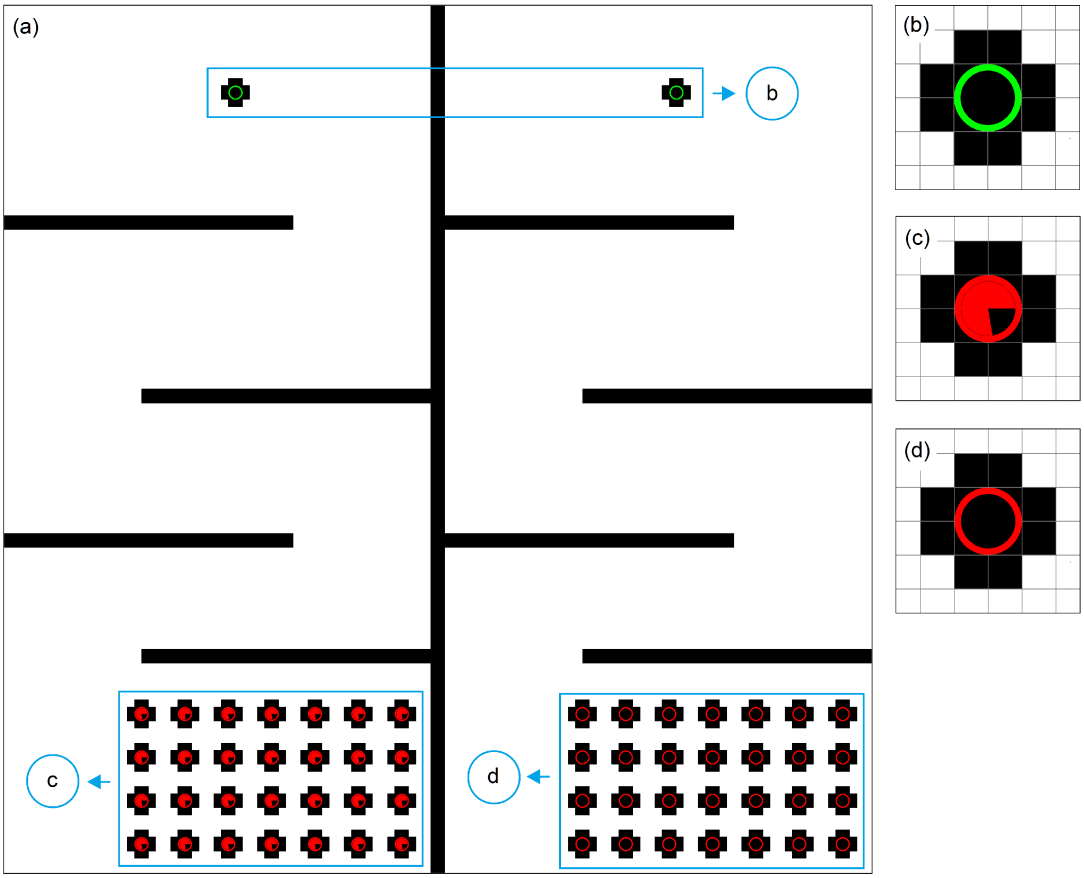

Figure 5.1: Situation disposition and initial conditions. (a): Overall view. Environment geometries and initial cell locations in the left and right compartments are the same. Thick line barriers are impermeable for ligands and form obstacles for cells. Both of the topmost cells are identical. All cells in the left bottom cluster are the same, all cells in the right bottom cluster are the same. (b): Detail of single topmost cell: CS on A_2 (green annulus), contains no receptors. (c): Detail of single bottom cell in the left compartment: CS on A_1 (red annulus), receptor amount: 233 on A_1 (red sector). (d): Detail of single bottom cell in the right compartment: CS on A_1, receptor amount: 0.25 on A_1. The receptor amount is too smal to be visible on the pie graph, Division treshold = 300.

The environment lattice is a square 120×120 panes, divided vertically into two halves by a barrier two panes thick, impermeable for cells and diffusible ligands.[46] The right half contains model of chronic inflammation, the left half models physiological inflammatory response. The only difference between the halves is in receptor amounts on A_1 in the bottom cells. On the left side, the receptor amount in a single cell is *233* while on the right it is *0.25*, i. e. roughly three orders of magnitude lower. Zygotic graph is as follows in Fig. 5.2.

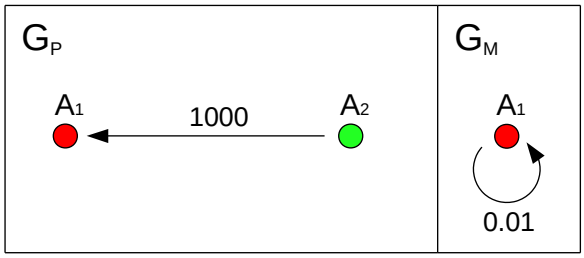

Figure 5.2: Zygotic graph. $G_R = G_A = \emptyset$. Colors (altrnatively) represent given ligands.

Regarding decays, there is $k_{ma}^{A_1} = 0.3$, $k_{sd}^{A_1} = 0.0001$. All the other decays are zero. Concerning relevant parameter values, there is $D = 0.2$, *Min gradient* $= 0.001$, *Ks change threshold* $=$ *1E-5, Division threshold* $= 300$, and *Membrane capacity* $= 301$. $K_d = 0$ for each vax (reaction). Parameters regarding divisions are not important. Since receptor graph is empty, cells in our scenario are not adding receptors and thus they are not dividing.

The two top cells in Fig. 5.1 serve as producing sources of A_1, being in CS on A_2 in every step. The bottom cells in the left part have receptors on A_1, thus feeling A_1 and cleaving it by membrane enzymatic activity. The bottom right cells also feel A_1 having receptors on it. However, due to small receptor amount local A_1 removal due to membrane enzymatic activity is negligible in comparison with the left scenario, if concentration of A_1 is sufficiently high. In both scenarios, migration towards A_1 source will occur. Character of the migration in each of the scenarios will be in the focus of our interest.

Flowaround setting. Before stepping further, resolution of concentrations in the surroundings of a migrating cell is to be defined. In our scenario, flowaround will be used. As an underlying model for flowaround we consider 2D potential flow around

46 As we will see later, since flowaround is used in the model, part of the area of the barrier can be internally regarded accessible for diffusible ligands within the flowaround computation. However, since the the barrier is "thick" and flowaround surroundings for each cell is "small", altering ligand concentrations on the other side of the barrier by flowaround of nearby migrating cells is not possible.

a cylinder [95], [96]. For the time being we will assume that our cell has circular shape, supposing first it is placed in uniform parallel flows.

Let's consider a circle with radius r_0 having its center located at the coordinate system origin. Let U be a uniform flow in the x direction. As described in [95], the complex potential $w(z)$ for a flow around the circle is

$$w(z) = U\left(z + \frac{r_0^2}{z}\right), \tag{5.1}$$

and for the components u_x, u_y of the flow around the circle in the x and y direction respectively there holds

$$u_x - iu_y = \frac{dw}{dz}, \tag{5.2}$$

where i is imaginary unit. From (5.1) and (5.2) we get

$$u_x = U\left(1 - \frac{x^2 - y^2}{r^4} \cdot r_0^2\right),$$

$$u_y = -2U r_0^2 \cdot \frac{xy}{r^4},$$

where $r^2 = x^2 + y^2$. Let's now consider that the cell moves along the x axis with the same speed but in the opposite direction than U and there is no uniform flow in the environment. To get the flow components p, q in the x and y directions respectively around the moving cell, we have to subtract the original uniform flow U. Denoting V the cell speed in our situation, $V = -U$, and we have

$$p = V r_0^2 \cdot \frac{x^2 - y^2}{\left(x^2 + y^2\right)^2},$$

$$q = V r_0^2 \cdot \frac{2xy}{\left(x^2 + y^2\right)^2}. \tag{5.3}$$

Now we will wish to define flowaround for our discretized cell doing elementary movement in a horizontal direction, utilizing p and q. We are interested in flows across selected vertical or horizontal segments in the (virtual) surroundings of the cell. Flow F_{ab} across horizontal segment (x_a, y_b), $(x_a + \Delta x, y_b)$ will be computed as

$$F_{ab} = \int_{x_a}^{x_a + \Delta x} q(x, y_b)\, dx,$$

similarly flow G_{kl} across vertical segment (x_k, y_l), $(x_k, y_l + \Delta y)$ will be obtained as

$$G_{kl} = \int_{y_l}^{y_l + \Delta y} p(x_k, y)\, dy.$$

We can simply check that

$$\int p(x,y)dy = Vr_0^2 \cdot \frac{y}{x^2+y^2},$$

$$\int q(x,y)dx = -Vr_0^2 \cdot \frac{y}{x^2+y^2}.$$

For our particular cell shape we take $r = 2$. We will consider case of defining flowaround for elementary movement to the left, i. e. $V = -1$. The situation is sketched in Fig. 5.3.

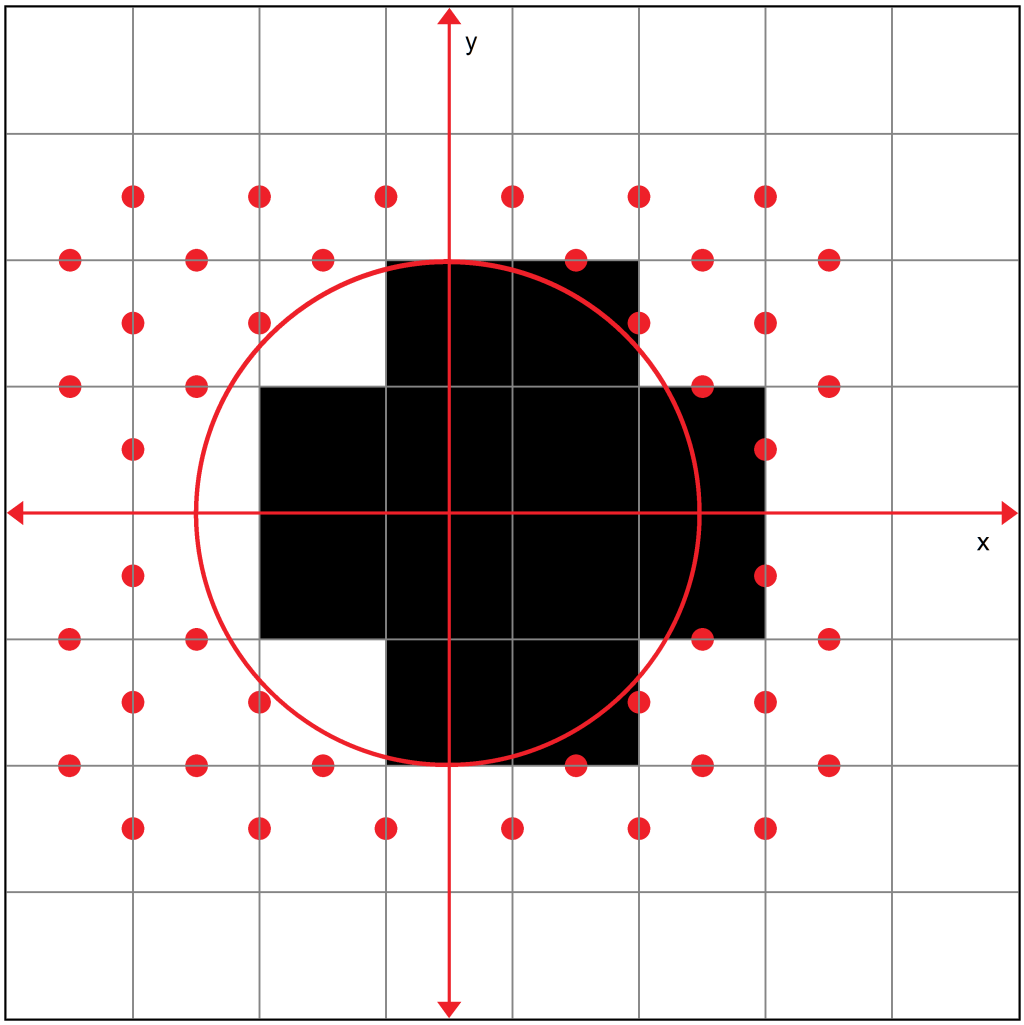

Figure 5.3: Defining flowaround for elementary cell movement to the left. The cell is shown at the starting position of the elementary movement. Flow field around the circle at the origin with horizontal speed -1 is determined. Flows across edges marked by dots are then computed based on the flow field. Two edges forming cell boundary and crossing y axis are treated in a separate way. Flows across the other edges are regarded zero.

Obviously from (5.3) in the flow field the flow across x axis is always zero, thus we excluded edges on the x axis from marking in Fig. 5.3 apriori. For the marked edges which intersect the circle, flow across the subsegment outside of the circle (only) is computed in flowaround definition. Further, let e be the upper edge crossing y axis and being part of the cell boundary. According to how flowaround was introduced in the model world, there can be no flux from or to panes that remain covered during cell movement. When taking the right half of e, meaning its subsegment with positive x coordinates, since flow field velocities are relatively high in its surroundings, we have decided to add the flow across this half-segment of e to the flow across the horizontal segment neighboring with e on the right in the flowaround definition. This operation has been performed symmetrically for the left half of e and the left horizontal neighbor of e. At the lower intersection of the cell boundary and the y axis the situation is analogical.

For elementary movements of the cell in the other directions the situation is analogous. Actually, due to symmetries of the flow field it is not difficult to realize that flowarounds in these cases are appropriate rotations of the flowaround "grid" for the left elementary movement.

Results. The simulation has been run for 50000 steps. Migration of the cells to the sources of A_1 is shown in snapshot series in Figs. 5.4, 5.5, and 5.6.

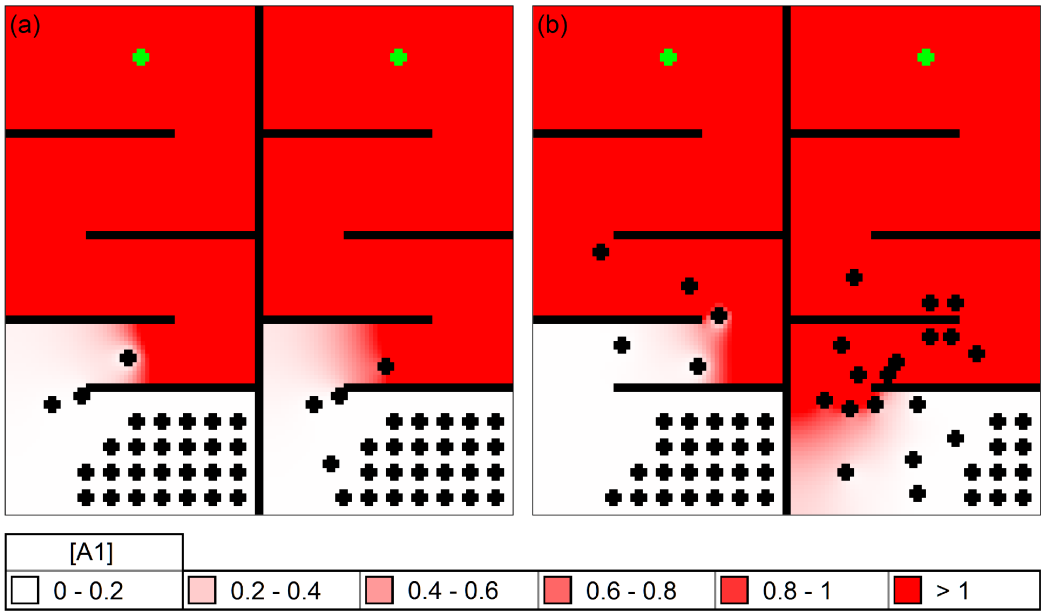

Figure 5.4: Migration starting phase. Green - producing cells. (a): Step 5000. After A_1 reaches detectable concentration in the area of the cells closest to the source, they start to migrate. This happens in the same time in both scenarios, migration patterns are similar. (b): Step 10000. In the right scenario, more cells started migration, concentration of A_1 in the area of the original cluster is higher than in the left scenario with the high membrane enzyme (receptors on A_1) concentration.

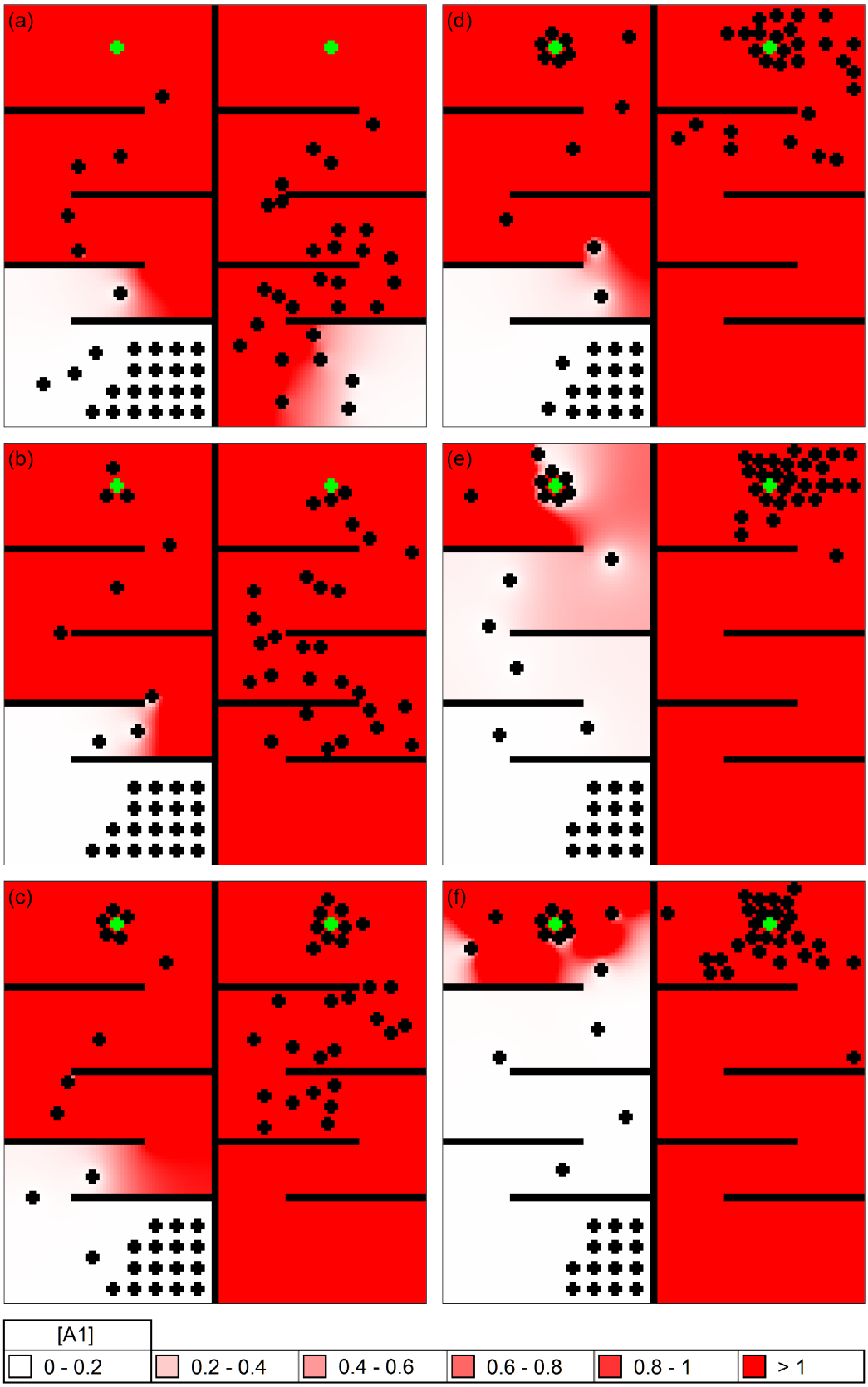

Figure 5.5: Cell translocation phase. Green – producing cells. (a): Step 15000. (b): Step 20000. (c) Step 25000. (d) Step 30000. (e) Step 35000. (f): Step 40000.

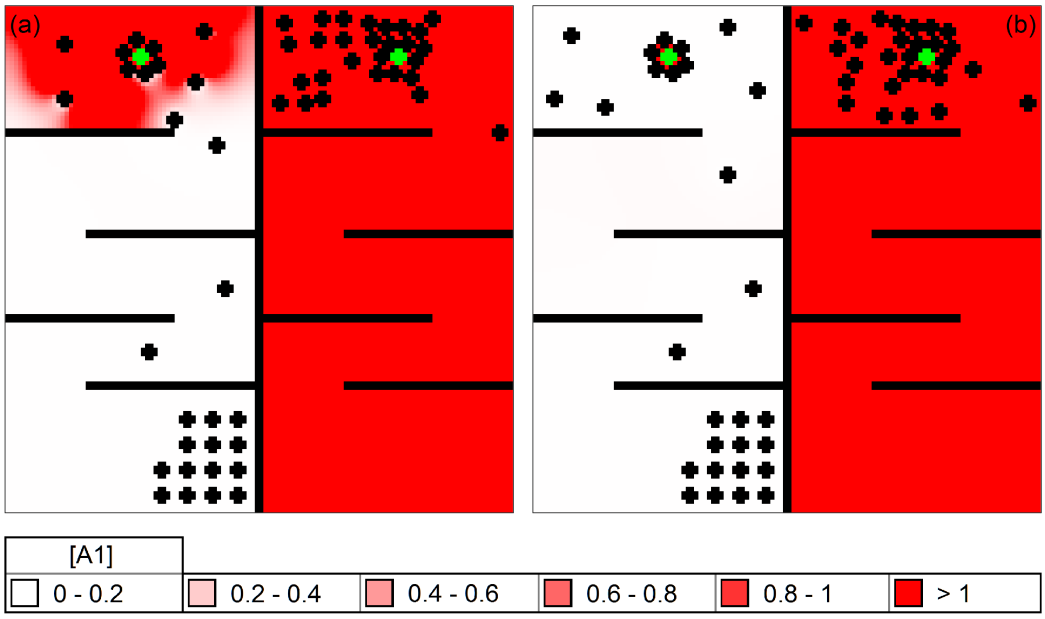

Figure 5.6: Post-translocation phase. Producing cells are colored green. (a): Step 45000. (b) Step 50000.

We can roughly divide the scenario development into three phases: Migration starting phase, cell translocation phase and post-translocation phase.

In the migration starting phase (Fig. 5.4) the first cells start movement after sensing A_1 that has spread from the producing cells. For some limited time, A_1 concentration in the surroundings of the migrating cells is relatively small, lower than cell receptor amount in either compartment.[47] In other words, in both compartments (all) receptors of the migratory cells are unsaturated, resulting in the same rate of cleavage of A_1 regarding pairs of corresponding cells per compartment. However, already in step 5000 (see Fig. 5.4 (a)) this mode of migration doesn't generally apply but due to its prior occurrence the situations look roughly similar. Further on, in the left compartment the intensive cleavage of A_1 by the migrating cells hinders its concentration increase in the area of the primary cluster. Thus most of the cells remain on their original locations. On the contrary, in the right compartment A_1 diffuses in higher concentrations to the region of the original cluster and many cells are recruited for migration (Fig. 5.4 (b)).

This trend continues and strengthens in the cell translocation phase (Fig. 5.5). On the left sides, smaller amount of rather consecutively migrating cells occur. On the right sides, all the cells move in a "cloud like" manner. After some time, all the cells in the right compartment translocate to the area near the producing cell. In the left compartment, only limited amount of cells translocate and many cells do not start migration at all. In both compartments, as the migrating cells are reaching the producing cell, the effective rate of production of A_1 to the (distant) environment gets

47 For the surroundings of the cells remaining in the clusters this holds as well.

lower. Firstly, membrane elements of a producing cell being adjacent to other cells do not secrete A_1. Secondly, at least for some periods the producing cells get surrounded by the attracting cells in a way that these form a barrier for diffusion, separating the producing cell from the rest of the environment. In the left compartment, when the effective production is blocked in this way the migratory cells remove A_1 from the most of the environment (Fig. 5.5 (f)). Also, although less migratory cells reach the producing one in the left compartment, they pack around the producing cell in a more structured way than in the other compartment. Substantial limitation of A_1 secretion to the distant environment appears sooner in the left compartment than in the right one.

In the post-translocation phase (Fig. 5.6), both scenarios reach kind of quasi-stable state. In the right compartment, all of the migratory cells are in the area near to the producing cell. In the left compartment, there is a shell around the producing cell that has formed in the prior phase, hindering A_1 to diffuse out up to occasional short term spills when some of the cells in the shell move slightly. Then there are several cells near to the shell that practically clear out such leakage of A_1 if it occurs.[48] When cleaving A_1, they are moving to places with its higher concentration where it "hasn't yet been cleaved", from the locations where A_1 "has been removed". This boosts the uptake. Further, there are two cells left nonmoving "roughly in the half of the way", where A_1 "has been cleared" already at the end of the prior stage.

Flowaround simulation. In our model we have incorporated flowaround based on potential flow around a moving circle. In the virtual surroundings of a cell where the flowaround is defined (cf. Fig. 5.3), near to the axis parallel to the cell movement flow components in front of the cell and at the back of the cell in the cell movement direction are relatively "big". Particularly, magnitude of flow velocities across the marked edges adjacent to the x axis in Fig. 5.3 is more than 0.5. In front of the cell in the movement direction, outflux from the panes at the border of the surroundings that are adjacent to these edges is less than the influx since there is by definition zero flux across their leading border-adjacent edges, instead of a positive value that gives the underlying potential flow field. This causes that part of the inflowing substances "accumulates" in these fields. It leads to artificial increase of concentration(s) in these panes. Behind the cell the situation is symmetric, artificial concentration decrease occurs in corresponding panes at the back of the moved cell. Followingly, these concentration changes cause bias in the concentration gradient in the proximity of a cell that performed elementary movement. In the areas where the ratio of original gradient magnitude to the substance concentration is low, this bias may be of nonnegligible impact. We have thus decided to perform parallel simulations using

48 Residual concentration (after clearing) of A_1 outside the shell is basically at values comparable with the cell migration treshold (*Min gradient)*.

infilling. Outcomes of the simulations (data not shown) were comparable with the ones using flowaround, confirming our results.

5.4 Discussion

We have created a model of cellular chemotactic migratory response in inflammatory conditions inspired by particular findings observed in rheumatoid arthritis and osteoarthritis [86]. Phenomenological results of our simulations align with the following conceptual model: We consider that in an inflammatory scenario there is a (focal) cue recruiting particular migratory component of the immune system. In the physiological conditions, amount of the cells adequate to the cue intensity will migrate to the place of the cue origin, inducing inflammation of intensity corresponding to the extent of the cause. In the chronic case, on the other hand, even for a small impulse the number of cells comming is unproportionally high, causing unadequate inflammatory reaction. In the result of [86] low amounts of membrane-bound enzyme DPP-IV were correlated with the chronical inflammation of rheumatoid arthritis while high amounts of DPP-IV did correlate with less inflammatory osteoarthritis. Our in-silico findings suggest following hypothesis: Low or negligible concentrations of the membrane-bound enzyme are directly responsible for the chronic inflammatory conditions causing unadequately high concentrations of immune cells in the locations of chemoattractant sources. Sole increase of membrane concentrations of the enzyme leads to the decrease of amount of these cells in the locations of the attractant origin, making the number of cells adequate to the the strength of the chemoattracting signal.

Fundamental conceptual difference between the two in-silico situations is following: In the no-cleavage scenario, each migratory cell is a solitaire. When it feels the chemoattractant, it follows its gradient regardless of what happens around, up to being blocked by obstacles or other cells. On the other hand, mere increase of membrane chemoattractant cleavage to reasonable level under otherwise the same conditions seems to grant kind of distributed intelligence to the cells, expressing itself in following properties:

- **Chemical localization.** The cells that set off a journey to the chemoattractant source decrease its influence on the cells that are behind, stopping or postponing their migration if the chemoattractant concentration is not very high. Viewed more globally, sufficient amount of the cells that migrated near to the source can effectively cause decrease of the chemoattractant concentration in the more distant environment to the extent that recruitment of other cells ends, terminating this phase of immune response.
- **Clearing.** If production of the chemoattractant stops or if it has been blocked, the cells in the closeness to the (former) cue source are able to effectively clear residual chemoattractant gradients (concentrations) by actively moving

towards local concentration maxima. In the same way occasional burst-like spills of the chemoattractant are reduced but longer term impulses can be quickly followed.

- **Reiteration.** The process of migration seems to be leaving some residual cells on the way in greater distance from the source, forming "further wave" of cells with the potential expressed in the previous point.
- **Migration structuring.** Membrane enzymatic cleavage locally structures the movement of the cells in presence of obstacles[49]. If we think of an individual cell in an area with initially constant concentration of the chemoattractant, the membrane cleavage forms a local "crater" in the concentration surface with the cell in the middle. If there are two cells in this way, (close to each other, say,) their craters will partially merge, leading to a concentration gradient around each cell in the direction away from the center of mass of the cell pair. Thus the cells will generally repel each other on the level of chemotaxis. Similarly, if a cell is close to a (zero flow) boundary, local concentration decrease will send the cell away from the boundary. In the conditions of migration of multitude of cells this property will reduce collisions. For a single cell in a narrow space, it will force it to migrate "in the middle".

As we have seen in [90], [93] cell crowding in agent-based migration scenarios may cause modeling and interpretational difficulties. In situations where the space is not filled with the cells too densely, chemoattractant membrane enzymatic cleavage offers a way of partial implicit reduction of cell crowding, making this cleavage a candidate for how this issue might have been tackled in corresponding biological motivations.

49 Being either in form of the (other) cells in the migrating collection or in form of other objects.

Conclusion

Particular models. We have created three models inspired by more or less concrete biological motivations.

In the lumen-formation model we have observed that cell migration together with directional divisions may be sufficient to form intercellular lumen, without need of either apoptosis or cellular polarisation. Additionally, lumen coalescing emerged for sufficiently close seeds, demonstrating that an elongated tubular structure may be generated by seeding individual cells “along the way“in appropriate intervals.

In the Diversified tumour Model, we have seen distinct growth phases connected to structuring analogical to histopathological tumour grading. Spontaneous decay acts as an overall driver influencing whether the in-silico tumour growth will stop or proceed to uncontrollable divisions. Membrane enzymatic activity looks to control local morphogenesis. Dedifferentiation has been observed in some scenarios, one of it's causes seems to be linked with specific subarea of the space of these parameters. The model offers a hypothesis for occurrence of observable progression of malignancy from an originally benign tumour on one hand and for appearance of aggressive neoplasms with no detectable precursor on the other hand as parametric variants of a single scenario.

In the third model we were focused on analyzing chemotaxis in chronic and physiologically relevant inflammations. Taking clinically observed correlation between chronic inflammatory conditions and decreased presence of a chemoattractant-cleaving membrane-bound enzyme in migratory immune cells, our simulations propose cause – consequence relationship to be behind. Particularly, the model suggests that adding appropriate amount of the membrane enzyme transforms the chronic inflammatory behavior into a response adequate to the strength of an inflammatory stimulus. It has been observed that local cell-cell and cell-boundary microrepellence structures the migrating cell community, making membrane enzymatic activity a candidate for a way of natural reduction of cell crowding.

Modeling approach and methodological conclusion. We have described a generic hybrid cell-based approach for simulating behavior of systems of cells. When looking at various cell-based modeling methodologies via the optics of the agent-based paradigm we can recognize two conceptual directions. In the first one, there is a kind of high freedom and variability in means of expressing rules for the cell agents. Examples of these approaches are generally cellular automata or agent-based modeling. One can implement cell decision logic as though developing a program in an arbitrary programming language. In the other direction there is a concept or mechanism ingrained in the approach specifying or limiting how things are expressed, unless substantial extension of the model alone is done. Representatives

of these methodologies are cellular Potts model or IBCell. In the former, energy minimization principle drives the basic cell behavior. If one wants to axiomatize or implement some sort of cellular behavior, usually a new term is added to the expression for the total energy. In IBCell the fluid mechanics model outlines a way of elementary articulation.

Generally, the conceptual and expressive apparatus of a modeling approach with such an incorporated principle specifies kind of “language” or “grammar”, a way of thinking of the topics of interest, formulating hypotheses and obtaining results. Physical, chemical or biological plausibility determines extent or scope of relevancy of the results one gets. Transparency of capturing the underlying principles in given “language” per se increases their traceability in the resulting models, simplifying assessment of the framework and particular outcomes not only from the point of view of biological motivations.

In our approach we used chemical substances, vax reactions, and zygotic graph as basic expression units. While playing the role of variables, the substances obey elementary chemical rules in their dynamics. Upon this, vax equilibrium is articulated as a key building block of receptor-ligand interactions, acting as a transparent expressive entity in the reaction-diffusion scenario as well. The zygotic graph then captures the idea of a simplified genome, where the elementary behaviors the cell can exhibit are encoded. More particularly, it specifies subsets of ”genes” expressed in parallel in specified intensities, each such pattern realizing concrete functionality a cell can perform or a “type“ a cell can instantiate. Cummulative states then uniquely represent these patterns. Although simplified, we regard this concept to exhibit low level of axiom “artificiality“ while being rather simple and transparent. Its conceptual advantage is that interpretation of particular axiomatizations offers itself in terms of expression intensities of individual genes or productions of individual proteins. Although this “direct link” needn't capture the real biology, it generates a hypothesis stating “how would the world look like if the gene / protein scheme was that simple”. It offers the first step of approximation, a simplified domain for model tuning. Generally, partial mismatch with real genetics and proteomics may help to discern between what is the fabric and what is the fine tuning in the real scenario.

Usability and possibilities of our approach have been demonstrated in the particular models. They show that relatively uncomplicated zygotic graphs can produce nontrivial organized behavior. This emphasizes system understanding of the situation rather than direct gene-phenotype linking. The models suggest that physical and chemical behaviors and consequences in a scenario play substantial conceptual role in its functional structure and variability. As an example we take membrane enzymatic activity. It may be surely attributed to a gene encoding the enzyme of interest or to the functionality of the part of the intracellular machinery responsible

for the enzyme's correct synthesis and membrane localization. However, an important part of the picture resides in the spatio-temporal dynamics of the environment containing the enzyme's diffusive substrate when a cell or cells are only seen as solid objects with the enzyme on their surfaces. Having this building block, chemotaxis then adds another level of behaviors. In the immune response model, properties of this character strongly participate. In the emergent results the zygotic graph or “genetic” logic then only simply uses given behaviors in order to achieve its goals. Translating this to the agent-based view, an emphasis on seeing the world from the perspective of the agent remains in our approach. However, the rest of the world is not or no longer viewed as a set of passive compounds in comparison with the active agents. It is rather a functionally and conceptually rich site. The idea is that the agents harness building blocks of the environment which are of a nature of system dynamics rather than being only simple environmental constituents. When creating a model, these system dynamics components may be used if known before in order to build the scenario. However, they can be observed aposteriori as emergent results, as it was in the chronic inflammation model. The specific expressive “language” of our approach supports the idea of the environment as a key conceptual and functional player in execution of the cell logic.

Perspectives. The greatest problem of mathematical and computer modeling of biological cell systems is a lack of directly testable hypotheses. Rather than apriori extending our approach in various ways it seems to be beneficial to seek scenarios of biological experimentation where the correspondence of conditions with the model world is as strong as possible. Potential model extensions would then aim to increase the compatibility in order to get close to generating hypotheses that could be suitable for experimental verification.

When looking at our concrete models, cell migration with membrane enzymatic activity can be a promising direction. The problem per se seems to offer space for theoretical in-silico exploration. Also, in vitro experiments where migratory cells are seeded on a flat surface look to be relevant and reachable. Generally, in-vitro scenarios with defined geometry and 2D cell arrangements with only a thin layer of medium are suitable candidates for our modeling analysis.

In the lumen formation model, growth termination is currently not covered. Analysis of structure generation with different 2D patterns of seeding may bring understanding of the model in greater scope.

In DTM, various models of physiological tissues can be made susceptible to the cancerous stimulus. Analyzing scenario progressions and properties in a way similar to the current model could bring understanding to tissue morphologies and dynamics under various grades in different types of cancers.

Bibliography

[1] M. Balek, V. Bednar, T. Bily, M. Karasek. Microscopic tumor growth module for ContraCancrum project. *IFMBE Proceedings*, 25(4):1957–1960, 2009

[2] H. Lodish, A. Berk, S. L. Zipursky, P. Matsudaria, D. Baltimore, J. E. Darnell. *Molecular Cell Biology*, chap. 2. W. H. Freeman and Company, New York, 4th edition, 2000

[3] Ph. Ciarlet, J. L. Lions eds. *Handbook for Numerical Analysis*, p. 715–1022. North Holland, 2000

[4] W. Jost. *Diffusion in solids, liquids, gases*. Academic Press, NewYork, 1970

[5] G. An, Q. Mi, J. Dutta-Moscato, Y. Vodovotz. Agent-based models in translational systems biology. *Wiley Interdiscip. Rev. Syst. Biol. Med.*, 1(2): 159–171, 2009

[6] M. Hwang, M. Garbey, S. A. Bercelt, and R. Tran-Son-Tay. Rule-Based Simulation of Multi-Cellular Biological Systems—A Review of Modeling Techniques. *Cell Mol. Bioeng.*, 2(3):285–294, 2009

[7] B. H. Mele, F. Giannino, Ch. E. Vincenot, S. Mazzoleni, and F. Cartení. Cell-Based Models in Plant Developmental Biology: Insights into Hybrid Approaches. *Front. Environ. Sci.*, 3:73, 2015

[8] S. Wolfram. Statistical mechanics of cellular automata. *Rev. Mod. Phys.*, 55(3):601–644, 1983

[9] G. Cheng, B. B. Youssef, P. Markenscoff, and K. Zygourakis. Cell population dynamics modulate the rates of tissue growth processes. *Biophys. J.*, 90:713–724, 2006

[10] D.Basanta, H. Hatzikirou, and A. Deutsch. Studying the emergence of invasiveness in tumours using the game theory. *Eur. Phys. J. B*, 63:393–397, 2008

[11] S. C. Ferreira Jr., M. L. Martins, and M. J. Vilela. Reaction-diffusion model for the growth of avascular tumor. *Phys. Rev. E*, 65:021907, 2002

[12] S. D. Shumate, and M. El-Shenawee. Computational model of ductal carcinoma in-situ: the effects of contact inhibition on pattern formation. *IEEE Transactions on biomedical engineering*, 5:1341–1347, 2009

[13] J. A. Engelberg, G. E. P. Ropella, and C. A. Hunt. Essential operating principles for tumor spheroid growth. *BMC Syst. Biol.*, 2:110, 2008

[14] M. J. Simpson, A. Merrifield, K. A. Landman, and B. D. Hughes. Simulating invasion with cellular automata: connecting cell-scale and population-scale properties. *Phys. Rev. E*, 76:021918, 2007

[15] E. Bonabeau. Agent-based modeling: methods and techniques for simulating human systems. *Proc. Natl Acad. Sci. USA*, 99:7280–7287, 2002.

[16] B. C. Thorne, A. M. Bailey, D. W. DeSimone, and S. M. Peirce. Agent-based modeling of multicell morphogenic processes during development. *Birth Defects Res. C Embryo Today*, 81:344–353, 2007.

[17] A. L. Bauer, T. L. Jackson, and Y. Jiang. A Cell-Based Model Exhibiting Branching and Anastomosis during tumor-Induced Angiogenesis. *Biophys. J.*, 92(9):3105–3121, 2007

[18] S. Turner, J. A. Sherratt, and D. Cameron. Tamoxifen treatment failure in cancer and the nonlinear dynamics of TGFbeta. *J. Theor. Biol.*, 229:101–111, 2004

[19] J. Galle, M. Hoffmann, and G. Aust. From single cells to tissue architecture—a bottom-up approach to modelling the spatio-temporal organisation of complex multi-cellular systems. *J. Math. Biol.*, 58:261–283, 2009

[20] M. Niazi, and A. Hussain. Agent-based computing from multi-agent systems to agent-based Models: a visual survey. *Scientometrics*, 89:479, 2011

[21] M. M. Palm, and R. M. H. Merks. Vascular networks due to dynamically arrested crystalline ordering of elongated cells. *Phys. Rev. E*, 87:012725, 2013

[22] A. J. Kabla. Collective cell migration: leadership, invasion and segregation. *J. R. Soc. Interface*, 9:3268–3278, 2012

[23] M. Zajac, G. L. Jones, and J. A. Glazier. Simulating convergent extension by way of anisotropic differential adhesion. *J. Theor. Biol.*, 222:247–259, 2003

[24] R. M. H. Merks, M. Guravage, D. Inzé, and G. T. S. Beemster. Virtualleaf: an open-source framework for cell-based modeling of plant tissue growth and development. *Plant Physiol.*, 155, 656–666, 2011

[25] R. M. H. Merks, S. V. Brodsky, M. S. Goligorksy, S. A. Newman, and J. A. Glazier. Cell elongation is key to in silico replication of in vitro vasculogenesis and subsequent remodeling. *Dev. Biol.*, 289:44–54, 2006

[26] S. D. Hester, J. M. Belmonte, J. S. Gens, S. G. Clendenon, and J. A. Glazier. A multi-cell, multi-scale model of vertebrate segmentation and somite formation. *Plos Comput. Biol.*, 7:e1002155, 2011

[27] Y. Jiang, J. Pjesivac-Grbovic, Ch. Cantrell, and J. P. Freyer. A Multiscale Model for Avascular tumor Growth. *Biophysical Journal*, 89:3884–3894, 2005

[28] R. M. H. Merks, J. A. Glazier. A cell-centered approach to developmental biology. *Physica A*, 352(1):113–130, 2005

[29] J. A. Izaguirre, R. Chaturvedi, C. Huang, T. Cickovski, J. Coffland, G. Thomas, G. Forgacs, M. Alber, G. Hentschel, S. A. Newman and J. A. Glazier. Compucell, a multi-model framework for simulation of morphogenesis. *Bioinformatics*, 20:1129–1137, 2004

[30] J. Jeon, V. Quaranta, and P. T. Cummings. An off-lattice hybrid discrete-continuum model of tumor growth and invasion. *Biophysical Journal*, 98:37–47, 2010

[31] Y. Kim, M. A. Stolarska, H. G. Othmer. A hybrid model for tumor spheroid growth in vitro, I: theoretical development and early results. Mathematical Models and Methods in Applied Sciences, 17:1773–1798, 2007

[32] M. A. Stolarska, Y. Kim, H. G. Othmer. Multi-scale models of cell and tissue dynamics. *Phil. Trans. R. Soc. A*, 367:3525–3553, 2009

[33] F. A. Meineke, C. S. Potten, and M. Loeffler. Cell migration and organization in the intestinal crypt using a lattice-free model. *Cell Prolif.*, 34:253–266, 2001

[34] G. Schaller, M. Meyer-Hermann. Multicellular tumor spheroid in an off-lattice Voronoi-Delaunay cell model. *Physical Review E*, 71:051910, 2005

[35] S. Checa, and P. J. Prendergast. A mechanobiological model for tissue differentiation that includes angiogenesis: A lattice-based modeling approach. *Ann. Biomed. Eng.*, 37:129–145, 2009

[36] K. A. Rejniak. A single-cell approach in modeling the dynamics of tumor microregions. *Mathematical Biosciences and Engineering*, 2(3):643–655, 2005

[37] K. A. Rejniak, R. H. Dillon. A single cell based model of the ductal tumour microarchitecture. *Computational and Mathematical Methods in Medicine*, 8:51–69, 2007

[38] N. V. Mantzaris, S. Webb, H. G. Othmer. Mathematical modeling of tumor-induced angiogenesis. *J. Math. Biol.*, 49:111–187, 2004

[39] B. Lubarsky and M. A. Krasnow. Tube Morphogenesis: Making and Shaping Biological Tubes. *Cell*, 112:19–28, 2003

[40] S. E. M. Boas and R. M. H. Merks. Synergy of cell–cell repulsion and vacuolation in a computational model of lumen formation. *J. R. Soc. Interface*, 11: 20131049, 2014

[41] J. A. Glazier and F. Graner. Simulation of the differential adhesion driven rearrangement of biological cells. *Phys. Rev. E*, 47:2128–2154, 1993

[42] F. Graner and J. A. Glazier. Simulation of biological cell sorting using a two-dimensional extended Potts model. *Phys. Rev. Lett*, 69:2013–2016, 1992

[43] M. J. Harding, H. F. McGraw, and A. Nechiporuk. The roles and regulation of multicellular rosette structures during morphogenesis. *Development*, 141:2549–2558, 2014

[44] A. Villasenor, D. C. Chong, M. Henkemeyer, and O. Cleaver. Epithelial dynamics of pancreatic branching morphogenesis. *Development*, 137:4295–4305, 2010

[45] J. Tang, H. Enderling, S. Becker-Weimann, Ch. Pham, A. Polyzos, Chen-Yi Chen, and S. V. Costes. Phenotypic transition maps of 3D breast acini obtained by imaging-guided agent-based modeling. *Integr. Biol.*, 3: 408–421, 2011

[46] K. Marias, V. Sakkalis, A. Roniotis, C. Farmaki, G. Stamatakos, D. Dionysiou, S. Giatili, N. Uzunoglou, N. Graf, R. Bohle, E. Messe, P. V. Coveney, S. Manos, S. Wan, A. Folarin, S. Nagl, P. Büchler, T. Bardyn, M. Reyes, G. Clapworthy, N. Mcfarlane, E. Liu, T. Bily, M. Balek, M. Karasek, V. Bednar, J. Sabczynski, R. Opfer, S. Renisch, I. C. Carlsen. Clinically Oriented Translational Cancer Multilevel Modeling: The ContraCancrum Project. *IFMBE Proceedings*, 25(4):2124–2127, 2009

[47] K.Marias, V.Sakkalis, A.Roniotis, I.Karatzanis, G.Stamatakos, D.Dionysiou, S.Giatili, N.Uzunoglou, N.Graf, R.Bohle, E.Messe, H.Stenzhorn, Y.-J.Kim, P.Coveney, S.Zasada, S.Wan, A.Folarin, P.Büchler, T.Bardyn, S.Bauer, M.Reyes, G.Clapworthy, E.Liu, T.Bily, V.Bednar, M.Karasek, A.Franz, R.Grewer and J.Sabczynski. ContraCancrum: Clinically Oriented Translational Cancer Multilevel Modelling. *Proc. 4th International Advanced Research Workshop on In Silico Oncology and Cancer Investigation (IARWISOCI 2011)*, 62–64, Athens, 2010

[48] G. S. Stamatakos, D. Dionysiou, S. Giatili, E. Kolokotroni, E. Georgiadi, A. Roniotis,V. Sakkalis, P. Coveney, S. Wan, S. Manos, S. Zasada, A. Folarin, P. Büchler, T. Bardyn, S. Bauer, M. Reyes, T. Bily, V. Bednar, M. Karasek, N. Graf, R. Bohle, E. Meese, Y.-J. Kim, H. Stenzhorn, G. Clapworthy, E. Liu, J. Sabczynski and K. Marias. The ContraCancrum Oncosimulator: Integrating Biomechanisms Across Scales in the Clinical Context. Proc. 4th International Advanced Research Workshop on In Silico Oncology and Cancer Investigation (IARWISOCI 2011), Athens, 65–67, 2010

[49] K. A. Rejniak, A. R. A. Anderson. A Computational Study of the Development of Epithelial Acini: I. Sufficient Conditions for the Formation of a Hollow Structure. *Bull. Math. Biol.*, 70:677–712, 2008

[50] K. A. Rejniak, A. R. A. Anderson. A Computational Study of the Development of Epithelial Acini: II. Necessary Conditions for Structure and Lumen Stability. *Bull. Math. Biol.*, 70:1450–1479, 2008

[51] Y. Sun and Q. Wang. Modeling and simulations of multicellular aggregate self-assembly in biofabrication using kinetic Monte Carlo methods. *Soft Matter*, 9:2172–2186, 2013

[52] A. B. Bortz, M. H. Kalos and J. L. Lebowitz. A New Algorithm for Monte Carlo Simulation of Ising Spin Systems. *J. Comput. Phys.*, 17:10–18, 1975

[53] P. A. Fleming, W. S. Argraves, C. Gentile, A. Neagu, G. Forgacs, and Ch. J. Drake. Fusion of uniluminal vascular spheroids: a model for assembly of blood vessels. *Dev Dyn.*, 239(2):398–406, 2010

[54] M. N. Nakatsu, R. C.A. Sainson, J. N. Aoto, K. L. Taylor, M. Aitkenhead, S. Pérez-del-Pulgar, P. M. Carpenter, and Ch. C. W. Hughes. Angiogenic sprouting and capillary lumen formation modeled by human umbilical vein endothelial cells (HUVEC) in fibrin gels: the role of fibroblasts and Angiopoietin-1. *Microvascular Research*, 66:102–112, 2003

[55] D. J. Andrew, A. J. Ewald. Morphogenesis of epithelial tubes: insights into tube formation, elongation, and elaboration. *Dev. Biol.*, 341:34–55, 2010

[56] M. A. Schlüter, and B. Margolis. Apical Lumen Formation in Renal Epithelia. *J. Am. Soc. Nephrol.*, 20:1444 –1452, 2009

[57] D. M. Bryant, K. E. Mostov. From cells to organs: building polarized tissue. *Nat. Rev. Mol. Cell Biol.*, 9:887–901, 2008

[58] S. Sigurbjörnsdóttir, R. Mathew, and M. Leptin. Molecular mechanisms of de novo lumen formation. *Nature Reviews Molecular Cell Biology*, 15:665 – 676, 2014

[59] E. Rodriguez-Boulan, A. Musch, A. LeBivic. Epithelial trafficking: new routes to familiar places. *Curr. Opin. Cell Biol.*, 16:436–442, 2004

[60] A. J. Blasky, A. Mangan, and R. Prekeris. Polarized protein transport and lumen formation during epithelial tissue morphogenesis. *Annu Rev Cell Dev Biol.*, 31:575–91, 2015

[61] E. Lammert and J. Axnick. Vascular Lumen Formation. *Cold Spring Harb.Perspect. Med.*, 2(4):a006619, 2012

[62] M. L. Iruela-Arispe, and G. E. Davis. Cellular and Molecular Mechanisms of Vascular Lumen Formation. *Developmental Cell*, 16:222–231, 2009

[63] M. S. Charpentier, P. Tandon, C. E. Trincot, E. K. Koutleva, F. L. Conlon. A Distinct Mechanism of Vascular Lumen Formation in Xenopus Requires EGFL7. *Plos One*, 10(2):e0116086, 2015

[64] M. R. Grant, K. E. Mostov, T. D. Tlsty, and C. A. Hunt. Simulating Properties of In Vitro Epithelial Cell Morphogenesis. *Plos Comput. Biol.*, 2(10):e129, 2006

[65] S. H. J. Kim and C. A. Hunt. Composite Cell Agent Model of Epithelial Culture In Vitro. *Proceedings of the 2011 Workshop on Agent-Directed Simulation*, ADS '11, pages 45–51, 2011

[66] V. Mironov, T. Boland, T. Trusk, G. Forgacs, and R. R. Markwald. Organ printing: computer-aided jet-based 3D tissue engineering. *Trends Biotechnol.*, 21:157–161, 2003

[67] *Farlex Partner Medical Dictionary.* Retrieved from http://medical-dictionary.thefreedictionary.com/lumen, June 2016

[68] Z. Wang, J. D. Butner, R. Kerketta, V. Cristini, and T. S. Deisboeck. Simulating Cancer Growth with Multiscale Agent-Based Modeling. *Semin. Cancer Biol.*, 30:70–78, 2015

[69] J. Werfel, S. Krause, A. G. Bischof, R. J. Mannix, H. Tobin, Y. Bar-Yam, R. M. Bellin, D. E. Ingber. How changes in extracellular matrix mechanics and gene expression variability might combine to drive cancer progression. *Plos One*, 8(10):e76122, 2013

[70] S. L. Spencer, R. A. Gerety, K. J. Pienta, S. Forrest. Modeling Somatic Evolution in tumorigenesis. *Plos Comput. Biol.*, 2(8):e108, 2006

[71] D. Hanahan, R. Weinberg. The hallmarks of cancer. *Cell*, 100:57–70, 2000

[72] P. Vineis, A. Schatzkin, and J. D. Potter. Models of carcinogenesis: an overview. *Carcinogenesis*, 31(10):1703–1709, 2010

[73] K. A. Rejniak, and A. R. A. Anderson. Hybrid Models of tumor Growth. *Wiley Interdiscip. Rev. Sys.t Biol. Med.*, 3(1):115–125, 2011

[74] T. Roose, S. J. Chapman, P. K. Maini. Mathematical Models of Avascular tumor Growth. *SIAM Rev.*, 49(2):179–208, 2007

[75] T. Reya, S. J. Morrison, M. F. Clarke, and I. L. Weissman. Stem cells, cancer, and cancer stem cells. *Nature*, 414:105–111, 2001

[76] A. Szabó, and R. M. H. Merks. Cellular Potts modeling of tumor growth, tumor invasion, and tumor evolution. *Front. Oncol.*, 3:87, 2013

[77] A. Sottoriva, L. Vermeulen, and S. Tavaré. Modeling evolutionary dynamics of epigenetic mutations in hierarchically organized tumors. *Plos Comput. Biol.*, 7:e1001132, 2011

[78] A. Sottoriva, J. J. C. Verhoeff, T. Borovski, S. K. McWeeney, L. Naumov, J. P. Medema, P. M. A. Sloot, and L. Vermeulen. Cancer stem cell tumor model reveals invasive morphology and increased phenotypical heterogeneity. *Cancer Res.*, 70:46–56, 2010.

[79] H. Enderling, L. Hlatky, and P. Hahnfeldt. Migration rules: tumours are conglomerates of self-metastases. *British Journal of Cancer*, 100:1917–1925, 2009

[80] H. Enderling, A. R. A. Anderson, M. A. J. Chaplain, A. Beheshti, L. Hlatky, and P. Hahnfeldt. Paradoxical dependencies of tumor dormancy and progression on basic cell kinetics. *Cancer Res.*, 69:8814–8821, 2009

[81] A. V. Ivshina, J. George, O. Senko, B. Mow, T. C. Putti, J. Smeds, T. Lindahl, Y. Pawitan, P. Hall, H. Nordgren, J. E. L. Wong, E. T. Liu, J. Bergh, V. A. Kuznetsov, and L. D. Miller. Genetic Reclassification of Histologic Grade Delineates New Clinical Subtypes of Breast Cancer. *Cancer Res.*, 66(21):10292–301, 2006

[82] H. Ohgaki and P. Kleihues. Genetic alterations and signaling pathways in the evolution of gliomas. *Cancer Sci.*, 100(12):2235–41, 2009.

[83] D. Loessner, J. P. Little, G. J. Pettet, and D. W. Hutmacher. A multiscale road map of cancer spheroids – incorporating experimental and mathematical modelling to understand cancer progression. *Journal of Cell Science*, 126:2761–2771, 2013.

[84] F. L. Greene, D. L. Page, I. D. Fleming, A. G. Fritz, Ch. M. Balch, D. G. Haller, M. Morrow. *AJCC Cancer Staging Manual*, chap. 1. Springer, New York, 6th edition, 2002.

[85] H. Ohgaki and P. Kleihues. Genetic Pathways to Primary and Secondary Glioblastoma. *Am. J. Pathol.*, 170:1445–53, 2007

[86] L. Sromova, H. Mareckova, L. Sedova, E. Balaziova, A. Sedo. Dipeptidyl peptidase-IV in synovial fluid and in synovial fluid mononuclear cells of patients with rheumatoid arthritis. *Clinica Chimica Acta*, 411:1046–1050, 2010

[87] A.-M. Lambeir, P. Proost, Ch. Durinx, G. Bal, K. Senten, K.Augustyns, S. Scharpe, J. V. Damme, and I. De Meester. Kinetic Investigation of Chemokine Truncation by CD26/Dipeptidyl Peptidase IV Reveals a Striking Selectivity within the Chemokine Family. *J. Biol. Chem.*, 276(32):29839–29845, 2001

[88] T. Nanki, K. Hayashida, H. S. El-Gabalawy, S. Suson, K. Shi, H. J. Girschick, S. Yavuz, and P. E. Lipsky. Stromal Cell-Derived Factor-1-CXC Chemokine Receptor 4 Interactions Play a Central Role in CD4+ T Cell Accumulation in Rheumatoid Arthritis Synovium. *J. Immunol.*, 165:6590–6598, 2000.

[89] T. Bennike, U. Ayturk, C. M. Haslauer, J. W. Froehlich, B. L. Proffen, O. Barnaby, S. Birkelund, M. M. Murray, M. L. Warman, A. Stensballe, and H. Steen. A Normative Study of the Synovial Fluid Proteome from Healthy Porcine Knee Joints. *J. Proteome Res.*, 13(10):4377–4387, 2014

[90] T. Riggs, A. Walts, N. Perry, L. Bickle, J. N. Lynch, A. Myers, J. Flynn, J. J. Linderman, M. J. Miller, D. E. Kirschner. A comparison of random vs. chemotaxis-driven contacts of T cells with dendritic cells during repertoire scanning. *J. Theor. Biol.*, 250(4):732–751, 2008

[91] Ch. Tokarski, S. Hummert, F. Mech, M. T. Figge, S. Germerodt, A. Schroeter, and S. Schuster. Agent-based modeling approach of immunedefense against spores of opportunistic human pathogenic fungi. *Front. Microbiol.*, 3:129, 2012

[92] S. Tisue, U. Wilensky. NetLogo: Design and implementation of a multi-agent modeling environment. In *Proceedings of the Agent 2004 Conference on Social Dynamics: Interaction, Reflexivity and Emergence*, Chicago, IL, 2004

[93] R. M. A. Vroomans, A. F. M. Marée, R. J. de Boer, J. B. Beltman. Chemotactic Migration of T Cells towards Dendritic Cells Promotes the Detection of Rare Antigens. *Plos Comput. Biol.*, 8(11): e1002763, 2012

[94] V. Baldazzi, P. Paci, M. Bernaschi, and F. Castiglione. Modeling lymphocyte homing and encounters in lymph nodes. *BMC Bioinformatics*, 10:387, 2009

[95] Y. Nakayama, R. F. Boucher. *Introduction to Fluid Mechanics*, chap. 12. Butterworth-Heinemann, Oxford, 1st edition, 1999

[96] P. J. Pritchard. *Fox and McDonald's Introduction to Fluid Mechanics*, chap. 6. John Wiley & Sons, Inc., New Jersey, 8th edition, 2011

[97] M. S. Alber, M. A. Kiskowski, J. A. Glazier, Y. Jiang. On cellular automaton approaches to modeling biological cells. In: J. Rosenthal, D. S. Gilliam, editors. Mathematical Systems Theory in Biology, Communications, Computation, and Finance, p. 1-40. Springer-Verlag, New York, 2003

[98] K. Bartha, H. Rieger. Vascular network remodeling via vessel cooption, regression and growth in tumors. J. Theor. Biol., 241:903–918, 2006

[99] S. Dormann, A. Deutsch. Modeling self-organized avascular tumor growth with a hybrid cellular automaton. Silico Biol., 2:0035, 2002

[100] P. Gerlee, A. R. A. Anderson. An evolutionary hybrid cellular automaton model of solid tumor growth. J. Theor. Biol., 246:583–603, 2007

[101] J. Galle, M. Loeffler, D. Drasdo. Modeling the effect of deregulated proliferation and apoptosis on the growth dynamics of epithelial cell populations in vitro. Biophys. J., 88:62–75, 2005

[102] V. Galvão, J. G. V. Miranda, R. Ribeiro-dos-Santos. Development of a two-dimensional agent-based model for chronic chagasic cardiomyopathy after stem cell transplantation. Bioinformatics, 24:2051–2056, 2008

[103] N. Grabe, K. Neuber. A multicellular systems biology model predicts epidermal morphology, kinetics and Ca^{2+} flow. Bioinformatics, 21:3541–3547, 2005

[104] Z. Guo, P. M. A. Sloot, J. C. Tay. A hybrid agent-based approach for modeling microbiological systems. J. Theor. Biol., 255:163–175, 2008

[105] A. R. Kansal, S. Torquato, G. R. Harsh IV, E. A. Chiocca, T. S. Deisboeck. Simulated brain tumor growth dynamics using a three-dimensional cellular automaton. J. Theor. Biol., 203:367–382, 2000

[106] Y. Mansury, T. S. Deisboeck. The impact of "search precision" in an agent-based tumor model. J. Theor. Biol., 224:325–337, 2003

[107] M. J. Piotrowska, S. D. Angus. A quantitative cellular automaton model of in vitro multicellular spheroid tumour growth. J. Theor. Biol., 258:165–178, 2009

[108] M. A. Pérez, P. J. Prendergast. Random-walk models of cell dispersal included in mechanobiological simulations of tissue differentiation. J. Biomech., 40:2244–2253, 2007

[109] S. H. Robertson, C. K. Smith, A. L. Langhans, S. E. McLinden, M. A. Oberhardt, K. R. Jakab, B. Dzamba, D. W. DeSimone, J. A. Papin, S. M. Peirce. Multiscale computational analysis of Xenopus laevis morphogenesis reveals key insights of systems-level behavior. BMC Syst. Biol., 1:46, 2007

[110] E. L. Stott, N. F. Britton, J. A. Glazier, M. Zajac. Stochastic simulation of benign avascular tumour growth using the Potts model. Math. Comput. Model., 30:183–198, 1999.

[111] G. Schaller, M. Meyer-Hermann. A modelling approach towards epidermal homoeostasis control. J. Theor. Biol., 247:554–573, 2007

[112] D. C. Walker, J. Southgate, G. Hill, M. Holcombe, D. R. Hose, S. M. Wood, S. Mac Neil, R. H. Smallwood. The epitheliome: agent-based modelling of the social behaviour of cells. BioSystems, 76:89–100, 2004

[113] L. Zhang, C. A. Athale, T. S. Deisboeck. Development of a three-dimensional multiscale agent-based tumor model: simulating gene-protein interaction profiles, cell phenotypes and multicellular patterns in brain cancer. J. Theor. Biol., 244:96–107, 2007

[114] G. S. Stamatakos, et al.. Clinically optimized version of the cellular/tissue models. ContraCancrum restricted Deliverable D4.3, 2011

[115] V. Bednář. Počítačové predikce pohybu buněk (Computer Predictions of Cell Movement). Master's Thesis (in Czech), Charles University, 2002

List of Abbreviations

ABM: agent-based models

CA: cellular automata

CPM: cellular Potts model

CS: cummulative state

CSC: cancer stem cell

DCs: dendritic cells

DPP-IV: dipeptidyl peptidase-IV

DTM: Diversifier tumour Model

FMNC: synovial fluid mononuclear cells

IBCell: immersed boundary cell model

MCS: monte carlo step

OA: osteoarthritis

PDE: partial differential equations

RA: rheumatoid arthritis

SDF: stromal-cell derived factor-1α

SF: synovial fluid